arXiv:2507.09865v1 [math.OC] 14 Jul 2025

# GROMOV-WASSERSTEIN BARYCENTERS: THE ANALYSIS PROBLEM

ROCÍO DÍAZ MARTÍN, IVAN V. MEDRI, AND JAMES M. MURPHY

ABSTRACT. This paper considers the problem of estimating a matrix that encodes pairwise distances in a finite metric space–or, more generally, the edge weight matrix of a network–under the barycentric coding model (BCM) with respect to the Gromov-Wasserstein (GW) distance function. We frame this task as estimating the unknown barycentric coordinates with respect to the GW distance, assuming that the target matrix (or kernel) belongs to the set of GW barycenters of a finite collection of known templates. In the language of harmonic analysis, if computing GW barycenters can be viewed as a synthesis problem, this paper aims to solve the corresponding analysis problem. We propose two methods: one utilizing fixed-point iteration for computing GW barycenters, and another employing a differentiation-based approach to the GW structure using a blow-up technique. Finally, we demonstrate the application of the proposed GW analysis approach in a series of numerical experiments and applications to machine learning.

## 1. INTRODUCTION

The *barycentric coding model* refers to a data representation framework that leverages the concept of expressing points in a convex set as barycentric combinations of its vertices. This approach is widely used in geometry, signal processing, and machine learning (ML), where data are represented via coordinates relative to specific reference points–sometimes called anchors, landmarks, or templates–rather than in a traditional Cartesian coordinate system or in terms of an algebraic basis of vectors [16]. While these notions–which include principal component analysis [44], nonnegative matrix factorization [33], and archetypal analysis [17]–are most natural in a vector space, they can be adapted to metric spaces via notions of *barycenter or Fréchet mean*, which do not always coincide with the convex combinations of some vertices of the set. The applications of modeling with barycentric coordinates range from data compression–where barycentric coding reduces dimensionality or redundancy by encoding data in terms of a few reference points (particularly in structured datasets)–to generative modeling, clustering, and embedding in ML–where data points are represented relative to cluster centroids–among other uses [72, 27, 67, 19, 59].

These models allow for *synthesis* and *analysis* of points in a metric space with distance $dist(\cdot,\cdot)$, through variational problems relative to given reference points $\mathbf{x}^1,\dots,\mathbf{x}^S$. For the *synthesis problem*, given a vector of non-negative coefficients $\lambda = (\lambda_1,\dots,\lambda_S)$ in the $(S-1)$-dimensional simplex $\Delta_{S-1}$, one seeks a point in the space minimizing the following objective:

$$\mathbf{x}_\lambda \in \arg\min_{\mathbf{x}} \sum_{s=1}^{S} \lambda_s \, dist^2(\mathbf{x}^s, \mathbf{x}); \tag{1}$$

where powers $p \geq 1$ other than 2 can also be considered. One can also 'project' a point $\mathbf{y}$ onto the collection of such synthesized points $\{\mathbf{x}_\lambda\}_{\lambda\in\Delta_{S-1}}$ by solving the *analysis problem*:

$$\lambda_{\mathbf{y}} \in \arg\min_{\lambda\in\Delta_{S-1}} d_a^2(\mathbf{y}, \mathbf{x}_\lambda), \tag{2}$$

*Key words and phrases.* Barycentric Coding Model, Gromov-Wasserstein Distance, Harmonic Analysis, Optimal Transport, Signal Processing.

where $d_a(\cdot,\cdot)$ is a discrepancy function (e.g., $d_a = dist$ or another metric in the space or even a weaker notion of dissimilarity that still identifies indiscernibles). We refer to the collection of points generated via (1) for fixed templates $\{\mathbf{x}^s\}_{s=1}^S$ as a *barycentric coding model* (BCM). Consequently, the barycenter of a set of templates for given weights $\lambda$ provides an alternative way of combining elements, one that better reflects the underlying geometry of the space while still preserving the dimensionality reduction properties of the representation.

This framework has been extensively used in classical optimal transport (OT), where the space of probability measures is endowed with the Wasserstein distance [49, 64, 65]. Foundational works on Wasserstein barycenters include [1, 18, 8, 32, 71], with more recent developments such as [68, 25, 35, 69] and extensions to dictionary learning [51, 41].

As an illustration, consider the space of discrete probability measures with finite support on $\mathbb{R}$, equipped with the 2-Wasserstein metric $W_2(\cdot,\cdot)$. Let the template measures be $\delta_0$ and $\delta_1$, where $\delta_x$ denotes the Dirac measure centered at $x$. The corresponding barycenter space consists of the set $\{\delta_t : t \in [0,1]\}$, which is obtained by solving the synthesis problem (1) in this specific setting. In other words, each measure $\mu = \delta_t$ minimizes the functional $\mu \mapsto t\,W_2^2(\delta_0,\mu) + (1-t)\,W_2^2(\delta_1,\mu)$. Hence, we can interpret the coordinates of the measure $\delta_t$ with respect to the templates $\delta_0$ and $\delta_1$ as the vector $(t, 1-t)$ in $\Delta_1$. In this simple example, barycenters correspond to convex combinations of the points 0 and 1–that is, Euclidean barycenters. In more general settings, however, measures or distributions have the ability to represent more complex data than individual points in space. For instance, Figure 1 compares interpolation between two weighted point clouds using Wasserstein geometry versus Euclidean geometry. Interpolating between two templates can be understood as constructing the barycentric space generated by those reference templates. Specifically, if $\mu_0$ and $\mu_1$ are the probability distributions corresponding to two templates, and $\pi$ is an OT plan between them in the 2-Wasserstein sense, then the interpolated measure $\mu_t$ defined as the pushforward of $\pi$ under the map $(x,y) \mapsto (1-t)x+ty$, that is, $\mu_t := ((1-t)x+ty)_\#\pi$ for $t \in [0,1]$, coincides with the Wasserstein barycenter of $\mu_0$ and $\mu_1$ with respective weights $(1-t)$ and $t$:

$$\mu_t = \arg\min_{\mu} \left\{(1-t)W_2^2(\mu,\mu_0) + tW_2^2(\mu,\mu_1)\right\}. \tag{3}$$

While classical OT relies on a shared underlying domain to compare probability measures, many modern applications involve distributions supported on different, potentially non-Euclidean, metric spaces. In such settings, Gromov-Wasserstein (GW) theory offers a natural generalization, enabling meaningful comparisons by aligning the intrinsic geometries of the underlying spaces themselves. The GW distance [38, 40] has emerged as a powerful tool in object matching problems, as it compares probability measures across different metric spaces by jointly aligning both structural (edge-based) and nodal (feature-based) similarities [26]. This perspective builds upon classical notions of shape similarity–such as the Hausdorff distance, the Wasserstein distance, and the Hausdorff-Wasserstein distance [38]–and can be viewed as a measure-theoretic relaxation of the Gromov-Hausdorff distance introduced in [24].

These innovations have led to applications across diverse domains, ranging from quantum chemistry [46] to natural language processing [3], enhancing fundamental tasks such as clustering [15], dimensionality reduction [61], shape correspondence [30], shape analysis [39], computer vision [52], and inference-based simulation [28]. Extensions to unbalanced settings have been explored [5, 9, 34, 54, 75], along with other variants, such as Sliced GW [58], and Fused GW–a simultaneous extension of Wasserstein and GW distances–[63, 62, 57]. However, GW distance computation is challenging due to requiring to solve a non-convex quadratic program; approximations include linearized [7] and entropy-regularized [46, 55, 48] GW.

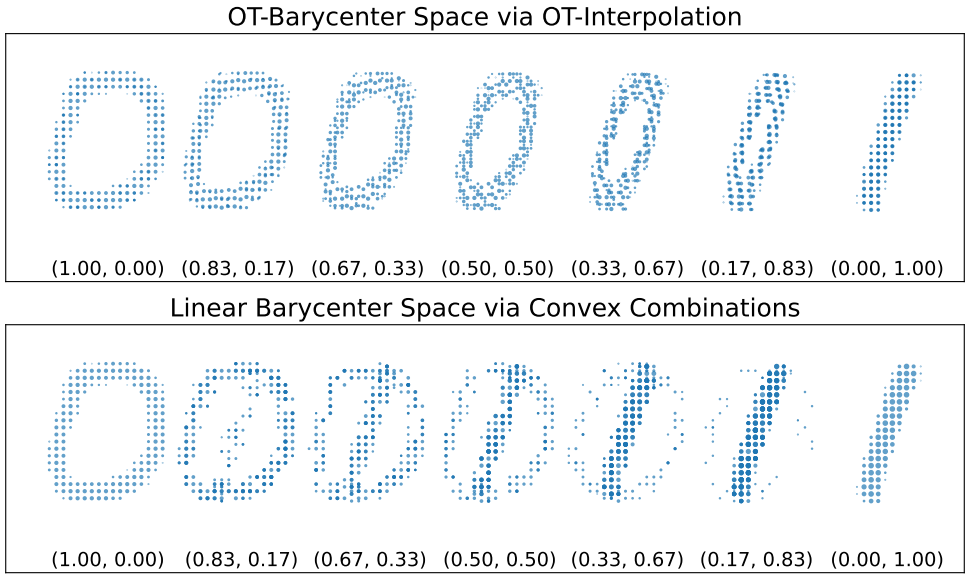



**Figure 1.** Illustration of different barycenter spaces between two point clouds selected from the Point Cloud MNIST 2D dataset [23], shown for various $t \in [0,1]$ with interpolation coordinates $(1-t,t)$ on the horizontal axis. Top: OT interpolations (with respect to the 2-Wasserstein geometry). Bottom: Linear interpolations (with respect to the Euclidean geometry).

In the context of GW, data consist of different configurations of nodes with weighted edges. Thus, instead of working with measures $\mu$ defined on a common underlying space, as in classical OT, we consider objects of the form $\mathbb{X} = (X, \omega_X, \mu_X)$, where $(X, \mu_X)$ is a probability space and $\omega_X : X \times X \to \mathbb{R}$ is a $\mu_X \otimes \mu_X$-measurable function. The function $\omega_X$ may represent a metric on $X$, in which case $\mathbb{X}$ is referred to as a *metric measure space* (mm-space). More generally, $\omega_X$ can be any function encoding *edge weights*, in which case the 3-tuple is called a *network* or a *shape*. If the set $X$ consists of finitely many points or *nodes*, then $\omega_X$ and $\mu_X$ admit matrix and vector representations, denoted by $\mathbf{X}$ and p, respectively. For short, we will sometimes use $(\mathbf{X}, \mathrm{p})$ to encode $(X, \omega_X, \mu_X)$. We refer to the space of networks endowed with the GW metric (see Section 2) as *GW space*.

Using these objects, the *GW synthesis problem* takes the form of (1) with the distance $dist(\cdot,\cdot)$ replaced by the GW metric: given templates $\{\mathbb{X}^s\}_{s=1}^S$, the goal is to solve

$$\Delta_{S-1} \ni \lambda \longmapsto \mathbb{Y}_\lambda \in \arg\min_{\mathbb{Y}} \sum_{s=1}^{S} \lambda_s \, GW^2(\mathbb{X}^s, \mathbb{Y}). \tag{4}$$

We call the collection generated by (4), for fixed templates and varying coefficients $\lambda \in \Delta_{S-1}$, a *GW barycenter space* or *Gromov–Wasserstein barycentric coding model* (GW-BCM).

One of the main differences between the 2-Wasserstein distance and the GW distance lies in how they support barycenter constructions. In the $W_2$ setting, barycenters between two or more measures can be constructed via displacement interpolation using OT maps under regularity assumptions [36, 1]. This interpolation aligns mass in a common ambient space and is underpinned by the pseudo-Riemannian structure of Wasserstein space [71]. In contrast, GW distance compares measures on different metric spaces by optimizing over structural correspondences rather than spatial displacements. While geodesics between two metric measure spaces exist in GW space and can yield meaningful barycenters (see Figure 2), there is no analogous displacement interpolation for more than two templates. This reflects the absence of a pseudo-Riemannian framework (in the classical sense [42, 4]), limiting the direct geometric interpretation of GW barycenters.

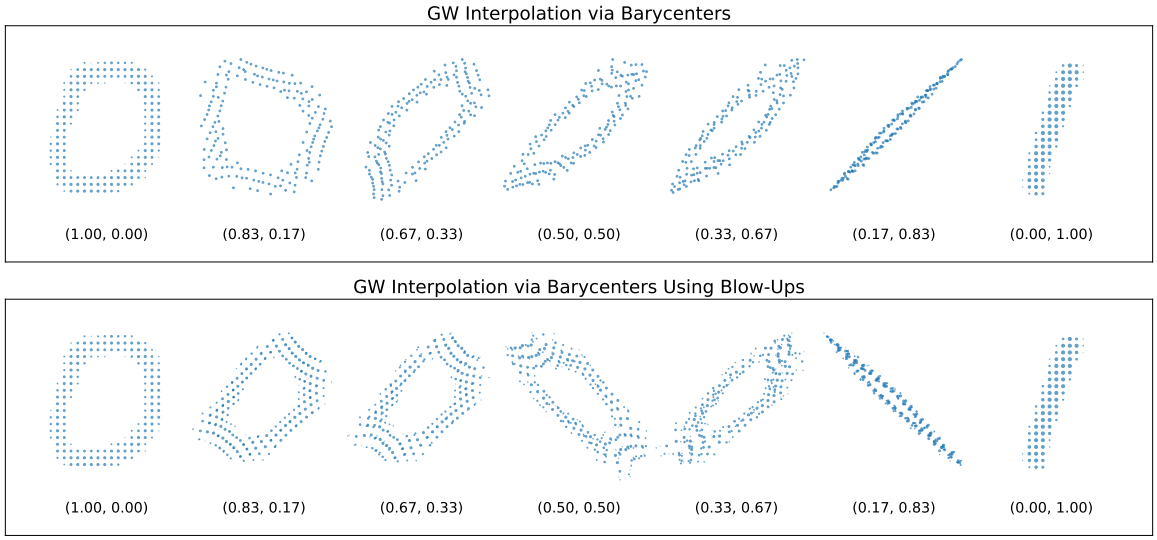



**Figure 2.** Illustration of GW barycenters between two point clouds from the Point Cloud MNIST 2D dataset [23], shown for various $t \in [0,1]$ with interpolation coordinates $(1-t,t)$ on the horizontal axis. The top subplot uses the function `ot.gromov.gromov_barycenters` from the POT Library [21] (based on [46]). The bottom subplot uses the blow-up technique from [13], which appropriately realigns the nodes and enlarges the template matrices $\mathbf{X}^0$ (zero shape) and $\mathbf{X}^1$ (one shape), creating new versions $\mathbf{X}_b^0$ and $\mathbf{X}_b^1$ of the same size, so that the GW barycenters can be interpreted as convex combinations $(1-t)\mathbf{X}_b^0 + t\mathbf{X}_b^1$ (see Remark B.9 in App. B.3). MDS embedding is used for visualization.

In this article, we focus on estimating the unknown GW barycentric coordinates of a point (or, more precisely, a network) under the barycentric coding model within the Gromov–Wasserstein framework (GW-BCM), a task we refer to as the *GW analysis problem*. That is, given a network $\mathbb{Y}$ we aim to formalize and solve

$$\lambda_{\mathbb{Y}} \in \underset{\lambda \in \Delta_{S-1}}{\arg\min}\, d_a^2(\mathbb{Y}, \mathbb{Y}_\lambda), \tag{5}$$

where $\mathbb{Y}_\lambda$ is generated by the GW-BCM (4), for some appropriate dissimilarity metric $d_a(\cdot,\cdot)$. In other words, assuming a given network is a GW barycenter of a set of templates $\{\mathbb{X}^s\}_{s=1}^S$, our goal is to recover the corresponding vector of weights $\lambda$. See Figure 2 for an illustration.

In this work, the synthesis problem–constructing GW barycenters–is addressed primarily to support the formulation of the GW-BCM assumption and the corresponding analysis problem. Since the minimization in (4) ranges over a very large *space of spaces* $\mathbb{Y}$, we restrict to spaces with finite many nodes for tractability. We further consider simplified versions of the general GW barycenter space generated by (4) (see also (32)). In the first simplification ((10) in Section 3), inspired by [46], we fix the cardinality of the set $Y$ and the measure $\mu_Y$ in $\mathbb{Y} = (Y, \omega_Y, \mu_Y)$. In the second ((33) in Section 4), we focus on critical points of the objective in (4) as in [14]. Relationships are discussed in Section 4.5.

1.1. **Summary of Contributions.** We primarily consider finite spaces and propose two distinct approaches to tackle the GW analysis problem (5):

(1) A method developed from a fixed-point scheme for the GW synthesis problem (4), relying on matrix optimization over the networks' weight matrices $\mathbf{Y}$.
(2) A gradient-based method motivated by an interpretation of GW barycenters not necessarily as exact minimizers of (4), but rather as critical points of a functional on the GW space.

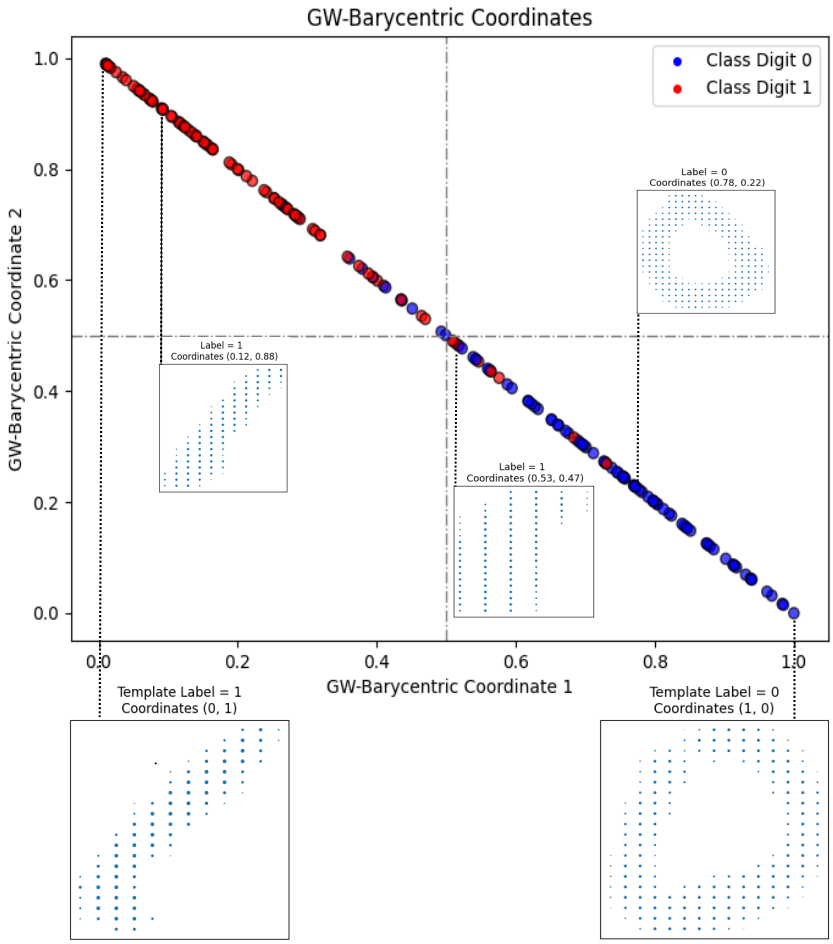



**Figure 3.** Visualization of the GW barycenter space as GW barycenter coordinates, using the Point Cloud MNIST 2D dataset [23]. Two point clouds serve as templates: one for digit 0s at $(1, 0)$ and one for digit 1s at $(0, 1)$. Using our proposed Algorithm 2, we compute GW barycenter coordinates for 200 random samples and plot them with blue dots for label 0 and red dots for label 1. Additionally, three corresponding point clouds are shown for illustration. Point clouds clearly corresponding to a digit 0 lie closer to the 0 template (coordinates near (1,0)), while those representing digit 1 are closer to the 1 template (coordinates near (0,1)).

Regarding (1), we adopt the following simple idea, which can be applied beyond the context of GW. Consider a finite set of templates $\mathbb{X}^s = (\mathbf{X}^s, \mathrm{p}^s)$, $s = 1, \dots, S$. Given a weight vector $\lambda \in \Delta_{S-1}$, consider GW synthesis problem (4), where the minimization is performed over $\mathbb{Y} = (\mathbf{Y}, \mathrm{q})$, with fixed matrix size $M$ for $\mathbf{Y}$ and a fixed probability vector q [46]. Assume that the GW synthesis problem (4) can be solved via a fixed-point iteration of the form $\mathbf{Y}_n = \rho_\lambda(\mathbf{Y}_{n-1})$. Then, if $(\mathbf{Y}, \mathrm{q})$ lies in the GW barycenter space generated by the templates, the matrix $\mathbf{Y}$ must be a fixed point of the corresponding iterative scheme. That is, there exists an unknown 'coordinate' vector $\lambda_{\mathbf{Y}}$ such that $\mathbf{Y} = \rho_{\lambda_{\mathbf{Y}}}(\mathbf{Y})$. To recover $\lambda_{\mathbf{Y}}$, we differentiate a chosen matrix norm $\|\mathbf{Y} - \rho_\lambda(\mathbf{Y})\|$ with respect to $\lambda$ and find its minimum at $\lambda = \lambda_{\mathbf{Y}}$. In summary, to generate GW barycenters, we employ a simplified version of the iterative scheme proposed in [46], and show in Theorem 3.3 that elements of the barycenter space are fixed points of this iteration. Building on this, Theorem 3.6 provides an exact recovery method for $\lambda_{\mathbf{Y}}$, for any $\mathbf{Y}$ in the GW barycenter space, formulated as a convex quadratic program and implemented in Algorithm 2. See Figure 3 for an illustration of its applicability.

Regarding (2), we interpret GW barycenters $\mathbb{Y}_\lambda$ as *Karcher means* of the template set $\{\mathbb{X}^s\}_{s=1}^S$ with respect to the weights $\lambda$, in the sense that $\mathbb{Y}_\lambda$ is a critical point of the objective functional in the GW synthesis problem (4)–that is, it satisfies the first-order condition [29]. To define a notion of gradients in GW space, we leverage a 'Riemannian-like structure', that endows the space of networks equipped with the GW distance with a tangent space framework [13, 14, 56]. To this end, we employ the *blow-up* technique introduced in [14] in the context of finite spaces. This approach enables the comparison of networks $\mathbb{X} = (\mathbf{X}, \mathrm{p})$ and $\mathbb{Y} = (\mathbf{Y}, \mathrm{q})$ of different sizes (i.e., where $\mathbf{X}$ is an $N \times N$ matrix and $\mathbf{Y}$ is an $M \times M$ matrix potentially with $M \neq N$) by converting GW OT plans into maps between new networks $\mathbb{X}_b = (\mathbf{X}_b, \mathrm{p}_b)$ and $\mathbb{Y}_b = (\mathbf{Y}_b, \mathrm{q}_b)$ of the same size. These new networks are *weakly isomorphic* (see Definition 2.3) to the original ones, and thus the GW dissimilarity is preserved: $GW(\mathbb{X}, \mathbb{Y}) = GW(\mathbb{X}_b, \mathbb{Y}_b)$. After establishing how to define directional derivatives and gradients in GW space, and drawing inspiration from [68, 69], we solve the GW analysis problem (5) as another convex quadratic program; see Theorem 4.7 and the corresponding implementation in Algorithm 4.

1.2. **Organization of the Paper.** Section 2 reviews the GW distance. Our main results, their proofs, and new algorithms are presented in Section 3 and Section 4, which address the GW analysis problem via two approaches: a fixed-point method (3) and a gradient-based method (4). 5 presents experiments on 2D and 3D point clouds that serve as a proof-of-concept for the analytical results. Conclusions follow in 6. The Appendix includes: additional context on the BCM framework in App. A; background proofs and examples in App. B; computational complexity of the proposed GW analysis algorithms in App. C; further experimental results in App. D; and an additional discussion on the computation of GW barycenters and $W_2$-barycenters in App. E. The code to reproduce the experiments of this paper is available online at https://github.com/RocioDM/GW_BCM.

1.3. **Notation.** In general, superscripts will be used for the templates and subscripts for the synthesized objects. We denote by $[S] := \{1, \dots, S\}$ the set of indices from 1 to $S$. The space of *weights* $\Delta_{S-1}$, also known as a *standard simplex* or *probability simplex*, is

$$\Delta_{S-1} := \{\lambda = (\lambda_1, \dots, \lambda_S) \in \mathbb{R}^S \mid \lambda_s \geq 0 \ \ \forall s \in [S], \text{ and } \sum_{s\in[S]} \lambda_s = 1\}.$$

If p is a vector and $\mathbf{X}$ a matrix, when there is no ambiguity regarding whether we are referring to entries or coordinates, we will write $\mathrm{p}[i] = \mathrm{p}_i$ and $\mathbf{X}[i, j] = \mathbf{X}_{ij}$. We recall that the *Frobenius norm* of a real-valued square matrix $\mathbf{X}$ is defined as $\|\mathbf{X}\|_{\mathrm{Frob}} := \sqrt{\mathrm{tr}(\mathbf{X}^T\mathbf{X})}$, where $\mathbf{X}^T$ stands for transpose. The component-wise (Hadamard) product between matrices is denoted by $(\mathbf{X} \odot \mathbf{Y})_{jl} := \mathbf{X}_{jl}\mathbf{Y}_{jl}$. For a vector q, the matrix $\frac{1}{\mathrm{q}\mathrm{q}^T}$ is defined by $\left(\frac{1}{\mathrm{q}\mathrm{q}^T}\right)[j, l] := \frac{1}{\mathrm{q}_j \mathrm{q}_l}$.

Given two (Borel) measure spaces $(X, \mu_X)$ and $(Y, \mu_Y)$, we say that the measure $\mu_Y$ is the *pushforward* of the measure $\mu_X$ by a measurable map $\varphi : X \to Y$, denoted by $\varphi_\# \mu_X = \mu_Y$, if $\mu_Y(A) = \mu_X(\{x \in X \mid \varphi(x) \in A\})$ for every measurable set $A \subseteq Y$. Given $\omega : Y \times Y \to \mathbb{R}$, we use the *pullback* notation $\varphi^*\omega(x, x') := \omega(\varphi(x), \varphi(x'))$, for all $x, x' \in X$. A *coupling* or *transport plan* $\pi$ between $\mu_X$ and $\mu_Y$, denoted $\pi \in \Pi(\mu, \nu)$, is a probability measure on the product space $X \times Y$ with marginals $\mu_X$, $\mu_Y$. In the case of finite discrete measures, $\mu_X = \sum_{i=1}^N \mathrm{p}_i \delta_{x_i}$ and $\mu_Y = \sum_{j=1}^M \mathrm{q}_j \delta_{y_j}$, each coupling can be identified with a matrix in

$$\Pi(\mathrm{p}, \mathrm{q}) := \{\pi \in \mathbb{R}^{N\times M} \mid \pi_{ij} \geq 0, \forall i, j\,; \sum_{j\in[M]} \pi_{ij} = \mathrm{p}_i \,\forall i \text{ and } \sum_{i\in[N]} \pi_{ij} = \mathrm{q}_j \,\forall j\}.$$

## 2. Gromov-Wasserstein (GW) Distances

The Gromov-Wasserstein (GW) distance endows the space of metric measure spaces with a well-defined metric structure. Moreover, it serves as a discrepancy measure for comparing more general structures.

**Definition 2.1** ([38, 7, 56, 13]). *Let $(X, \mu_X)$ be a probability space, where $X$ is a Polish space*[1]*, and $\mu_X$ is a fully supported Borel probability measure on $X$.*

*(1) If the set $X$ is endowed with a metric $d_X : X \times X \to \mathbb{R}_{\geq 0}$, then the triple $\mathbb{X} = (X, d_X, \mu_X)$ is called a* metric measure space *(mm-space).*

*(2) If $g_X$ is a symmetric function in $L^2(X \times X, \mu_X \otimes \mu_X)$ (i.e., $g_X(x, x') = g_X(x', x)$), then the triple $\mathbb{X} = (X, g_X, \mu_X)$ is called a* gauge measure space *(gm-space).*[2]

*(3) If $\omega_X : X \times X \to \mathbb{R}$ is any square-integrable function, i.e., $\omega_X \in L^2(X \times X, \mu_X \otimes \mu_X)$, then the triple $\mathbb{X} = (X, \omega_X, \mu_X)$ is called a* network *(or* shape*).*

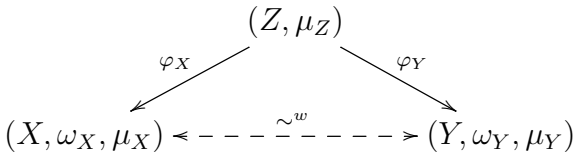
The natural hierarchy among the above structures can be expressed by the following chain of inclusions: mm-spaces $\subset$ gm-spaces $\subset$ networks.

**Definition 2.2** ([38, 13]). *Let $1 \leq p < \infty$. The* $p$-Gromov-Wasserstein problem *between two networks $\mathbb{X} = (X, \omega_X, \mu_X)$ and $\mathbb{Y} = (Y, \omega_Y, \mu_Y)$ is formulated as*[3]*:*

$$GW(\mathbb{X}, \mathbb{Y}) = \inf_{\pi \in \Pi(\mu_X, \mu_Y)} \left( \int_{X \times Y} \int_{X \times Y} |\omega_X(x, x') - \omega_Y(y, y')|^p d\pi(x, y) d\pi(x', y') \right)^{\frac{1}{p}}. \quad (6)$$

Roughly speaking, if $\pi(x, y)$ encodes the mass transported from location $x \in X$ to the point $y \in Y$, we can interpret that (6) optimizes over all possible plans $\pi$ so that when transporting mass from the points $x$ and $x'$ to $y$ and $y'$, the internal weights/dissimilarities $\omega_X(x, x')$ and $\omega_Y(y, y')$ are preserved or are as close as possible. The typical choice is $p = 2$, and for simplicity, we will assume this case. Accordingly, we denote $GW_2(\cdot, \cdot)$ simply as $GW(\cdot, \cdot)$. More general loss functions beyond $|\cdot|^p$, such as the KL-divergence [46] or the inner product GW problem [73], have also been considered in the literature.

**Definition 2.3** ([13]). *We say that two mm-spaces $\mathbb{X} = (X, d_X, \mu_X)$, $\mathbb{Y} = (Y, d_Y, \mu_Y)$ are* strongly isomorphic*, denoted $\mathbb{X} \sim \mathbb{Y}$, if there exists a Borel measurable surjective isometry $\varphi : X \to Y$ ($d_X(x, x') = d_Y(\varphi(x), \varphi(x'))$) with Borel measurable inverse such that $\varphi_{\#}\mu_X = \mu_Y$. We say that two networks $\mathbb{X} = (X, \omega_X, \mu_X)$, $\mathbb{Y} = (Y, \omega_Y, \mu_Y)$ are* weakly isomorphic*, denoted $\mathbb{X} \sim^w \mathbb{Y}$, if there exists a Borel probability space $(Z, \mu_Z)$ and measurable maps $\varphi_X : Z \to X$ and $\varphi_Y : Z \to Y$ such that $(\varphi_X)_{\#}\mu_Z = \mu_X$, $(\varphi_Y)_{\#}\mu_Z = \mu_Y$, and $\|(\varphi_X)^* \omega_X - (\varphi_Y)^* \omega_Y\|_\infty = 0$.*




For a simple visualization of weak isomorphic networks, see Figure 4 (and also Figure 10 described by Example B.7 in App. B). It is clear that if two networks are strongly isomorphic, then they are also weakly isomorphic. Moreover, if two networks are weakly isomorphic and have the structure of mm-spaces, then they are strongly isomorphic; see Proposition B.6 in App. B.3 for the finite case.

[1](i.e., a separable and completely metrizable topological space equipped with the Borel $\sigma$-algebra)

[2]For example, one may take squared-distances $g_X(x, x') = d_X^2(x, x')$.

[3](for simplicity, assume $X$ and $Y$ to be compact, so that (6) takes a finite value)

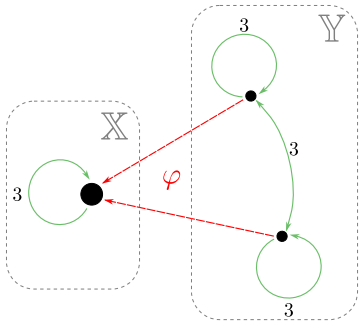
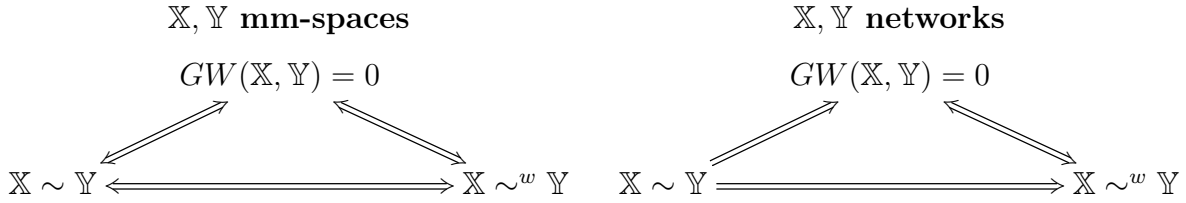



**Figure 4.** Illustration of weakly isomorphic networks $\mathbb{X}$ and $\mathbb{Y}$. The network $\mathbb{X}$ consists of one point (i.e., $X$ is a singleton) with unit mass (i.e., $\mu_X$ is the delta-measure), and $\omega_X$ represented by the $1 \times 1$ matrix $\mathbf{X} = (3)$. The network $\mathbb{Y}$ is given by the probability space $(Y, \mu_Y)$ consisting of two points with equal mass, and $\omega_Y$ represented by the $2 \times 2$ matrix $\mathbf{Y} = \begin{pmatrix} 3 & 3 \\ 3 & 3 \end{pmatrix}$. The pivoting space $(Z, \mu_Z)$ in Definition 2.3 can be taken as $(Y, \mu_Y)$, with $\varphi_X = \varphi$ (red assignment) and $\varphi_Y$ the identity map.

Consider the equivalence relation on the space of of networks given by

$$\mathbb{X} \sim \mathbb{X}' \quad \text{if and only if} \quad GW(\mathbb{X}, \mathbb{X}') = 0. \tag{7}$$

Then, $GW(\cdot, \cdot)$ defines a metric on the quotient space of mm-spaces under this equivalence relation. Moreover, (7) coincides with the notion of *strong isomorphism* [38, Thm. 5.1]. The extension of the GW discrepancy from mm-spaces to general networks is not necessarily a metric modulo strong isomorphisms [13, Rem. 2.5 and Fig. 2]. However, in analogy to Gromov–Hausdorff distance [12], in [13, Thms. 2.3 and 2.4] the authors prove that GW in (6) is a pseudo-metric in the space of networks (i.e, non-negative, symmetric and satisfies the triangle inequality). Moreover, $GW(\mathbb{X}, \mathbb{Y}) = 0$ if and only if $\mathbb{X}$ and $\mathbb{Y}$ are *weakly isomorphic*. As a summary, we provide the following diagram:




In this paper, we consider general *networks* as described in Definition 2.1, up to the equivalence relation induced by *weak isomorphisms*. Specifically, let $\mathcal{GW}$ denote the space of equivalence classes of networks under the weak isomorphism relation $\sim^w$. Given a network $\mathbb{Y} = (Y, \omega_Y, \mu_Y)$, we denote its equivalence class by $[\mathbb{Y}]$.

2.1. **GW on Finite Spaces.** We follow the approach in [38, Sec. 7], where the author introduces a computationally motivated formulation of the GW problem (see also [46]).

From now on, we focus on *finite* spaces $X = \{x_i\}_{i=1}^{N_\mathbf{X}}$, where $N_\mathbf{X} \in \mathbb{N}$ denotes the finite number of nodes. Finite networks can be represented as square matrices equipped with a probability measure on the columns (or equivalently, on the rows). Specifically, we encode the information of the triple $(X, \omega_X, \mu_X)$ as a pair $(\mathbf{X}, \mathrm{p}_\mathbf{X})$, where:

- $\mathrm{p}_\mathbf{X} = (\mathrm{p}_\mathbf{X}[1], \dots, \mathrm{p}_\mathbf{X}[N_\mathbf{X}]) \in \mathbb{R}^{N_\mathbf{X}}$, with $\mathrm{p}_\mathbf{X}[j] > 0 \ \forall j \in [N_\mathbf{X}]$ and $\sum_{j \in [N_\mathbf{X}]} \mathrm{p}_\mathbf{X}[j] = 1$, encodes the discrete measure $\mu_X$ supported on the $N_\mathbf{X}$ points; that is,

$$\mu_X = \sum_{j=1}^{N_\mathbf{X}} \mathrm{p}_\mathbf{X}[j] \delta_{x_j}.$$

- $\mathbf{X} \in \mathbb{R}^{N_\mathbf{X} \times N_\mathbf{X}}$ is a real $N_\mathbf{X} \times N_\mathbf{X}$ matrix, sometimes referred to as a *dissimilarity matrix*, where each entry $(i, j)$ represents the interaction between nodes $x_i$ and $x_j$; that is,

$$\omega_X(x_i, x_j) = \mathbf{X}_{ij}.$$

To simplify the notation, we omit the subscript and simply write p instead of $\mathrm{p}_\mathbf{X}$, and $N$ instead of $N_\mathbf{X}$. For convenience, we denote the space of such probability vectors p by $\mathcal{P}_N$.

To match the definition of mm-spaces, $\mathbf{X}$ should correspond with a distance matrix, $\mathbf{X}_{ij} = d_X(x_i, x_j)$, $\forall i, j \in [N]$, must therefore satisfy certain structural properties (at least, symmetry, non-negativity, and a zero diagonal). In this work, we adopt a more general abstraction where $\mathbf{X}$ need not represent a distance matrix and may encode arbitrary pairwise relations[4].

Given $(\mathbf{X}, \mathrm{p}) \in \mathbb{R}^{N\times N} \times \mathcal{P}_N$, $(\mathbf{Y}, \mathrm{q}) \in \mathbb{R}^{M\times M} \times \mathcal{P}_M$, the GW optimization problem in (6) adopts the form:

$$GW((\mathbf{X}, \mathrm{p}), (\mathbf{Y}, \mathrm{q}))^2 = \min_{\pi\in\Pi(\mathrm{p},\mathrm{q})} \sum_{i\in[N],j\in[M]} \sum_{k\in[N],l\in[M]} |\mathbf{X}_{ik} - \mathbf{Y}_{jl}|^2 \pi_{ij}\pi_{kl}. \tag{8}$$

It is a quadratic optimization problem with linear constraints, with no guarantees to be convex in general, and a minimizer is always attained [38]. When considering symmetric positive (semi)definite matrices, (8) is convex. For completeness, we provide a proof of this result in Proposition B.1 in App. B.1. However, we note that distance matrices $\mathbf{X}_{ij} = d_X(x_i, x_j)$ are not generally positive semidefinite.

## 3. Fixed-Point Iteration for Gromov-Wasserstein Barycenters

In this section, we begin by revisiting one of the most widely used approaches for synthesizing GW barycenters [46], but without incorporating any regularization term (3.1). We then show that this iterative scheme constitutes a fixed-point iteration (Theorem 3.3 and its Corollary 3.4). Building on this, in Section 3.2 we present our new contributions on solving the GW analysis problem, including Theorem 3.6 and Algorithm 2.

### 3.1. GW Barycenters via a Fixed-Point Approach: The Synthesis Problem.

Consider finitely many templates $(\mathbf{X}^s, \mathrm{p}^s) \in \mathbb{R}^{N^s\times N^s} \times \mathcal{P}_{N^s}$, for $s \in [S]$, where $S \in \mathbb{N}$. The GW synthesis problem studied in [46] can be formulated as follows. For $M \in \mathbb{N}$ and $\mathrm{q} \in \mathcal{P}_M$, consider the following restricted version of (4):

$$\Delta_{S-1} \ni \lambda \longmapsto \mathbf{Y}_\lambda \in \operatorname*{arg\,min}_{\mathbf{Y}\in\mathbb{R}^{M\times M}} \sum_{s\in[S]} \lambda_s\, GW((\mathbf{X}^s, \mathrm{p}^s), (\mathbf{Y}, \mathrm{q}))^2. \tag{9}$$

See Proposition B.4 in App. B.2 for a discussion on the existence of a minimum in (9). If the general synthesis problem (1) is replaced by (9), we define the following barycentric space.

**Definition 3.1.** *Let $\{(\mathbf{X}^s, \mathrm{p}^s) \in \mathbb{R}^{N^s\times N^s} \times \mathcal{P}_{N^s}\}_{s\in[S]}$ be a finite set of templates. For $M \in \mathbb{N}$ and $\mathrm{q} \in \mathcal{P}_M$ a probability vector with all entries strictly positive, we define:*

$$\mathrm{Bary}_{M,\mathrm{q}}(\{(\mathbf{X}^s, \mathrm{p}^s)\}_{s\in[S]}) := \{\mathbf{Y}_\lambda \text{ as in (9)} \mid \lambda \in \Delta_{S-1}\}. \tag{10}$$

*That is, $\mathrm{Bary}_{M,\mathrm{q}}(\{(\mathbf{X}^s, \mathrm{p}^s)\}_{s\in[S]})$ is the set of solutions $\mathbf{Y}_\lambda$ of the GW synthesis problem (9) varying $\lambda \in \Delta_{S-1}$, where the size $M$ of $\mathbf{Y}_\lambda$ is fixed, as well as* q.

[4]This framework enables applications in settings such as graphs, where $\mathbf{X}$ could represent adjacency matrices or Laplacian matrices, thereby broadening the scope of potential use cases.

Notice that the problem in (9) involves minimizing over multiple variables:

$$\begin{aligned}&\min_{\mathbf{Y}\in\mathbb{R}^{M\times M}} \sum_{s\in[S]} \lambda_s GW((\mathbf{X}^s,\mathrm{p}^s),(\mathbf{Y},\mathrm{q}))^2\\ &= \min_{\mathbf{Y}\in\mathbb{R}^{M\times M}} \min_{\{\pi^s\in\Pi(\mathrm{p}^s,\mathrm{q})\}_{s=1}^S} \sum_{s\in[S]} \lambda_s \sum_{i\in[N^s],j\in[M]} \sum_{k\in[N^s],l\in[M]} |\mathbf{X}^s_{ik}-\mathbf{Y}_{jl}|^2\pi^s_{ij}\pi^s_{kl}. \end{aligned} \tag{11}$$

As mentioned in [46], when the variables are treated separatly, this optimization problem is convex with respect to $\mathbf{Y}$, but not with respect to $\{\pi^s\}_{s=1}^S$ (it is quadratic, but the associated form is not necessarily positive semidefinite)[5]. In what follows we recall [46, Prop. 3][6].

**Proposition 3.2** (Prop. 3 [46] - Revisited proof in App. B.2)**.** *Given $S\in\mathbb{N}$, consider templates $(\mathbf{X}^s,\mathrm{p}^s)\in\mathbb{R}^{N^s\times N^s}\times\mathcal{P}_{N^s}$ for each $s\in[S]$, and $\lambda\in\Delta_{S-1}$. Let $M\in\mathbb{N}$ and let $\mathrm{q}\in\mathcal{P}_M$ be a probability vector. For each $s\in[S]$, let $\pi^s$ be a coupling in $\Pi(\mathrm{p}^s,\mathrm{q})$. Consider the functional*[7]

$$\mathbb{R}^{M\times M}\ni\mathbf{Y}\longmapsto J_\lambda(\mathbf{Y}):=\sum_{s\in[S]}\lambda_s\sum_{i\in[N^s],j\in[M]}\sum_{k\in[N^s],l\in[M]}|\mathbf{X}^s_{ik}-\mathbf{Y}_{jl}|^2\pi^s_{ij}\pi^s_{kl}. \tag{12}$$

*Then, the minimization problem $\min_{\mathbf{Y}\in\mathbb{R}^{M\times M}} J_\lambda(\mathbf{Y})$ is well-defined. Moreover, if all the entries of* q *are strictly positive*[8]*, there exists a unique minimizer $\mathbf{Y}^*\in\mathbb{R}^{M\times M}$ given by:*

$$\mathbf{Y}^*_{jl}:=\frac{1}{\mathrm{q}_j\mathrm{q}_l}\sum_{s\in[S]}\lambda_s\left((\pi^s)^T\mathbf{X}^s\pi^s\right)_{jl},\qquad\forall l,j\in[M]. \tag{13}$$

The following result provides a closed-form expression for the elements of the GW barycenter space in Definition 3.1.

**Theorem 3.3.** *Let $M\in\mathbb{N}$ and $\mathrm{q}\in\mathcal{P}_M$ with all entries strictly positive. Let $\mathbf{Y}_\lambda\in\mathrm{Bary}_{M,\mathrm{q}}(\{(\mathbf{X}^s,\mathrm{p}^s)\}_{s\in[S]})$ for some $\lambda\in\Delta_{S-1}$. For each $s\in[S]$, let $\pi^{*s}$ be an optimal plan for $GW((\mathbf{X}^s,\mathrm{p}^s),(\mathbf{Y}_\lambda,\mathrm{q}))$, and consider $\mathbf{Y}^*_\lambda\in\mathbb{R}^{M\times M}$ as in (13), i.e., $\mathbf{Y}^*_\lambda:=\frac{1}{\mathrm{q}\mathrm{q}^T}\odot\sum_{s\in[S]}\lambda_s(\pi^{*s})^T\mathbf{X}^s\pi^{*s}$. Then $\mathbf{Y}_\lambda=\mathbf{Y}^*_\lambda$.*

*Proof.* As in (12), consider the functional $J_\lambda$ on $\mathbb{R}^{M\times M}$, defined in this case by:

$$\mathbf{Y}\longmapsto J_\lambda(\mathbf{Y}):=\sum_{s\in[S]}\lambda_s\sum_{i\in[N^s],j\in[M]}\sum_{k\in[N^s],l\in[M]}|\mathbf{X}^s_{ik}-\mathbf{Y}_{jl}|^2\pi^{*s}_{ij}\pi^{*s}_{kl}. \tag{14}$$

By Proposition 3.2, we know that it has a unique minimum given by $\mathbf{Y}^*_\lambda$. Indeed, from the fact that q has all its entries strictly positive, it follows that $J_\lambda$ is strictly convex.

[5]However, if the set of couplings $\{\pi^s\}_{s\in[S]}$ is not fixed in advance, then each $\pi^s$ may depend on $\mathbf{Y}$ (since it is optimal for $GW((\mathbf{X}^s,\mathrm{p}^s),(\mathbf{Y},\mathrm{q}))$), implying that (11) is not necessarily convex in $\mathbf{Y}$. This is due to the general fact that while the supremum of convex functions is convex, the minimum is not; that is, even if $x\mapsto h(x,y)$ is convex for each $y$, the function $g(x)=\min_y h(x,y)$ need not be convex.

[6]Although [46, Prop. 3] allows for more general loss functions in the GW problem, we restrict our attention to the standard case $|\cdot|^2$ for clarity and simplicity.

[7]If we were able to choose the couplings $\pi^s$ as the OT plans for each problem $GW((\mathbf{X}^s,\mathrm{p}^s),(\mathbf{Y},\mathrm{q}))$, then the functional $J_\lambda$ could be interpreted as a simplified version of the objective in (4) (see $G_\lambda$ in (31), Section 4) now acting over the space of matrices of fixed size, rather than over the space of networks, where the sizes of the dissimilarity matrices may vary and the probability distributions over the nodes are not predefined.

[8]The assumption that all entries of q are strictly positive ensures that every node in the shape carries some mass, which is a natural requirement. Indeed, Definition 2.1 already requires fully supported measures.

**Algorithm 1** Iterative GW Barycenter Synthesis

**Inputs:**
- Templates $\{(\mathbf{X}^s, \mathrm{p}^s)\}_{s\in[S]}$
- Weight vector $\lambda \in \Delta_{S-1}$
- Predefined size of the output barycentric matrix $M$
- $\mathrm{q} \in \mathcal{P}_M$ (usually uniform, i.e., $\mathrm{q} = \frac{1}{M}(1,\ldots,1) \in \mathbb{R}^M$)
- Initialization $\mathbf{Y}_0 \in \mathbb{R}^{M\times M}$

**Output:** GW barycentric matrix $\mathbf{Y} \in \mathbb{R}^{M\times M}$

Initialize $\mathbf{Y} \leftarrow \mathbf{Y}_0$
**repeat**
  **for** $s = 1, 2, \ldots, S$ **do**
    $\pi(\mathbf{Y}, s) \leftarrow$ optimal coupling for $GW((\mathbf{X}^s, \mathrm{p}^s), (\mathbf{Y}, \mathrm{q}))$
  **end for**
  Update $\mathbf{Y} \leftarrow \frac{1}{\mathrm{q}\mathrm{q}^T} \odot \sum_{s\in[S]} \lambda_s (\pi(\mathbf{Y}, s))^T \mathbf{X}^s \pi(\mathbf{Y}, s)$
**until** convergence
**return** $\mathbf{Y}$

Therefore,

$$
\begin{aligned}
J_\lambda(\mathbf{Y}^*_\lambda) &\leq J_\lambda(\mathbf{Y}_\lambda) \qquad \text{(due to Proposition 3.2)} \\
&= \sum_{s\in[S]} \lambda_s \sum_{i\in[N^s],j\in[M]} \sum_{k\in[N^s],l\in[M]} |\mathbf{X}^s_{ik} - (\mathbf{Y}_\lambda)_{jl}|^2 \pi^{*s}_{ij} \pi^{*s}_{kl} \\
&= \sum_{s\in[S]} \lambda_s GW((\mathbf{X}^s, \mathrm{p}^s), (\mathbf{Y}_\lambda, \mathrm{q}))^2 \quad \text{(since } \pi^{*s} \text{ optimal for } GW((\mathbf{X}^s, \mathrm{p}^s), (\mathbf{Y}_\lambda, \mathrm{q}))\text{)} \\
&= \min_{\mathbf{Y}\in\mathbb{R}^{M\times M}} \sum_{s\in[S]} \lambda_s GW((\mathbf{X}^s, \mathrm{p}^s), (\mathbf{Y}, \mathrm{q}))^2 \quad \text{(since } \mathbf{Y}_\lambda \in \mathrm{Bary}_{M,\mathrm{q}}(\{(\mathbf{X}^s, \mathrm{p}^s)\}_{s\in[S]})\text{)} \\
&= \min_{\mathbf{Y}\in\mathbb{R}^{M\times M}} \sum_{s\in[S]} \lambda_s \min_{\pi^s\in\Pi(\mathrm{p}^s,\mathrm{q})} \sum_{i\in[N^s],j\in[M]} \sum_{k\in[N^s],l\in[M]} |\mathbf{X}^s_{ik} - \mathbf{Y}_{jl}|^2 \pi^s_{ij} \pi^s_{kl} \\
&\leq \min_{\mathbf{Y}\in\mathbb{R}^{M\times M}} \sum_{s\in[S]} \lambda_s \sum_{i\in[N^s],j\in[M]} \sum_{k\in[N^s],l\in[M]} |\mathbf{X}^s_{ik} - \mathbf{Y}_{jl}|^2 \pi^{*s}_{ij} \pi^{*s}_{kl} \\
&= \min_{\mathbf{Y}\in\mathbb{R}^{M\times M}} J_\lambda(\mathbf{Y}) \\
&= J_\lambda(\mathbf{Y}^*_\lambda) \qquad \text{(due to Proposition 3.2).}
\end{aligned}
$$

As a consequence, $\mathbf{Y}_\lambda$ is another minimum of the function (14). Therefore, $\mathbf{Y}_\lambda = \mathbf{Y}^*_\lambda$. □

As a direct consequence, the algebraic form of GW barycenters in (10) is captured by:

$$
\mathrm{Bary}_{M,\mathrm{q}}(\{(\mathbf{X}^s, \mathrm{p}^s)\}_{s\in[S]}) \subseteq \left\{ \frac{1}{\mathrm{q}\mathrm{q}^T} \odot \sum_{s\in[S]} \lambda_s (\pi^s)^T \mathbf{X}^s \pi^s \mid \pi^s \in \Pi(\mathrm{p}^s, \mathrm{q}),\ \lambda \in \Delta_{S-1} \right\}.
$$

The following corollary is a simple consequence of Theorem 3.3. It guarantees that Algorithm 1, which is a simplified version of the iteration scheme proposed in [46] to compute GW barycenters, has a fixed point (albeit does not guarantee convergence).

**Corollary 3.4.** *Consider templates* $\{(\mathbf{X}^s, \mathrm{p}^s)\}_{s=1}^S$, $M \in \mathbb{N}$, $\mathrm{q} \in \mathcal{P}_M$ *with all entries strictly positive, and* $\lambda \in \Delta_{S-1}$. *Given any real matrix* $\mathbf{Y}$ *of size* $M \times M$, *let* $\pi(\mathbf{Y}, s) \in \Pi(\mathrm{p}^s, \mathrm{q})$ *denote an optimal plan for* $GW((\mathbf{X}^s, \mathrm{p}^s), (\mathbf{Y}, \mathrm{q}))$. *Consider the following operator in* $\mathbb{R}^{M\times M}$:

$$\rho_\lambda(\mathbf{Y}) := \frac{1}{\mathrm{q}\mathrm{q}^T} \odot \sum_{s\in[S]} \lambda_s \left(\pi(\mathbf{Y}, s)\right)^T \mathbf{X}^s \pi(\mathbf{Y}, s) \qquad \forall\, \mathbf{Y} \in \mathbb{R}^{M\times M}. \tag{15}$$

*Then, every matrix in* $\mathrm{Bary}_{M,\mathrm{q}}(\{(\mathbf{X}^s, \mathrm{p}^s)\}_{s\in[S]})$ *that is a solution for* (9) *with weights* $\lambda$ *is a fixed point of the map* $\rho_\lambda$.

*Proof.* Given $\lambda \in \Delta_{S-1}$, let $\mathbf{Y}_\lambda$ be a solution to the synthesis problem (9). Thus, $\mathbf{Y}_\lambda \in \mathrm{Bary}_{M,\mathrm{q}}(\{(\mathbf{X}^s, \mathrm{p}^s)\}_{s\in[S]})$. Then, by Theorem 3.3 we have that $\mathbf{Y}_\lambda$ is a fixed point of $\rho_\lambda$:

$$\rho_\lambda(\mathbf{Y}_\lambda) = \frac{1}{\mathrm{q}\mathrm{q}^T} \odot \sum_{s\in[S]} \lambda_s (\pi(\mathbf{Y}_\lambda, s))^T \mathbf{X}^s \pi(\mathbf{Y}_\lambda, s) = \mathbf{Y}_\lambda^* = \mathbf{Y}_\lambda.$$

□

Algorithm 1 can be viewed as applying the function $\rho_\lambda$ iteratively, which is guaranteed to have a fixed point. In the statement of Corollary 3.4, we use the notation $\pi(\mathbf{Y}, s)$ to emphasize the dependence on $\mathbf{Y}$, as it is optimal for the GW problem $GW((\mathbf{X}^s, \mathrm{p}^s), (\mathbf{Y}, \mathrm{q}))$.

**Remark 3.5** (See also Example B.5 in App. B.2)**.** *Theorem 3.3 implies that formula* (13) *for* $\mathbf{Y}_\lambda^*$ *does not depend on the initial choice of GW OT plans* $\{\pi^{*s}\}_{s\in[S]}$. *Indeed, let* $\mathbf{Y}_\lambda \in \mathrm{Bary}_{M,\mathrm{q}}(\{(\mathbf{X}^s, \mathrm{p}^s)\}_{s\in[S]})$ *for some* $\lambda \in \Delta_{S-1}$. *For each* $s \in [S]$, *let* $\pi^{*s}$ *and* $\widetilde{\pi}^{*s}$ *be couplings in* $\Pi(\mathrm{p}^s, \mathrm{q})$ *both optimal for* $GW((\mathbf{X}^s, \mathrm{p}^s), (\mathbf{Y}_\lambda, \mathrm{q}))$. *Then, Theorem 3.3 implies that*

$$\frac{1}{\mathrm{q}\mathrm{q}^T} \odot \sum_{s\in[S]} \lambda_s (\pi^{*s})^T \mathbf{X}^s \pi^{*s} = \mathbf{Y}_\lambda = \frac{1}{\mathrm{q}\mathrm{q}^T} \odot \sum_{s\in[S]} \lambda_s (\widetilde{\pi}^{*s})^T \mathbf{X}^s \widetilde{\pi}^{*s}.$$

3.2. **GW Barycenters via a Fixed-Point Approach: The Analysis Problem.** Let us fix finitely many templates $(\mathbf{X}^s, \mathrm{p}^s) \in \mathbb{R}^{N^s\times N^s} \times \mathcal{P}_{N^s}$, for $s \in [S]$. Let $M \in \mathbb{N}$ and $\mathrm{q} \in \mathcal{P}_M$. In this section, we consider the following version of the *GW analysis problem* introduced in (5):

$$\mathbb{R}^{M\times M} \ni \mathbf{Y} \longmapsto \lambda_{\mathbf{Y}} := \operatorname*{arg\,min}_{\lambda\in\Delta_{S-1}} d_a(\mathbf{Y}, \mathbf{Y}_\lambda)^2, \tag{16}$$

where $\mathbf{Y}_\lambda \in \mathrm{Bary}_{M,\mathrm{q}}(\{(\mathbf{X}^s, \mathrm{p}^s)\}_{s\in[S]})$, i.e., it is a solution of the GW synthesis problem (9) corresponding to weight vector $\lambda$. The function $d_a(\cdot,\cdot)$ denotes a divergence measure on the space of $M \times M$ real matrices, which is to be specified.

Theorem 3.6 below solves the GW analysis problem (16) under the GW-BCM hypothesis, that is, assuming that $\mathbf{Y} \in \mathbb{R}^{M\times M}$ belongs to the GW barycenter space given in Definition 3.1 (in symbols, $\mathbf{Y} \in \mathrm{Bary}_{M,\mathrm{q}}(\{(\mathbf{X}^s, \mathrm{p}^s)\}_{s\in[S]})$). Under this hypothesis, Theorem 3.3 implies that

$$\mathbf{Y} = \frac{1}{\mathrm{q}\mathrm{q}^T} \odot \sum_{s\in[S]} (\lambda_{\mathbf{Y}})_s (\pi^s)^T \mathbf{X}^s \pi^s, \qquad \text{for some } \lambda_{\mathbf{Y}} \in \Delta_{S-1}, \tag{17}$$

where, for each $s \in [S]$, $\pi^s$ is an optimal plan for $GW((\mathbf{X}^s, \mathrm{p}^s), (\mathbf{Y}, \mathrm{q}))$. It is important to notice that each $\pi^s$ depends on the input $\mathbf{Y}$, but, by Remark 3.5, we could consider another set of optimal plans $\{\widetilde{\pi}^s\}_{s=1}^S$ and the expression (17) would not differ. Let us simplify our notation by defining, for each $s \in [S]$, the matrices

$$F(\mathbf{Y}, s) := \frac{1}{\mathrm{q}\mathrm{q}^T} \odot (\pi^s)^T \mathbf{X}^s \pi^s \in \mathbb{R}^{M\times M}. \tag{18}$$

This implies that problem (16) for the given $\mathbf{Y} \in \mathrm{Bary}_{M,\mathrm{q}}(\{(\mathbf{X}^s, \mathrm{p}^s)\}_{s=1}^S)$ coincides with

$$\lambda_{\mathbf{Y}} := \underset{\lambda \in \Delta_{S-1}}{\arg\min}\, d_a^2 \left( \mathbf{Y}, \sum_{s\in[S]} \lambda_s F(\mathbf{Y}, s) \right). \tag{19}$$

In other words, we aim to minimize the functional $\Theta : \mathbb{R}^S \to [0, \infty)$ defined by

$$\Theta(\lambda) := d_a^2 \left( \mathbf{Y}, \sum_{s\in[S]} \lambda_s F(\mathbf{Y}, s) \right) \tag{20}$$

over the convex set $\Delta_{S-1}$. As the choice of divergence $d_a(\cdot,\cdot)$ does not affect result (as pointed out in Remark A.2), in Theorem 3.6 we will adopt $d_a(\mathbf{X}, \mathbf{Y}) = \|\mathbf{Y} - \mathbf{X}\|_{\mathrm{Frob}}$[9].

**Theorem 3.6.** *Let $\{(\mathbf{X}^s, \mathrm{p}^s) \in \mathbb{R}^{N^s \times N^s} \times \mathcal{P}_{N^s}\}_{s\in[S]}$, $M \in \mathbb{N}$, $(\mathbf{Y}, \mathrm{q}) \in \mathbb{R}^{M\times M} \times \mathcal{P}_M$. Let $F(\mathbf{Y}, s)$ be as in (18), for each $s \in [S]$, and consider the loss $d_a(\mathbf{X}, \mathbf{Y}) = \|\mathbf{Y} - \mathbf{X}\|_{\mathrm{Frob}}$ in the formulation of the GW analysis problem (16). If $\mathbf{Y} \in \mathrm{Bary}_{M,\mathrm{q}}(\{(\mathbf{X}^s, \mathrm{p}^s)\}_{s\in[S]})$, then the corresponding weight vector $\lambda_{\mathbf{Y}} \in \Delta_{S-1}$ associated with $\mathbf{Y}$ is given by a solution of the following convex quadratic minimization problem:*

$$\min_{\lambda\in\Delta_{S-1}} \lambda^T \mathcal{Q} \lambda, \quad \text{where } \mathcal{Q}_{sr} := \mathrm{tr}\left( (F(\mathbf{Y}, s) - \mathbf{Y})^T (F(\mathbf{Y}, r) - \mathbf{Y}) \right) \ \ \forall s, r \in [S]. \tag{21}$$

*Equivalently, $\lambda_{\mathbf{Y}}$ is a solution of the following linear problem:*

$$K\lambda = b \qquad \text{subject to } \lambda \in \Delta_{S-1} \subset \mathbb{R}^S, \tag{22}$$

*where $K \in \mathbb{R}^{S\times S}$ and $b \in \mathbb{R}^S$ are given by*

$$K_{sr} := \mathrm{tr}\left( F(\mathbf{Y}, s)^T F(\mathbf{Y}, r) \right) \quad \forall s, r \in [S], \quad b_s := \mathrm{tr}\left( \mathbf{Y}^T F(\mathbf{Y}, s) \right) \quad \forall s \in [S]. \tag{23}$$

*Proof.* Let $\mathbf{Y} \in \mathrm{Bary}_{M,\mathrm{q}}(\{(\mathbf{X}^s, \mathrm{p}^s)\}_{s=1}^S)$. Under the choice of the Frobenius norm $\|\cdot\|_{\mathrm{Frob}}$ in $\mathbb{R}^{M\times M}$, the nonnegative functional $\Theta$ in (20) can be written as

$$\begin{aligned}
\Theta(\lambda) &= \mathrm{tr}\left( \left( \sum_{s\in[S]} \lambda_s F(\mathbf{Y}, s) - \mathbf{Y} \right)^T \left( \sum_{r\in[S]} \lambda_r F(\mathbf{Y}, r) - \mathbf{Y} \right) \right) \\
&= \sum_{s,r\in[S]} \lambda_s \lambda_r \underbrace{\mathrm{tr}\left( (F(\mathbf{Y}, s) - \mathbf{Y})^T (F(\mathbf{Y}, r) - \mathbf{Y}) \right)}_{\mathcal{Q}_{sr}} \\
&= \lambda^T \mathcal{Q} \lambda.
\end{aligned}$$

Due to (17), the GW barycentric coordinate vector $\lambda_{\mathbf{Y}}$ is such that $\Theta(\lambda_{\mathbf{Y}}) = \lambda_{\mathbf{Y}}^T \mathcal{Q} \lambda_{\mathbf{Y}} = 0$. Equivalently, $\lambda_{\mathbf{Y}}$ is a solution of the quadratic minimization problem (21), that is,

$$\lambda_{\mathbf{Y}} \in \underset{\lambda\in\Delta_{S-1}}{\arg\min}\, \lambda^T \mathcal{Q} \lambda.$$

The matrix $\mathcal{Q}$ is symmetric and positive semidefinite. This holds since it is the Gram matrix of the system of matrices $\{F(\mathbf{Y}, s) - \mathbf{Y}\}_{s=1}^S$ with respect to the inner product in $\mathbb{R}^{M\times M}$ given by $\langle A, B\rangle = \mathrm{tr}(A^T B)$, and it is well-known that all Gram matrices are symmetric positive semidefinite [53]. Thus, $\Theta$ is convex and non-negative as a function over the whole $\mathbb{R}^S$. So, critical points of $\Theta$ are global minima. Moreover, we can decompose

$$\lambda^T \mathcal{Q} \lambda = \mathrm{tr}\left( \mathbf{Y}^T \mathbf{Y} \right) - 2 \sum_{s\in[S]} \lambda_s b_s + \sum_{s\in[S]} \sum_{r\in[S]} \lambda_s \lambda_r K_{sr},$$

[9](which, in particular, is invariant under orthogonal transformations)

**Algorithm 2** Analysis: GW Barycenter Coordinates

**Inputs:**
- Templates $\{(\mathbf{X}^s, \mathrm{p}^s)_{s\in[S]}\}$
- Shape/Network $\mathbf{Y} \in \mathbb{R}^{M\times M}$, $\mathrm{q} \in \mathcal{P}_M$

**Output:** Weight vector $\lambda$

**for** $s = 1, 2, \ldots, S$ **do**
  $\pi(\mathbf{Y}, s) \leftarrow$ optimal coupling for $GW((\mathbf{X}^s, \mathrm{p}^s), (\mathbf{Y}, \mathrm{q}))$
  $F(\mathbf{Y}, s) \leftarrow \pi(\mathbf{Y}, s)^T \mathbf{X}^s \pi(\mathbf{Y}, s)$
**end for**
**for** $s = 1, 2, \ldots, S$ **do**
  **for** $r = s, s+1, \ldots, S$ **do**
    $\mathcal{Q}_{sr} = \mathrm{tr}\left((F(\mathbf{Y}, s) - \mathbf{Y})^T (F(\mathbf{Y}, s) - \mathbf{Y})\right)$
    $\mathcal{Q}_{rs} = \mathcal{Q}_{sr}$
  **end for**
**end for**
$\lambda \leftarrow \arg\min_{\lambda\in\Delta_{S-1}} \lambda^T \mathcal{Q} \lambda$
**return** $\lambda$

where $K \in \mathbb{R}^{S\times S}$ and $b \in \mathbb{R}^S$ are given by (23). Thus, minimizing $\Theta(\lambda)$ over the simplex $\Delta_{S-1}$ is equivalent to solving the quadratic program

$$\min_{\lambda\in\Delta_{S-1}} \lambda^T K \lambda - 2\lambda^T b, \tag{24}$$

and the critical points of $\Theta$ are the solutions of the linear problem $K\lambda = b$. As a conclusion, the vector solutions $\lambda \in \mathbb{R}^S$ of the linear system $K\lambda = b$ are global minima of $\Theta$. These solutions might not be unique but under the GW-BCM condition (i.e., assuming $\mathbf{Y} \in \mathrm{Bary}_{M,\mathrm{q}}(\{(\mathbf{X}^s, \mathrm{p}^s)\}_{s=1}^S)$), it is guaranteed that there exists at least one solution $\lambda_{\mathbf{Y}}$ in $\Delta_{S-1}$. In other words, the solutions of (21) (or (24)) are given by (22). □

Algorithm 2 implements the analysis scheme laid out in Theorem 3.6, and we refer the reader to App. C for an analysis of its computational complexity.

## 4. A Gradient Method for Gromov-Wasserstein Barycenters

In [14], given a network $\mathbb{X}$, the authors provide a way of computing directional derivatives of the functional $\mathbb{Y} \longmapsto GW^2(\mathbb{X}, \mathbb{Y})$ in the direction of vectors in a 'tangent space' at $\mathbb{Y}$ [6, 13, 56]. Thus, in Sections 4.1, 4.2, and 4.3 we shift to a different approach that allows to compute gradients of functionals in GW space using a blow-up technique, and thus defining a weaker version of GW barycenters as Karcher means. This culminates in our new contributions to the GW analysis problem (4.4), including Theorem 4.7 and Algorithm 4. Connections between the fixed-point and gradient-based approaches are discussed in Section 4.5.

### 4.1. Tangent Space, Exponential Map, Directional Derivatives, and Gradients.

As introduced in Section 2, let $\mathcal{GW}$ be the Gromov-Wasserstein space of equivalence classes of networks under weak isomorphism $\sim^w$. Thus, two networks $\mathbb{Y}$ and $\mathbb{Y}'$ belong to the same class $[\mathbb{Y}]$ if and only if $GW(\mathbb{Y}, \mathbb{Y}') = 0$. In this case, a GW OT plan $\pi$ realizing $GW(\mathbb{Y}, \mathbb{Y}') = 0$ is referred to as a *self-coupling*. In [14], the authors define a *formal tangent structure* on the GW space $\mathcal{GW}$ as follows: the *tangent space* of $\mathcal{GW}$ at a network

class $[\mathbb{Y}]$ is given by[10]

$$\mathrm{Tan}_{[\mathbb{Y}]} = \left( \bigcup_{(Y,\omega_Y,\mu_Y)\in[\mathbb{Y}]} L^2(Y\times Y, \mu_Y\otimes\mu_Y) \right) / \simeq \tag{25}$$

where the quotient is taken under the following equivalence relation defined by self-couplings: given $v \in L^2(Y\times Y,\mu_Y\otimes\mu_Y)$, $v' \in L^2(Y'\times Y',\mu_{Y'}\otimes\mu_{Y'})$, for $(Y,\omega_Y,\mu_Y)$, $(Y',\omega_{Y'},\mu_{Y'})$ in $[\mathbb{Y}]$, we say that $v \simeq v'$ if and only if there a self-coupling $\pi\in\Pi(\mu_Y,\mu_{Y'})$ such that

$$\omega_Y(y_1,y_2)=\omega_{Y'}(y_1',y_2') \quad \text{and} \quad v(y_1,y_2)=v'(y_1',y_2') \qquad a.e.\,\pi(y_1,y_1')\pi(y_2,y_2').$$

We denote the class of $v$ as $[v]$. Each space $\mathrm{Tan}_{[\mathbb{Y}]}$ is equipped with the inner product[11]

$$\langle [v],[v']\rangle_{\mathrm{Tan}_{[\mathbb{Y}]}} := \langle (\varphi_Y)^* v, (\varphi_{Y'})^* v'\rangle_{L^2(Z\times Z,\mu_Z\otimes\mu_Z)},$$

where the measure space $(Z,\mu_Z)$ and the functions $\varphi_Y : Z\to Y$, $\varphi_{Y'}: Z\to Y'$ are as in Definition 2.3 of weak isomorphism between $\mathbb{Y}$ and $\mathbb{Y}'$ (i.e., a *common resolution*). Notice that, when considering finite networks $(Y=\{y_j\}_{j=1}^M,\omega_Y,\mu_Y=\sum_{j=}^M \mathrm{q}_j\delta_{y_j})$, the $L^2$-space $L^2(Y\times Y,\mu_Y\otimes\mu_Y)$ can be identified with $\mathbb{R}^{M\times M}$ equipped with an inner product induced by a weighted version of the Frobenius norm:

$$\langle A,B\rangle_{L^2(Y\times Y,\mu_Y\otimes\mu_Y)} = \sum_{i,j\in[M]} A_{ij}B_{ij}\mathrm{q}_i\mathrm{q}_j =: \mathrm{tr}_{\mathrm{q}}(A^TB), \tag{26}$$

where $\mathrm{tr}_{\mathrm{q}}$ denotes the trace inner product weighted by $\mathrm{q}\otimes\mathrm{q}\in\mathbb{R}^{M\times M}$.[12]

The *exponential* map $Exp_{[\mathbb{Y}]}:\mathrm{Tan}_{[\mathbb{Y}]}\longrightarrow\mathcal{GM}$ is defined as:

$$[v]\longmapsto[(Y,\omega_Y+v,\mu_Y)] \qquad \text{for } v\in L^2(Y\times Y,\mu_Y\otimes\mu_Y). \tag{27}$$

Using our shorthand notation $(\mathbf{Y},\mathrm{q})\in\mathbb{R}^{M\times M}\times\mathcal{P}_M$ to denote a representative of $[\mathbb{Y}]$, (27) can be identified with the map $v\mapsto(\mathbf{Y}+v,\mathrm{q})$ for all $v\in\mathbb{R}^{M\times M}$.

**Definition 4.1** ([13]). *Given a functional over the GW space, $G:\mathcal{GW}\to\mathbb{R}$, its* directional derivative *in the direction of $[v]\in\mathrm{Tan}_{[\mathbb{Y}]}$ is defined by*

$$D_vG([\mathbb{Y}]) := \lim_{t\searrow 0}\frac{G(Exp_{[\mathbb{Y}]}([tv]))-G([\mathbb{Y}])}{t}, \tag{28}$$

*and its* gradient[13] *by a vector $\nabla G([\mathbb{Y}])\in\mathrm{Tan}_{[\mathbb{Y}]}$ satisfying*

$$D_vG([\mathbb{Y}]) = \langle [v],\nabla G([\mathbb{Y}])\rangle_{\mathrm{Tan}_{[\mathbb{Y}]}}, \qquad \forall [v]\in\mathrm{Tan}_{[\mathbb{Y}]}. \tag{29}$$

4.2. **Blow-Ups.** In [14], particular representatives of the equivalence classes under weak isomorphisms were considered using a *blow-up* technique, which we will describe[14]. This blow-up idea avoids the need to fix a size $M$ in advance, as required in the in the approach of [46] and reviewed in this paper when studying the GW synthesis problem (10) in Section 3.1.

[10] If we consider only the space of classes of mm-spaces or gm-spaces under the strong isomorphism defined in Definition 2.3, then each $L^2$-space in (25) is restricted to its subspace of symmetric functions.

[11] i.e., a well-defined, symmetric, positive semidefinite bilinear form on the quotient space $\mathrm{Tan}_{[\mathbb{Y}]}$, which is modeled on Hilbert spaces.

[12] To ensure that this defines a norm, we assume that $\mathrm{q}_j>0$ for all $j\in[M]$, meaning that the support of $\mu_Y$ consists precisely of the $M$ distinct points $\{y_j\}_{j=1}^M$, as required in Definition 2.1.

[13] If $G:\mathcal{GW}\to\mathbb{R}$ is differentiable, that is, if all the directional derivatives (28) exist, and if, moreover, its gradient at $[\mathbb{Y}]$, as defined via the *Riesz representation* (29), exists, then it is unique (see [14, Lem. 7] and the references therein).

[14] In a broader sense, this idea is similar to that of the *barycentric projection* widely used in linear OT [66] in order to get transport maps from OT plans. See also [7] for the GW case.

**Definition 4.2** ([13, 14]). *Consider finite networks* $(X = \{x_i\}_{i=1}^N, \omega_X, \mu_X)$ *and* $(Y = \{y_j\}_{j=1}^M, \omega_Y, \mu_Y)$*, which we simply denote as* $(\mathbf{X}, \mathrm{p}) \in \mathbb{R}^{N\times N} \times \mathcal{P}_N$ *and* $(\mathbf{Y}, \mathrm{q}) \in \mathbb{R}^{M\times M} \times \mathcal{P}_M$[15]*. Let* $\pi \in \Pi(\mathrm{p}, \mathrm{q})$ *be a coupling between* p *and* q*. Consider the vectors* $u(x) = (u(x_1), \dots u(x_N))$ *and* $v(y) = (v(y_1), \dots, v(y_M))$ *given by*

$$u(x_i) := |\{j \in [M] \mid \pi(x_i, y_j) > 0\}| \quad \text{and} \quad v(y_j) := |\{i \in [N] \mid \pi(x_i, y_j) > 0\}|.$$

*We define:*

- *New sets of nodes*

$$X_b := \bigcup_{i\in[N],\, 1\le k_i\le u(x_i)} (x_i, k_i) \qquad \text{and} \qquad Y_b := \bigcup_{j\in[M],\, 1\le l_j\le v(y_j)} (y_j, l_j).$$

- *New probability vectors supported on such nodes*

$$\mathrm{p}_b[i, k_i] := \pi(\{x_i, y_{k_i}\}) \qquad \text{and} \qquad \mathrm{q}_b[j, l_j] := \pi(\{x_{l_j}, y_j\}),$$

  *along with new probability measures* $\mu_{X_b} := \sum \mathrm{p}_b[i, k_i]\delta_{(x_i,k_i)}$, $\mu_{Y_b} := \sum \mathrm{q}_b[j, l_j]\delta_{(y_j,l_j)}$.
- *New weight functions* $\omega_{X_b}$, $\omega_{Y_b}$*, represented by the following matrices*

$$\mathbf{X}_b[(i, k_i), (i', k_{i'})] := \mathbf{X}[i, i'] \qquad \text{and} \qquad \mathbf{Y}_b[(j, l_j), (j', l_{j'})] := \mathbf{Y}[j, j'].$$

*The new spaces* $\mathbb{X}_b = (X_b, \omega_{X_b}, \mu_{X_b})$ *and* $\mathbb{Y}_b = (Y_b, \omega_{Y_b}, \mu_{Y_b})$ *are called a* blow-up *of the original networks* $\mathbb{X} = (X, \omega_X, \mu_X)$ *and* $\mathbb{Y} = (Y, \omega_Y, \mu_Y)$.

Let $\mathbb{X}$ and $\mathbb{Y}$ be finite networks with $N$ and $M$ nodes, respectively, and $\mathbb{X}_b = (X_b, \omega_{X_b}, \mu_{X_b})$ and $\mathbb{Y}_b = (Y_b, \omega_{Y_b}, \mu_{Y_b})$, simply denoted by $(\mathbf{X}_b, \mathrm{p}_b)$ and $(\mathbf{Y}_b, \mathrm{q}_b)$, be as in Definition 4.2 with $\pi \in \Pi(\mathrm{p}, \mathrm{q})$ an $N \times M$ *optimal* coupling for $GW(\mathbb{X}, \mathbb{Y})$. Then, we have the following properties:

(1) $\mathbb{X}_b \sim^w \mathbb{X}$ and $\mathbb{Y}_b \sim^w \mathbb{Y}$. Thus, $GW(\mathbb{X}, \mathbb{Y}) = GW(\mathbb{X}_b, \mathbb{Y}_b)$.
(2) Same size: $|X_b| = |\mathrm{supp}(\pi)| = |Y_b|$. We denote this number by $M_b$.
(3) Alignment: One can construct a (possibly enlarged) optimal coupling $\pi_b \in \Pi(\mathrm{p}_b, \mathrm{q}_b)$ for $GW(\mathbb{X}_b, \mathbb{Y}_b)$ that induces an optimal GW-transport map $T : X_b \to Y_b$, which is a bijection[16], i.e., a permutation of the indices in $[M_b]$. As highlighted in [14], the crux of the blow-up construction relies on the observation that while $\mathbb{X}_b$ and $\mathbb{Y}_b$ maintain weak isomorphisms with $\mathbb{X}$ and $\mathbb{Y}$, respectively, the initial (optimal) transport plan $\pi$ between the original measures $\mu_X, \mu_Y$ supported on the original nodes $X, Y$ (represented the vectors $\mathrm{p}, \mathrm{q}$), lifts to a map $T$ between the new sets of nodes $X_b, Y_b$ such that $T_\# \mu_{X_b} = \mu_{Y_b}$:

$$\begin{array}{ccc} \mathbb{X} & \xrightarrow{\text{plan}} & \mathbb{Y} \\ {\scriptstyle\sim^w}\downarrow & & \downarrow{\scriptstyle\sim^w} \\ \mathbb{X}_b & \xrightarrow{\text{map}} & \mathbb{Y}_b \end{array}$$

For simplicity, after permuting and relabeling the nodes, if necessary, we will assume that $T$ is the identity map (i.e., we identify $X_b = Y_b$). Consequently, $\mathrm{p}_b = \mathrm{q}_b$, and $\pi_b$ can be regarded as the diagonal matrix with $\mathrm{q}_b$ as its diagonal entries, denoted as $\pi_b = \mathrm{diag}(\mathrm{q}_b)$. See Figure 5 for an illustration. Moreover,

$$GW^2(\mathbb{X}, \mathbb{Y}) = \sum_{j,k\in[M_b]} |\mathbf{X}_b[j, k] - \mathbf{Y}_b[j, k]|^2 \, \mathrm{q}_b[j]\mathrm{q}_b[k] = \mathrm{tr}_{\mathrm{q}_b}\left((\mathbf{X}_b - \mathbf{Y}_b)^T(\mathbf{X}_b - \mathbf{Y}_b)\right). \quad (30)$$

[15](we recall the notation $\omega_X(x_i, x_{i'}) = \mathbf{X}[i, i']$, $\omega_Y(y_j, y_{j'}) = \mathbf{Y}[j, j']$, $\mu_X = \sum_{i=1}^N \mathrm{p}[i]\delta_{x_i}$, $\mu_Y = \sum_{i=1}^M \mathrm{q}[j]\delta_{y_j}$)

[16]See [20] for existence of optimal GW maps in the context of mm-spaces under strong isomorphisms.

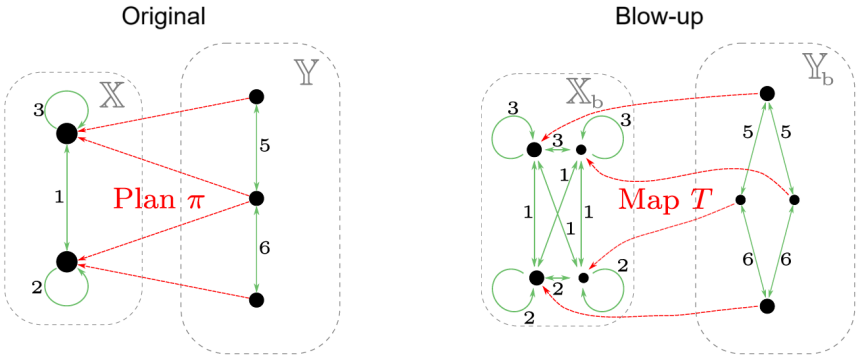



**Figure 5.** Blow-up illustration.

Expression (30) shows that, after blow-up, the GW distance becomes a Frobenius norm with weight depending on an optimal GW assignment between the pair of networks.

If we consider multiple templates $\{[\mathbb{X}^s]\}_{s=1}^S$ for $S \geq 1$, given a class $[\mathbb{Y}]$, Algorithm 3 is a *general blow-up*, which facilitates the alignment of each template representative $\mathbb{X}^s = (X^s, \omega_{X^s}, \mu_{X^s})$ with a representative $\mathbb{Y} = (Y, \omega_Y, \mu_Y)$, ensuring that the new spaces $Y_b = X_b^1 = \cdots = X_b^S$ all contain the same number of nodes ($M_b$), share the same mass distribution $\mathrm{q}_b$ across the nodes, and the identity map is optimal for each GW problem between $\mathbb{X}_b^s$ and $\mathbb{Y}_b$ ($s \in [S]$). Note that the optimal plans between $\mathbb{X}_b^s, \mathbb{X}_b^r$, for $s \neq r$, are not necessarily the identity. The network $\mathbb{Y}$ plays a special role in this algorithm, and thus when we apply it to templates $\{[\mathbb{X}^s]\}_{s=1}^S$, we say that we perform *an optimal blow-up with respect to* $\mathbb{Y}$.

**Proposition 4.3** (Prop. 8 [14] - Revisited proof in App. B.3)**.** *For a fixed family of classes of finite templates* $\{[\mathbb{X}^s]\}_{s=1}^S$ *and* $\lambda \in \Delta_{S-1}$*, consider the objective functional in* (4) *given by*

$$G_\lambda([\mathbb{Y}]) := \frac{1}{2} \sum_{s=1}^S \lambda_s GW^2(\mathbb{X}^s, \mathbb{Y}). \tag{31}$$

*Then* $\nabla G_\lambda([\mathbb{Y}])$ *can be identified, after an optimal blow-up of the templates with respect to* $\mathbb{Y}$*, with the square matrix* $\sum_{s=1}^S \lambda_s \mathbf{X}_b^s - \mathbf{Y}_b$.

4.3. **GW Barycenters via Blow-Up: The Synthesis Problem.** In the same spirit as Definition 3.1, we introduce the following general and weak forms of GW barycenters.

**Definition 4.4.** *Consider a collection of reference classes of finite networks* $\{[\mathbb{X}^s]\}_{s\in[S]}$*. The* GW barycenter space *generated by* $\{[\mathbb{X}^s]\}_{s\in[S]}$ *is defined by:*

$$\mathrm{Bary}(\{[\mathbb{X}^s]\}_{s=1}^S) := \{[\mathbb{Y}_\lambda] \mid \mathbb{Y}_\lambda \text{ is as in (4) for some } \lambda \in \Delta_{S-1}\}. \tag{32}$$

*The* weak GW barycenter space *generated by* $\{[\mathbb{X}^s]\}_{s\in[S]}$ *is defined by:*

$$\widetilde{\mathrm{Bary}}(\{[\mathbb{X}^s]\}_{s=1}^S) := \{[\mathbb{Y}_\lambda] \mid \nabla G_\lambda([\mathbb{Y}_\lambda]) = 0 \text{ for some } \lambda \in \Delta_{S-1}\}. \tag{33}$$

In (32) we consider all minimizers $[\mathbb{Y}_\lambda]$ of the general GW synthesis problem (4), with $\lambda \in \Delta_{S-1}$, that is, $[\mathbb{Y}_\lambda] \in \arg\min_{[\mathbb{Y}]} G_\lambda([\mathbb{Y}])$ (also referred to as *Fréchet means*). The number of nodes in the networks from the set (32), as well as the distribution of mass among them, is not predetermined in advance, unlike in the set $\mathrm{Bary}_{M,\mathrm{q}}(\{(\mathbf{X}^s, \mathrm{p}^s)\}_{s=1}^S)$ defined in (10). In contrast, the set given by (33) consists of the classes $[\mathbb{Y}_\lambda]$ that are critical points of the objective functional in the minimization problem (4), i.e., of the functional $G_\lambda$ defined in (31) for some $\lambda \in \Delta_{S-1}$ (also referred to as *Karcher means*).

**Algorithm 3** An Optimal Blow-Up of Multiple Templates With Respect to a Fixed Network

**Inputs:**
- Templates $\{(\mathbf{X}^s, \mathrm{p}^s) \in \mathbb{R}^{N^s \times N^s} \times \mathcal{P}_{N^s}\}_{s\in[S]}$
- Network $(\mathbf{Y}, \mathrm{q}) \in \mathbb{R}^{M\times M} \times \mathcal{P}_M$

**Output:**
- Blow-up size $M_b \in \mathbb{N}$
- Blow-up template matrices $\{\mathbf{X}_b^s\}_{s\in[S]}$ (all of size $M_b \times M_b$)
- Blow-up network $(\mathbf{Y}_b, \mathrm{q}_b) \in \mathbb{R}^{M_b\times M_b} \times \mathcal{P}_{M_b}$

**for** $s = 1, 2, \ldots, S$ **do**
  $\mathbf{X} \leftarrow \mathbf{X}^s$
  $\mathrm{p} \leftarrow \mathrm{p}^s$
  $\pi \leftarrow$ optimal plan for $GW((\mathbf{X}, \mathrm{p}), (\mathbf{Y}, \mathrm{q}))$
  $v_X, v_Y \leftarrow$ indices of non-null entries of $\pi$
  $M_b = \mathrm{len}(v_X)$
  Set $\mathrm{q}_b$ such that $\mathrm{q}_b[l] = \pi[v_X[l], v_Y[l]]$ for all $l \in [M_b]$
  $\mathrm{q} \leftarrow \mathrm{q}_b$
  Set $\mathbf{X}_b$ such that $\mathbf{X}_b[i, j] = \mathbf{X}[v_X[i], v_X[j]]$ for all $i, j \in [M_b]$
  Set $\mathbf{Y}_b$ such that $\mathbf{Y}_b[i, j] = \mathbf{Y}[v_Y[i], v_Y[j]]$ for all $i, j \in [M_b]$
  $\mathbf{X}_b^s \leftarrow \mathbf{X}_b$
  $\mathbf{Y} \leftarrow \mathbf{Y}_b$
  **for** $r = 1, 2, \ldots s-1$ **do**
    Set $\mathbf{X}_b$ such that $\mathbf{X}_b[i, j] = \mathbf{X}_b^r[v_Y[i], v_Y[j]]$ for all $i, j \in [M_b]$
    $\mathbf{X}_b^r \leftarrow \mathbf{X}_b$
  **end for**
**end for**
**return** $M_b$, $\mathbf{Y}_b, \mathrm{q}_b$, $\mathbf{X}_b^1, \ldots, \mathbf{X}_b^S$

**Lemma 4.5.** *In the space of finite networks, consider a collection of templates* $\{\mathbb{X}^s\}_{s\in[S]}$, *and another network* $\mathbb{Y}^*$. *Let* $\mathbb{X}_b^s = (\mathbf{X}_b^s, \mathrm{q}_b)$, *for* $s \in [S]$, *and* $\mathbb{Y}_b^* = (\mathbf{Y}_b^*, \mathrm{q}_b)$ *be an optimal blow-up of* $\{\mathbb{X}^s\}_{s\in[S]}$ *with respect to* $\mathbb{Y}^*$ *as in Algorithm 3.*

- *If* $[\mathbb{Y}^*] \in \widetilde{\mathrm{Bary}}(\{[\mathbb{X}^s]\}_{s=1}^S)$, *then* $\mathbb{Y}^* \sim^w \left(\sum_{s=1}^S \lambda_s \mathbf{X}_b^s, \mathrm{q}_b\right)$ *for some vector* $\lambda \in \Delta_{S-1}$.
- *If* $[\mathbb{Y}^*] \in \mathrm{Bary}(\{[\mathbb{X}^s]\}_{s=1}^S)$, *then* $\mathbb{Y}^* \sim^w \left(\sum_{s=1}^S \lambda_s \mathbf{X}_b^s, \mathrm{q}_b\right)$ *for some vector* $\lambda \in \Delta_{S-1}$.

*Proof.* If $[\mathbb{Y}^*] \in \widetilde{\mathrm{Bary}}(\{[\mathbb{X}^s]\}_{s=1}^S)$, then, using Proposition 4.3, we have $0 = \nabla G_\lambda[\mathbb{Y}^*] = \sum_{s=1}^S \lambda_s \mathbf{X}_b^s - \mathbf{Y}_b^*$. Thus, $\mathbb{Y}^* \sim^w (\mathbf{Y}_b^*, \mathrm{q}_b) = \left(\sum_{s=1}^S \lambda_s \mathbf{X}_b^s, \mathrm{q}_b\right)$, for some vector $\lambda \in \Delta_{S-1}$.

If $[\mathbb{Y}^*] \in \mathrm{Bary}(\{[\mathbb{X}^s]\}_{s=1}^S)$ then, due to the first-order optimality condition (see Remark B.10 in App. B.3), $[\mathbb{Y}^*] \in \widetilde{\mathrm{Bary}}(\{[\mathbb{X}^s]\}_{s=1}^S)$. Hence, $\mathbb{Y}^* \sim^w \left(\sum_{s=1}^S \lambda_s \mathbf{X}_b^s, \mathrm{q}_b\right)$. □

In App. B.3, we provide a direct proof of the last bullet point in Lemma 4.5 that does not rely on the first-order optimality condition, but instead builds on the fixed-point approach following the ideas of the proof of Theorem 3.3.

In Lemma 4.5, the blow-up technique can be interpreted as a *'change of coordinates'*, in which all nodes are re-aligned, relabeled, or reordered with respect to those of a GW barycenter $\mathbb{Y}^*$. Once this alignment is established, the new templates (which are weakly isomorphic to the original ones) have the same number of nodes and share a common mass distribution $\mathbf{q}_b$. The GW barycenter formula (for the weight matrix) will then take

the form $\sum_{s=1}^{S} \lambda_s \mathbf{X}_b^s$, which resembles an Euclidean barycenter[17]. This may indicate that the GW framework corresponds to the Euclidean geometry on the space of real square matrices of fixed size $(M_b \times M_b)$. However, there are many caveats. Appropriate mass must be distributed at the nodes of the network $\left(\sum_{s=1}^{S} \lambda_s \mathbf{X}_b^s, \mathrm{q}_b\right)$, namely the probability vector $\mathbf{q}_b$, which does not only depend on the templates but also on $\mathbb{Y}^*$. Also, the order or labels of the coordinates of $\sum_{s=1}^{S} \lambda_s \mathbf{X}_b^s$ depend on the blow-up template matrices $\{\mathbf{X}_b^s\}_{s\in[S]}$, which, in turn, are determined by optimal GW assignments with respect to $\mathbb{Y}^*$. Moreover, if a new vector $\lambda \in \Delta_{S-1}$ is chosen, the formula of the barycenter does no longer apply and new blow-ups of the templates must be taken respect to a new $\mathbb{Y}^*$. For further discussion, see Remark B.13 in App. B.3. We also refer the reader to App. E for an additional discussion on the parallels and differences between Wasserstein and GW barycenters, as well as the methods used to compute them.

4.4. **GW Barycenters via Blow-Up: The Analysis Problem.** As in Theorem 3.6, where we used the characterization of elements in $\mathrm{Bary}_{M,\mathrm{q}}(\{(\mathbf{X}^s, \mathrm{p}^s)\}_{s\in[S]})$ given by Theorem 3.3 to derive a method that exactly recovers the barycentric coordinates $\lambda$–leading to Algorithm 2 which also applies beyond strict barycenter inputs–we now use 4.6 to derive a method that exactly recovers the barycentric coordinates $\lambda$ for elements in $\widetilde{\mathrm{Bary}}(\{[\mathbb{X}^s]\}_{s\in[S]})$, and which likewise extends beyond exact barycenter inputs, giving rise to a subsequent procedure described in Algorithm 4.

**Proposition 4.6.** *Let $\{\mathbb{X}^s\}_{s=1}^S$ be finite templates and let $\lambda \in \Delta_{S-1}$. Let $\mathbb{Y}$ be a finite network class. Consider the blow-up matrices $\mathbf{X}_b^1, \ldots, \mathbf{X}_b^S$ and network $(\mathbf{Y}_b, \mathrm{q}_b)$ obtained with Algorithm 3. Then, $\|\nabla G_\lambda([\mathbb{Y}])\|^2_{\mathrm{Tan}_{[\mathbb{Y}]}} = \lambda^T \mathcal{A} \lambda$, where*

$$\mathcal{A}_{sr} := \mathrm{tr}_{\mathrm{q}_b}\left((\mathbf{X}_b^s - \mathbf{Y}_b)^T (\mathbf{X}_b^r - \mathbf{Y}_b)\right), \qquad \forall s, r \in [S]. \tag{34}$$

*Proof.* This proof is inspired by analysis in [68], and a consequence of Proposition 4.3. Since the networks involved in the statement have finitely many nodes, we can use (26) to express the inner product in the tangent space $\mathrm{Tan}_{[\mathbb{Y}]}$ as a weighted trace of matrices. Indeed, after blow-up all the matrices have the same size $M_b \times M_b$. Hence, we can consider the variant of Frobenius norm in the space of $M_b \times M_b$ square matrices weighted by $\mathrm{q}_b \otimes \mathrm{q}_b$:

$$\begin{aligned}
\|\nabla G_\lambda([\mathbb{Y}])\|^2_{\mathrm{Tan}_{[\mathbb{Y}]}} &= \mathrm{tr}_{\mathrm{q}_b}\left(\left(\sum_{s=1}^{S} \lambda_s \mathbf{X}_b^s - \mathbf{Y}_b\right)^T \left(\sum_{r=1}^{S} \lambda_r \mathbf{X}_b^r - \mathbf{Y}_b\right)\right) \\
&= \sum_{s,r=1}^{S} \lambda_s \lambda_r \underbrace{\mathrm{tr}_{\mathrm{q}_b}\left((\mathbf{X}_b^s - \mathbf{Y}_b)^T (\mathbf{X}_b^r - \mathbf{Y}_b)\right)}_{\mathcal{A}_{sr}} \\
&= \lambda^T \mathcal{A} \lambda.
\end{aligned}$$

□

**Theorem 4.7.** *Let $\{[\mathbb{X}^s]\}_{s\in[S]}$ be classes of finite networks. Given a finite class $[\mathbb{Y}]$, consider a blow-up $(\mathbf{Y}_b, \mathrm{q}_b)$, $\mathbf{X}_b^1, \ldots, \mathbf{X}_b^S$ as in Algorithm 3, and let $\mathcal{A}$ be the $S \times S$ matrix given by the expression (34) in 4.6. Then $[\mathbb{Y}] \in \widetilde{\mathrm{Bary}}(\{[\mathbb{X}^s]\}_{s\in[S]})$ if and only if*

$$\min_{\lambda \in \Delta_{S-1}} \lambda^T \mathcal{A} \lambda = 0, \tag{35}$$

*and the solution argument $\lambda_{\mathbb{Y}} \in \Delta_{S-1}$ is the corresponding weight vector to $[\mathbb{Y}]$ as a weak GW barycenter in the space given in (33). Equivalently, $\lambda_{\mathbb{Y}}$ solves the linear problem*

$$L\,\lambda = c \qquad \text{subject to } \lambda \in \Delta_{S-1} \subset \mathbb{R}^S, \tag{36}$$

[17](see (43) in App. A)

**Algorithm 4** Analysis: GW Barycenter Coordinates via Blow-up

**Inputs:**
- Templates $\{(\mathbf{X}^s, \mathrm{p}^s)_{s\in[S]}\}$
- Shape/Network: $\mathbf{Y} \in \mathbb{R}^{M\times M}$, $\mathrm{q} \in \mathcal{P}_M$

**Output:** Weight vector $\lambda$

$\mathbf{Y}_b, \mathrm{q}_b, \mathbf{X}_b^1, \dots, \mathbf{X}_b^S \leftarrow$ compute Blow-ups (i.e., apply Algorithm 3)
**for** $s = 1, 2, \dots, S$ **do**
  **for** $r = s, s+1, \dots, S$ **do**
    $\mathcal{A}_{sr} = \mathrm{tr}_{\mathrm{q}_b}\left((\mathbf{X}_b^s - \mathbf{Y}_b)^T(\mathbf{X}_b^r - \mathbf{Y}_b)\right)$
    $\mathcal{A}_{rs} = \mathcal{A}_{sr}$
  **end for**
**end for**
$\lambda \leftarrow \arg\min_{\lambda\in\Delta_{S-1}} \lambda^T\mathcal{A}\lambda$
**return** $\lambda$

*where* $L \in \mathbb{R}^{S\times S}$ *and* $c \in \mathbb{R}^S$ *are given by*

$$L_{sr} := \mathrm{tr}_{\mathrm{q}_b}\left((\mathbf{X}_b^s)^T\,\mathbf{X}_b^r\right) \quad \forall s, r \in [S], \qquad c_s := \mathrm{tr}_{\mathrm{q}_b}\left(\mathbf{Y}_b^T\,\mathbf{X}_b^s\right) \quad \forall s \in [S]. \tag{37}$$

*Proof.* First, let us prove that (35) defines a convex quadratic program. On the one hand, the set of restrictions $\Delta_{S-1}$ is a convex set. On the other hand, $\mathcal{A}$ is a symmetric positive semidefinite $S \times S$ matrix because it is the Gram matrix of the system of matrices $\{\mathbf{X}_b^s - \mathbf{Y}_b\}_{s=1}^S$ with respect to the inner product in $L^2(Y_b \times Y_b, \mu_{Y_b} \otimes \mu_{Y_b})$ (i.e., $(A, B) \mapsto \mathrm{tr}_{\mathrm{q}_b}(A^T B)$ for all $A, B \in \mathbb{R}^{M_b\times M_b}$) [53].

By definition, $[\mathbb{Y}] \in \widetilde{\mathrm{Bary}}(\{(\mathbf{X}^s)\}_{s=1}^S)$ if and only if $\nabla G_\lambda([\mathbb{Y}]) = 0$ for some $\lambda \in \Delta_{S-1}$. A vector is the zero vector if and only if its norm is zero, and $\|\nabla G_\lambda([\mathbb{Y}])\|_{\mathrm{Tan}_{[\mathbb{Y}]}} = 0$ for some $\lambda \in \Delta_{S-1}$ if and only if the problem (35) has a solution $\lambda \in \Delta_{S-1}$ (by 4.6).

Finally, we proceed as in the proof of Theorem 3.6. We have just proven that $\lambda \mapsto \lambda^T\mathcal{A}\lambda$ is non-negative and convex as a function over the whole $\mathbb{R}^S$. Therefore, its critical points ($\lambda \in \mathbb{R}^S$ such that $\mathcal{A}\lambda = 0$) are global minima. Moreover, we can express:

$$\lambda^T\mathcal{A}\lambda = \mathrm{tr}_{\mathrm{q}_b}\left(\mathbf{Y}_b^T\mathbf{Y}_b\right) - 2\sum_{s\in[S]}\lambda_s c_s + \sum_{s\in[S]}\sum_{r\in[S]}\lambda_s\lambda_r L_{sr},$$

where the matrix $L$ and the vector $c$ are given by (37). As a conclusion, the critical points can be expressed as the solutions $\lambda \in \mathbb{R}^S$ of the linear system $L\lambda = c$. These solutions might not be unique but under the GW-BCM condition (i.e., assuming $[\mathbb{Y}] \in \widetilde{\mathrm{Bary}}(\{[\mathbb{X}^s]\}_{s=1}^S)$) there exists at least one solution $\lambda_{\mathbb{Y}}$ in $\Delta_{S-1}$. That is, the solutions of (35) are given by (36). □

As a direct corollary, under the same hypothesis as Theorem 4.7, if $[\mathbb{Y}] \in \mathrm{Bary}(\{[\mathbb{X}^s]\}_{s\in[S]})$ *then* (35) is satisfied, and the solution argument $\lambda_{\mathbb{Y}}$ is its corresponding weight vector.

Algorithm 4 implements the analysis scheme laid out in Theorem 4.7, and we refer the reader to App. C for a discussion on its computational complexity.

4.5. **Relationship Between Fixed-Point and Gradient Approaches.** In this section, we relate the two strategies considered for addressing the GW synthesis and analysis problems: the fixed-point approach, which arises from interpreting the GW barycenters as fixed points of an iteration scheme (Sections 3.1 and 3.2), and the gradient-based approach, where we define weak GW barycenters as Karcher means (Sections 4.3 and 4.4).

Let $(\mathbf{X}^s, \mathrm{p}^s)$, for $s \in [S]$, and $(\mathbf{Y}, \mathrm{q})$ be representatives of the classes $\{[\mathbb{X}^s]\}_{s\in[S]}$ (templates) and $[\mathbb{Y}]$ (input shape) in $\mathcal{GM}$. Let us preprocess them obtaining $(\mathbf{X}_b^s, \mathrm{q}_b)$, $s \in [S]$,

and $(\mathbf{Y}_b, \mathrm{q}_b)$ in $\mathbb{R}^{M_b \times M_b} \times \mathcal{P}_{M_b}$, using the blow-up Algorithm 3. Consider GW OT plans $\pi_b^s = \mathrm{diag}(\mathrm{q}_b)$ for each problem $GW((\mathbf{X}_b^s, \mathrm{q}_b), (\mathbf{Y}_b, \mathrm{q}_b))$, with $s \in [S]$. Finally, in the approach outlined in Section 3, consider $M_b$ and $\mathrm{q}_b$ in place of $M$ and q. We observe that expression (13) becomes:

$$\frac{1}{\mathrm{q}_b(\mathrm{q}_b)^T} \odot \sum_{s\in[S]} \lambda_s (\pi_b^s)^T \mathbf{X}_b^s \pi_b^s = \frac{1}{\mathrm{q}_b(\mathrm{q}_b)^T} \odot \sum_{s\in[S]} \lambda_s \mathrm{diag}(\mathrm{q}_b) \mathbf{X}_b^s \mathrm{diag}(\mathrm{q}_b) = \sum_{s\in[S]} \lambda_s \mathbf{X}_b^s. \quad (38)$$

In other words, under the respective GW-BCM frameworks, the expression (13) from the fixed-point approach coincides with the expression in Lemma 4.5 satisfied by critical points $\nabla G_\lambda([\mathbb{X}]) = 0$ or minimizers of (4).

Moreover, when formulating the analysis problem (16) (or, equivalently, (19) under the GW-BCM assumption), we have the flexibility to consider any divergence. Therefore, if instead of considering the classical Frobenius norm $d_a(A, B) = \|A - B\|_{\mathrm{Frob}}$ in Theorem 3.6, we had used the variant of the Frobenius norm with weight $\mathrm{q}_b \otimes \mathrm{q}_b$, we would have obtained that the convex quadratic problems (21) and (35) coincide, as $\mathcal{Q} = \mathcal{A}$ (to compare their expressions given in (21) and (34), using that, from (38), one has $F(\mathbf{Y}_b, s) = \mathbf{X}_b^s$). Indeed, as functions from $\mathbb{R}^S$ to $[0, \infty)$, we would have $\Theta(\lambda) = \|G_\lambda([\mathbb{X}])\|^2_{\mathrm{Tan}_{[\mathbb{X}]}}$ (compare (20) and 4.6). In particular, the linear optimization problems (22) and (36) would coincide; that is, $K = L$ and $b = c$, as defined in (23) and (37). If one tries to reformulate problem (19) to coincide exactly with Section 4.4, one needs to compute $\mathrm{q}_b$ in advance. This involves solving one GW problem per template (as part of the blow-up procedure). The blow-up distribution $\mathrm{q}_b$ depends on $(\mathbf{Y}, \mathrm{q})$ but but generally differs from q.

## 5. Experimental Results

In this section, we experimentally assess the performance of our algorithms for solving the GW analysis problem. We also present applications to classification. Additional use cases involving point cloud corruptions are provided in App. D.4.

### 5.1. Reconstruction Performance of Algorithms 2 and 4 Under the GW-BCM.

In this section, we demonstrate the performance of the proposed GW analysis algorithms by applying them to 3D point cloud data: Figures 6 and 7 illustrate the application of Algorithms 2 and 4 on the ModelNet40 - Princeton 3D Object Dataset [70] consisting of 3D CAD models of 40 common object categories such as chairs, tables, airplanes, lamps, and more. In App. D.1 we provide additional 2D examples (Figures 15 and 16).

From the object category 'airplane' we select $S = 3$ templates and sample them to generate 3D point clouds with (varying) numbers of points $N^s$, $s = 1, 2, 3$ (see Figure 11 in App. D). We compute the associated $N^s \times N^s$ pairwise Euclidean distance matrices $\mathbf{X}^s$ within each point cloud ($s = 1, 2, 3$). We assign to each point uniform mass, that is, $\mathrm{p}^s = \frac{1}{N^s}(1, \ldots, 1) \in \mathbb{R}^{N^s}$, for $s = 1, 2, 3$. We consider either the uniform vector $\lambda = (\frac{1}{3}, \frac{1}{3}, \frac{1}{3}) \in \Delta_2$ or a random vector $\lambda \in \Delta_2$ drawn from a Dirichlet distribution with uniform parameters $\alpha = (1, 1, 1)$, which corresponds to the uniform distribution over the 2-simplex. For such a $\lambda$ and the selected templates, we synthesize a GW barycenter $M \times M$ matrix $\mathbf{Y}$ by using the function `ot.gromov.gromov_barycenters` from the POT Library [21] with a predetermined size $M$ and uniform probability $\mathrm{q} = \frac{1}{M}(1, \ldots, 1) \in \mathbb{R}^M$, which is based on a fixed-point algorithm in the spirit of Algorithm 1. Then, we apply Algorithm 2 or Algorithm 4 to the synthetic GW barycenter, q, and the templates $\{(\mathbf{X}^1, \mathrm{p}^1), (\mathbf{X}^2, \mathrm{p}^2), (\mathbf{X}^3, \mathrm{p}^3)\}$ to get the estimate $\widetilde{\lambda} \approx \lambda$.

In Figure 6 we consider $\lambda = (\frac{1}{3}, \frac{1}{3}, \frac{1}{3})$, and after estimation, we reconstruct the shape as:

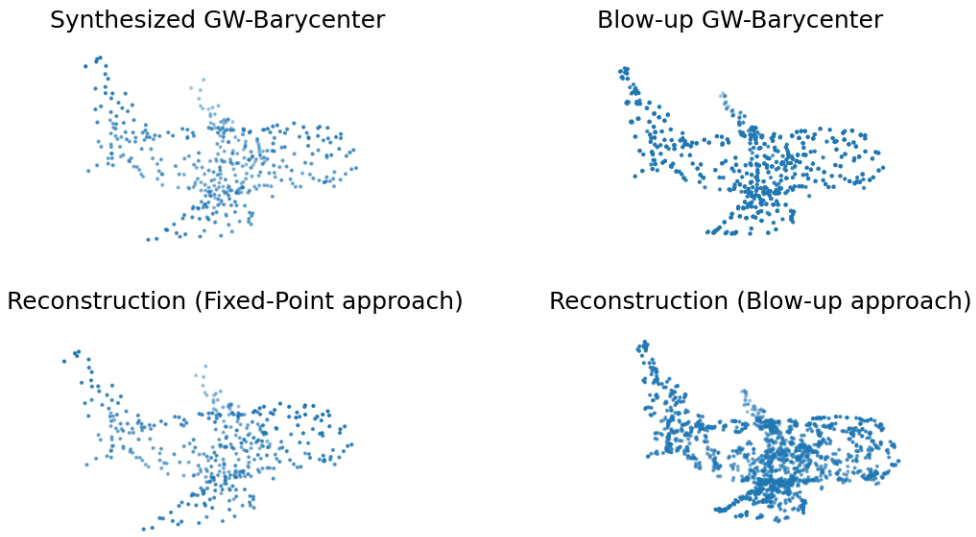



**Figure 6.** Reconstructions of synthetic GW barycenter. **Top Left:** MDS of synthetic GW barycenter with 3 templates and $\lambda = (\frac{1}{3}, \frac{1}{3}, \frac{1}{3})$, computed via `ot.gromov.gromov_barycenters` (POT Library) with $M = 400$ points and uniform mass q. **Bottom Left:** MDS of the matrix given by (39) after applying Algorithm 2 to estimate $\widetilde{\lambda} \approx \lambda$ (error of order $10^{-14}$). GW distance between shapes in top and bottom left panels: $GW((\mathbf{Y}, \mathrm{q}), (\mathbf{Y}_{\mathrm{bary}}, \mathrm{q})) \approx 10^{-16}$. **Top Right:** MDS of the synthetic GW barycenter after blow-up (i.e., using Algorithm 3 with synthesized GW barycenter (top left) and templates). GW distance between the two shapes in the top panel: $GW((\mathbf{Y}, \mathrm{q}), (\mathbf{Y}_b, \mathrm{q}_b)) \approx 10^{-16}$. **Bottom Right:** MDS of the matrix given by (40) after applying Algorithm 4 to estimate $\widetilde{\lambda} \approx \lambda$ (error of order $10^{-3}$). GW distance between shapes in top left and bottom right panels: $GW((\mathbf{Y}, \mathrm{q}), (\mathbf{Y}_{\mathrm{barybu}}, \mathrm{q}_b)) \approx 10^{-5}$.

- If we use Algorithm 2 for recovering the vector $\widetilde{\lambda} = (\widetilde{\lambda}_1, \widetilde{\lambda}_2, \widetilde{\lambda}_3)$, we compute the matrix

$$\mathbf{Y}_{\mathrm{bary}} := \frac{1}{\mathrm{q}\mathrm{q}^T} \odot \sum_{s=1}^{S} \widetilde{\lambda}_s (\pi(\mathbf{Y}, s))^T \mathbf{X}^s \pi(\mathbf{Y}, s) \in \mathbb{R}^{M \times M}, \tag{39}$$

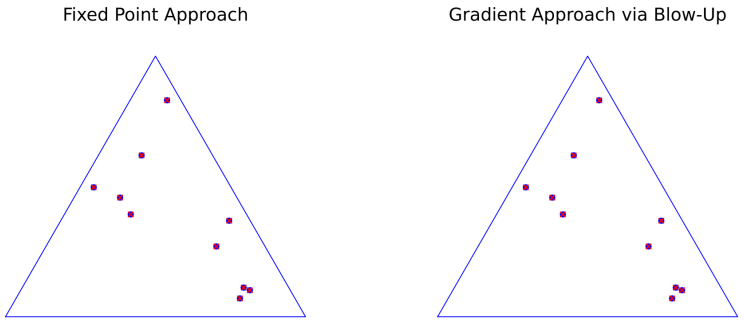
  where, for each $s \in [S]$, $\pi(\mathbf{Y}, s)$ is an optimal coupling for $GW((\mathbf{Y}, \mathrm{q}), (\mathbf{X}^s, \mathrm{p}^s))$ computed using the function `ot.gromov.gromov_wasserstein` from the POT Library.
- If we use Algorithm 4 for recovering a vector $\widetilde{\lambda} = (\widetilde{\lambda}_1, \widetilde{\lambda}_2, \widetilde{\lambda}_3)$, we compute the matrix

$$\mathbf{Y}_{\mathrm{barybu}} := \sum_{s=1}^{S} \widetilde{\lambda}_s \mathbf{X}_b^s \in \mathbb{R}^{M_b \times M_b}, \tag{40}$$

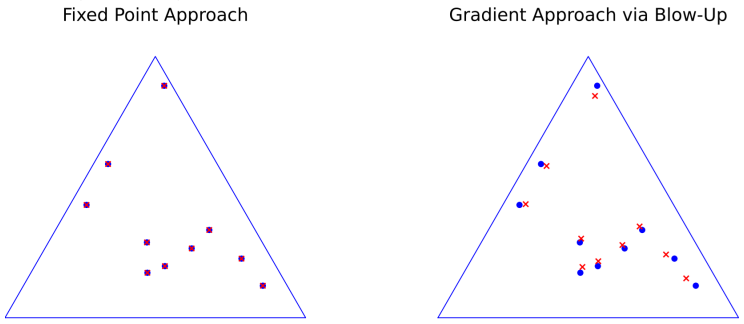
  where $\{\mathbf{X}_b^s\}_{s=1}^S$ are the blow-up matrices obtained after preprocessing via Algorithm 3 applied to the original templates with respect to $(\mathbf{Y}, \mathrm{q})$, and where $\mathrm{q}_b \in \mathcal{P}_{M_b}$ is also derived.

For visualization, we apply the classical multidimesional scaling embedding (MDS) [37] with 3 components to the synthetic GW barycenter matrix $\mathbf{Y}$ and the recovered matrices $\mathbf{Y}_{\mathrm{bary}}$ and $\mathbf{Y}_{\mathrm{barybu}}$ given by the two approaches (39) and (40), respectively. For assessing the reconstruction accuracy, we use the function `ot.gromov.gromov_wasserstein` from the POT Library to compute $GW((\mathbf{Y}, \mathrm{q}), (\mathbf{Y}_{\mathrm{bary}}, \mathrm{q}))$ and $GW((\mathbf{Y}, \mathrm{q}), (\mathbf{Y}_{\mathrm{barybu}}, \mathrm{q}_b))$.

In Figure 7 we estimate GW barycentric coordinates $\widetilde{\lambda} \approx \lambda$ for synthetic GW barycenters built with randomly generated $\lambda$. The only difference between Figures 7a and 7b is that, in the former, the point cloud templates are uniformly sampled, whereas in the latter, the sampling rates vary across templates. Additional visualizations are Figures 12, 13, 14.




**(a)** We use 3 templates, each *uniformly sampled* at 150 points. GW barycenters with $M = 150$ points were synthesized using `ot.gromov.gromov_barycenters` from the POT Library.




**(b)** We use the 3 templates, *sampled at varying rates* ranging from 50 to 150 points. GW barycenters with $M = 100$ points were synthesized using `ot.gromov.gromov_barycenters` from the POT Library.

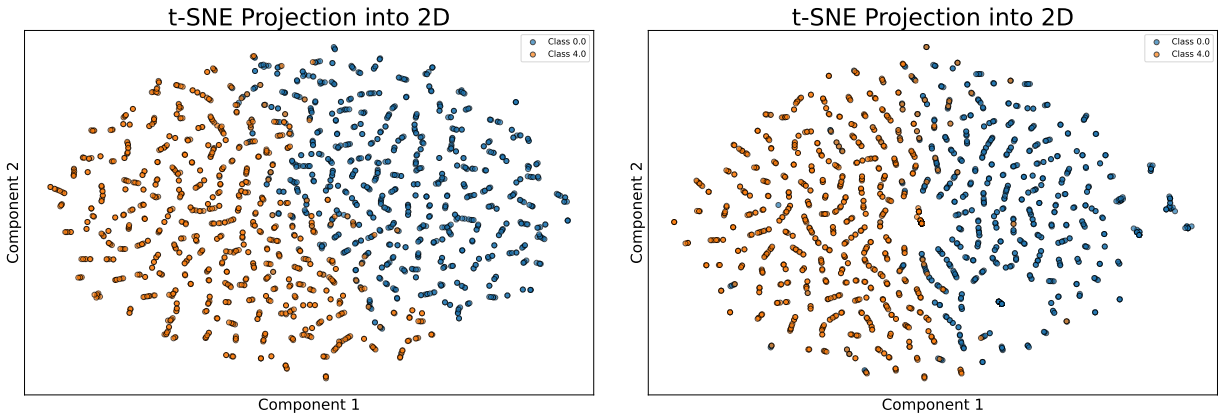
**Figure 7.** Depiction of 10 different randomly generated $\lambda \in \Delta_2$ (blue dots) and their estimation (red crosses) from synthesized GW barycenters using Algorithm 2 (left) and Algorithm 4 (right). Each $\lambda$ is represented as a convex combination of the vertices of an equilateral triangle.

5.2. **Classification.** Consider the task of identifying a sample's class label using small number of labeled objects (templates) from the dataset. 3 provides a visualization of how GW barycentric coordinates capture meaningful structure in the data: they separate (or cluster) the digit classes 0 and 1 in the Point Cloud MNIST 2D dataset [23]. The slight observed overlap suggests the presence of shared geometric features among certain point clouds from the two classes. For classification, after estimating the GW barycentric coordinates $\lambda$ of each sample, the predicted label can be assigned by selecting the index corresponding to the highest coordinate in the vector $\lambda$. Additional visualization is in Figure 21.

We now present a similar technique using t-SNE. Additional methods are given in App. D.3, all leveraging GW barycentric coordinates via Algorithms 2 and 4.

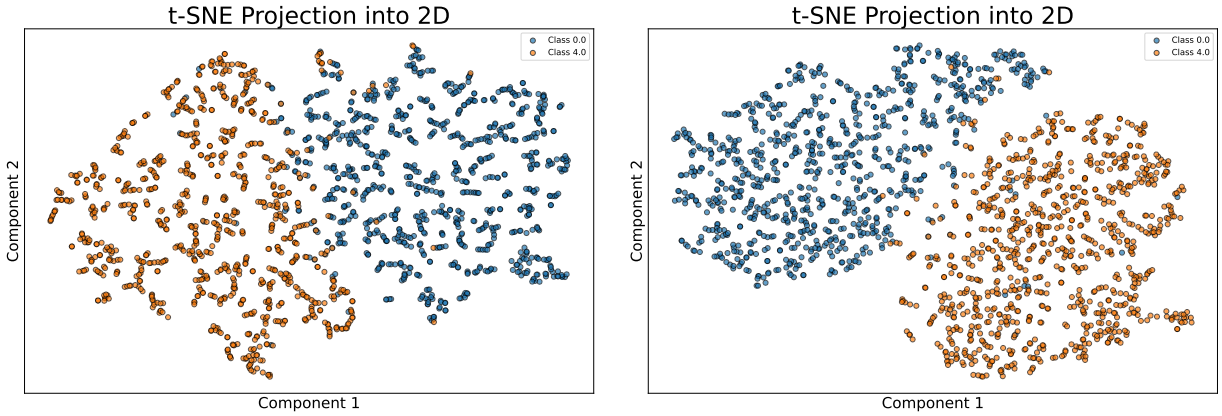
5.2.1. *t-SNE in the GW Barycentric Coordinate Space – Experimental Setup.* Assume there are $C$ classes in a dataset, and consider $k$ reference objects from each class.

(1) Randomly select templates from each class of the dataset ($k$ samples per class).
(2) For each sample in the dataset, compute GW barycentric coordinates with respect to the selected templates by applying either Algorithm 2 or Algorithm 4. Each sample is thus represented by a coordinate vector $\lambda \in \mathbb{R}^S$, where $S = k \times C$.
(3) Apply t-SNE (t-distributed Stochastic Neighbor Embedding) as a dimensionality reduction from $\mathbb{R}^S$ to $\mathbb{R}^2$, and visualize the result, coloring points by class label.
(4) Perform clustering using using K-Means (with $C$ number of classes) in the embedded space provided by t-SNE. Compute accuracy by comparing the predicted labels from clustering with the true labels. To assess whether the clustering correctly groups similar digits and to highlight common misclassification patterns, compute the *confusion matrix*.




**(a)** Fixed-point approach. **(b)** Blow-up approach.

**Figure 8.** t-SNE of estimated $\lambda$ coordinates. One-shot clustering accuracy (K-Means): 0.9, achieved using a single template per class for both (A) Algorithm 2 and (B) Algorithm 4.




**(a)** Three templates per class. **(b)** Six templates per class.

**Figure 9.** t-SNE of estimated $\lambda$ coordinates via Algorithm 2. Multiple templates per class: (A) 3, (B) 6. Clustering accuracy (K-Means): (A) 0.95, (B) 0.98.

As a proof-of-concept, we apply this methodology to the Point Cloud MNIST 2D dataset [23], considering $C = 2$ classes (digits 0 and 4) and $k = 1, 3, 6$ template objects from each class. Figures 8 and 9 show the resulting t-SNE embeddings in two dimensions (for 1800 random samples), while the associated K-Means clustering and confusion matrices are provided in App. D (Figures 17, 18, 19, and 20). Algorithms 2 and 4 perform comparably; however, Algorithm 4 is slower due to the preprocessing step (Algorithm 3) required to align samples with the templates. As more templates per class are included, the separation between classes in the t-SNE embedding becomes more pronounced.

## 6. Conclusions

This paper addresses the problem of recovering barycentric coordinates in the context of finite metric spaces, or more generally, networks with weighted dissimilarities between nodes, embedded via the Gromov–Wasserstein (GW) distance, referred to as the *GW analysis problem*. While the literature offers at least two established methods for computing GW barycenters, this work builds upon them and proposes two corresponding solutions to the GW analysis problem, each with its own algorithm. Moreover, we show that these two perspectives are not entirely independent: under suitable parameter choices, they share common ground. Notably, both proposed solutions correspond to critical points of

convex functions (Theorems 3.6 and 4.7). Finally, we introduce strategies for estimating barycentric coordinates that may remain useful even when the target object is not an exact GW barycenter.

This paper focuses on the case of discrete metric measure spaces (or discrete networks), although the GW framework also applies in the continuum setting. Extending our fixed-point and gradient-based approaches to a broader context is of interest. In addition, this paper does not establish a full equivalence between Karcher means and GW barycenters. In the case of classical OT, such an equivalence can be shown under certain assumptions [68]. Developing analogous conditions in the GW setting remains an open direction for future research.

## Acknowledgments

RDM and JMM were partially supported by DMS-2318894. JMM was partially supported by DMS-2309519. IVM was funded by NIH award GM130825 and ONR award N000142212505.

## Appendix A. Background: The Barycentric Coding Model (BCM)

Suppose B is a convex set in a vector space having finitely many *extreme points* $\mathbf{x}^1, \dots, \mathbf{x}^S$, for some $S \in \mathbb{N}$. That is, B is the *convex hull* of $\{\mathbf{x}^1, \dots, \mathbf{x}^S\}$: every point $\mathbf{x} \in \mathrm{B}$ can be expressed as

$$\mathbf{x} = \sum_{s\in[S]} \lambda_s \mathbf{x}^s, \qquad \text{for some } \lambda = (\lambda_1, \dots, \lambda_S) \in \Delta_{S-1}. \tag{41}$$

Reciprocally, since we are assuming that B is convex, we have that every convex combination of the points $\mathbf{x}^1, \dots, \mathbf{x}^S$ belongs to B. Hence, we have a correlation between points in B and its *barycentric coordinates* in $\Delta_{S-1}$ given by the relation (41): $\mathrm{B} \ni \mathbf{x} \longleftrightarrow \lambda \in \Delta_{S-1}$. Thus, given a vector of weights $\lambda \in \Delta_{S-1}$, one can *synthesize* a point in B by:

$$\Delta_{S-1} \ni \lambda \longmapsto \mathbf{x}_\lambda := \sum_{s\in[S]} \lambda_s \mathbf{x}^s \in \mathrm{B}. \tag{42}$$

In Euclidean spaces, (42) coincides with solving the barycenter problem

$$\Delta_{S-1} \ni \lambda \longmapsto \mathbf{x}_\lambda = \operatorname*{arg\,min}_{\mathbf{x}\in\mathbb{R}^n} \sum_{s\in[S]} \lambda_s \|\mathbf{x}^s - \mathbf{x}\|^2 \in \mathrm{B}. \tag{43}$$

On the other hand, one can *analyze* an element $\mathbf{x} \in \mathrm{B}$, by decomposing it into the set $\{\mathbf{x^1}, \dots, \mathbf{x^S}\}$ in terms of its *barycentric coordinates*. For example, if $\mathrm{B} \subset \mathbb{R}^n$, this corresponds to solving the following optimization problem:

$$\mathbf{x} \longmapsto \lambda_{\mathbf{x}} := \operatorname*{arg\,min}_{\lambda\in\Delta_{S-1}} \|\mathbf{x} - \sum_{s\in[S]} \lambda_s \mathbf{x}^s\|^2. \tag{44}$$

Moreover, one can extend (44) by considering $\mathbf{x} \in \mathbb{R}^n$ instead of restricting to $\mathbf{x} \in \mathrm{B}$. This amounts to projecting $\mathbf{x}$ onto B and retaining only the coordinates $\lambda_{\mathbf{x}}$ of the projected point[18]; consequently, the orthogonal projection of $\mathbf{x} \in \mathbb{R}^n$ onto the closed convex set B is given by $\sum_{s\in[S]} (\lambda_{\mathbf{x}})_s \mathbf{x}^s$ [60]. Moreover, problem (44) can be rewritten as

$$\mathbf{x} \longmapsto \lambda_{\mathbf{x}} := \operatorname*{arg\,min}_{\lambda\in\Delta_{S-1}} \|\mathbf{x} - \mathbf{x}_\lambda\|^2, \tag{45}$$

[18]Let $\Phi : \mathbb{R}^S \to \mathbb{R}^n$ be the matrix whose columns are the vectors $\mathbf{x}^1, \dots, \mathbf{x}^S$, and consider the quadratic function $f(\lambda) := \|\mathbf{x} - \sum_{s\in[S]} \lambda_s \mathbf{x}^s\|^2 = \|\mathbf{x} - \Phi\lambda\|^2$ for all $\lambda \in \Delta_{S-1}$. Since $f$ is continuous and the simplex is compact, a minimizer $\lambda_{\mathbf{x}}$ for problem (44) exists. Define $\mathbf{z} := \Phi\lambda_{\mathbf{x}} \in \mathrm{B}$. By construction and since $\mathrm{B} = \Phi(\Delta_{S-1})$, we have $\|\mathbf{x} - \mathbf{z}\| = \min_{\lambda\in\Delta_{S-1}} \|\mathbf{x} - \Phi\lambda\| = \min_{\mathbf{y}\in\mathrm{B}} \|\mathbf{x} - \mathbf{y}\|$. Thus, by convex analysis, this last property characterizes $\mathbf{z}$ as the unique orthogonal projection of $\mathbf{x}$ onto B (even if $\lambda_{\mathbf{x}}$ is not unique).

where $\mathbf{x}_\lambda$ is a synthesized element as in (42) or (43).

With more generality, let us consider an ambient space G that is not necessarily convex, nor contained in a vector space, but endowed with a metric $dist(\cdot,\cdot)$. Consider also a *divergence* $d_a(\cdot,\cdot)$, that is, a non-negative function defined on $\mathrm{G}\times\mathrm{G}$ satisfying the identity of indiscernibles (i.e., $d_a(\mathbf{x},\mathbf{y})=0$ if and only if $\mathbf{x}=\mathbf{y}$), but not necessarily symmetric and/or not necessarily satisfying the triangle inequality (for readability, it can be assumed $d_a(\cdot,\cdot)=dist(\cdot,\cdot)$). Given finitely many template points $\mathbf{x}^1,\dots,\mathbf{x}^S\in\mathrm{G}$, for some $S\in\mathbb{N}$, we can formulate the following *synthesis* and *analysis* problems, borrowing terminology from harmonic analysis. The *barycenter synthesis problem* is

$$\Delta_{S-1}\ni\lambda\longmapsto\mathbf{x}_\lambda\in\operatorname*{arg\,min}_{\mathbf{x}\in\mathrm{G}}\sum_{s\in[S]}\lambda_s\,dist^2(\mathbf{x}^s,\mathbf{x}). \tag{46}$$

The *barycenter analysis problem* is

$$\mathrm{G}\ni\mathbf{x}\longmapsto\lambda_{\mathbf{x}}\in\operatorname*{arg\,min}_{\lambda\in\Delta_{S-1}}d^2(\mathbf{x},\mathbf{x}_\lambda), \tag{47}$$

where each $\mathbf{x}_\lambda$ is any point defined in (46). Note that (46) and (47) are the generalizations of problem (43) and problem (44) (or (45)), respectively.

**Definition A.1.** *The* barycentric space *generated by the reference points* $\{\mathbf{x}^s\}_{s\in[S]}$ *is defined by* $\mathrm{Bary}(\{\mathbf{x}^s\}_{s\in[S]}):=\{\mathbf{x}_\lambda$ *solution of* (46) $\mid\ \lambda\in\Delta_{S-1}\}$.

**Remark A.2.** *Notice that* $\mathbf{x}\in\mathrm{Bary}(\{\mathbf{x}^s\}_{s\in[S]})$ *if and only if* $\mathbf{x}=\mathbf{x}_\lambda$ *for some* $\lambda\in\Delta_{S-1}$*; equivalently, if and only if* $d_a(\mathbf{x},\mathbf{x}_\lambda)=0$ *for some* $\lambda\in\Delta_{S-1}$, for any *choice of divergence* $d_a(\cdot,\cdot)$. *However, in general,* $\mathrm{Bary}(\{\mathbf{x}^s\}_{s\in[S]})$ *is not necessarily a convex set, in particular is not necessarily the convex hull of the points* $\{\mathbf{x}^s\}_{s\in[S]}$.

In this general context, the problem of estimating an unknown point $\mathbf{x}$ under the *barycentric coding model* (BCM) consists of assuming that $\mathbf{x}\in\mathrm{Bary}(\{\mathbf{x}^s\}_{s\in[S]})$ (*model*), for a fixed set of points $\{\mathbf{x}^s\}_{s\in[S]}$, and estimating the unknown barycentric coordinates $\lambda\in\Delta_{S-1}$ such that a solution $\mathbf{x}_\lambda$ of the optimization problem (46) approximates the original point $\mathbf{x}$.

## Appendix B. Generalities on the Gromov-Wasserstein Problem

### B.1. GW Distance.

**Proposition B.1.** *The minimization problem* (8) *is convex (respectively, strictly convex) if the input matrices* $\mathbf{X}$ *and* $\mathbf{Y}$ *are symmetric positive definite (respectively, symmetric positive definite).*

*Proof.* On the one hand, the set of couplings $\Pi(\mathrm{p},\mathrm{q})$ is convex. On the other hand, we first note that in general, by using the constraint $\pi\in\Pi(\mathrm{p},\mathrm{q})$, the cost function in the minimization problem (8) can be rewritten as

$$\begin{aligned}&\sum_{i\in[N],j\in[M]}\sum_{k\in[N],l\in[M]}|\mathbf{X}_{ik}-\mathbf{Y}_{jl}|^2\pi_{ij}\pi_{kl}\\&=\sum_{i,k\in[N]}(\mathbf{X}_{ik})^2\mathrm{p}_i\mathrm{p}_k-2\underbrace{\sum_{i,k\in[N],j,l\in[M]}\mathbf{X}_{ik}\mathbf{Y}_{jl}\pi_{ij}\pi_{kl}}_{\mathrm{tr}(\pi^T\mathbf{X}^T\pi\mathbf{Y})}+\sum_{j,l\in[M]}(\mathbf{Y}_{jl})^2\mathrm{q}_j\mathrm{q}_l,\end{aligned}$$

where only the second term depends on the coupling $\pi$. It is easy to check that, for each $i_0\in[N],j_0\in[M]$,

$$\frac{\partial}{\partial\pi_{i_0j_0}}\mathrm{tr}(\pi^T\mathbf{X}^T\pi\mathbf{Y})=2\sum_{k\in[N],l\in[M]}\mathbf{X}_{i_0k}\pi_{kl}\mathbf{Y}_{j_0l},$$

and

$$\frac{\partial^2}{\partial \pi_{k_0 l_0} \partial \pi_{i_0 j_0}} \mathrm{tr}(\pi^T \mathbf{X}^T \pi \mathbf{Y}) = 2\mathbf{X}_{i_0 k_0} \mathbf{Y}_{j_0 l_0}.$$

Thus, the first-order derivative of the functional $\pi \mapsto \mathrm{tr}(\pi^T \mathbf{X}^T \pi \mathbf{Y})$ with respect to $\pi$ is $2\mathbf{X}\pi\mathbf{Y}$ and the Hessian is $2(\mathbf{X} \otimes \mathbf{Y})$, where $\otimes$ denotes the Kronecker product.

If both $\mathbf{X}$ and $\mathbf{Y}$ are symmetric positive semidefinite matrices, then so it is $\mathbf{X} \otimes \mathbf{Y}$ because the eigenvalues of the $MN \times MN$ matrix $\mathbf{X} \otimes \mathbf{Y}$ are given by the products of the eigenvalues of $\mathbf{X}$ and $\mathbf{Y}$. Thus, in this case the minimization problem (8) is convex (it is strictly convex if the input matrices $\mathbf{X}$ and $\mathbf{Y}$ are symmetric positive definite). □

**Remark B.2.** *See also* [14]*, where the above result is proven in the case where* $\mathbf{X}$ *and* $\mathbf{Y}$ *are symmetric positive definite matrices, using the Cholesky decomposition of the given matrices.*

B.2. **GW Synthesis Problem – Fixed-Point Iteration Scheme.** In this section we consider the GW synthesis problem (9). First, for completeness, we provide a proof of Proposition 3.2 (see also [46, Prop. 3]), followed by several remarks.

*Proof of Proposition 3.2.* Notice that, as in the proof of Proposition B.1, if we use the marginal constraints $\pi^s \in \Pi(\mathrm{p}^s, \mathrm{q})$, that is,

$$\sum_{j \in [M]} \pi^s_{ij} = \mathrm{p}^s_i \qquad \forall i \in [N^s] \qquad \text{and} \qquad \sum_{i \in [N^s]} \pi^s_{ij} = \mathrm{q}_j \qquad \forall j \in [M],$$

then the objective function $J_\lambda$ can be rewritten as

$$0 \le J_\lambda(\mathbf{Y}) = \sum_{s \in [S]} \lambda_s \sum_{i \in [N^s], j \in [M]} \sum_{k \in [N^s], l \in [M]} |\mathbf{X}^s_{ik} - \mathbf{Y}_{jl}|^2 \pi^s_{ij} \pi^s_{kl} \tag{48}$$

$$= \sum_{s \in [S]} \sum_{i,k \in [N]} \lambda_s (\mathbf{X}^s_{ik})^2 \mathrm{p}^s_i \mathrm{p}^s_k + \sum_{j,l \in [M]} (\mathbf{Y}_{jl})^2 \mathrm{q}_j \mathrm{q}_l$$

$$- 2 \sum_{s \in [S]} \sum_{i \in [N^s], j \in [M]} \sum_{k \in [N^s], l \in [M]} \lambda_s \mathbf{X}^s_{ik} \mathbf{Y}_{jl} \pi^s_{ij} \pi^s_{kl}. \tag{49}$$

Thus, $J_\lambda$ is continuous, convex, and nonnegative, (i.e., $J_\lambda(\mathbf{Y}) \ge 0$ for all $\mathbf{Y} \in \mathbb{R}^{M \times M}$). It is easy to check that if $\{\pi^s\}_{s \in [S]}$ are fixed, minimizing $J_\lambda$ over $\mathbf{Y} \in \mathbb{R}^{M \times M}$ yields the gradient expression:

$$\frac{\partial J_\lambda}{\partial \mathbf{Y}_{j_0 l_0}} = 2\, \mathrm{q}_{j_0} \mathrm{q}_{l_0} \mathbf{Y}_{j_0 l_0} - 2 \sum_{s \in [S]} \lambda_s \sum_{i,k \in [N^s]} \mathbf{X}^s_{ik} \pi^s_{ij_0} \pi^s_{kl_0}. \tag{50}$$

The Hessian of $J_\lambda$ is a $M^2 \times M^2$ diagonal matrix with diagonal entries given by:

$$\frac{\partial^2 J_\lambda}{\partial \mathbf{Y}^2_{j_0 l_0}} = 2\, \mathrm{q}_{j_0} \mathrm{q}_{l_0}, \qquad \forall l_0, j_0 \in [M].$$

In general, since $\mathrm{q}_j \ge 0$ for all $j$, the Hessian is positive semidefinite, and therefore, by convexity and the fact that the objective function is nonnegative, a minimizer exists. Moreover, if $\mathrm{q}_j > 0$ for all $j$, the Hessian is positive definite, implying that the problem admits a unique global minimum. The entries of the minimum $\mathbf{Y}^* \in \mathbb{R}^{M \times M}$ are characterized by setting the gradient expression (50) to zero, yielding the closed-form solution (13).

□

**Remark B.3.** *Notice that if* $\{\mathbf{X}^s\}_{s \in [S]}$ *are symmetric, then formula* (13) *defines a symmetric matrix* $\mathbf{Y}^*$*. Similarly, if the matrices* $\{\mathbf{X}^s\}_{s \in [S]}$ *have non-negative entries or are positive semidefinite, then* $\mathbf{Y}^*$ *will also have non-negative entries or be positive semidefinite* [46, Prop. 3]*. However, in general,* $\mathbf{Y}^*$ *does not have zero-trace (or zero-diagonal), even*

*if the template matrices* $\{\mathbf{X}^s\}_{s\in[S]}$ *have zero trace. Therefore, even if the templates are distance matrices,* $\mathbf{Y}^*$ *given by* (13) *does not necessarily define a distance matrix.*

**Proposition B.4** (Existence of a Solution for the GW Synthesis Problem (9))**.** *Consider a set of finite templates* $\{(\mathbf{X}^s, \mathrm{p}^s) \in \mathbb{R}^{N^s\times N^s} \times \mathcal{P}_{N^s}\}_{s\in[S]}$*. Fix* $\lambda \in \Delta_{S-1}$*, a size* $M \in \mathbb{N}$*, and a probability vector* $\mathrm{q} \in \mathcal{P}_M$*. Consider the functional* $H : \mathbb{R}^{M\times M} \times \Pi(\mathrm{p}^1, \mathrm{q}) \times \cdots \times \Pi(\mathrm{p}^S, \mathrm{q}) \to \mathbb{R}$ *given by*

$$H(\mathbf{Y}, \pi^1, \dots, \pi^S) := \sum_{s\in[S]} \lambda_s \sum_{i\in[N^s],j\in[M]} \sum_{k\in[N^s],l\in[M]} |\mathbf{X}^s_{ik} - \mathbf{Y}_{jl}|^2 \pi^s_{ij}\pi^s_{kl}.$$

*If we assume the extra hypothesis that all fixed matrices* $\mathbf{X}^1, \dots, \mathbf{X}^S$ *and the variable matrix* $\mathbf{Y}$ *have non-negative entries, then there exists a minimizer* $(\mathbf{Y}^*, (\pi^1)^*, \dots, (\pi^S)^*)$ *of* $H$ *and problem* (9) *has at least one solution* $\mathbf{Y}_\lambda$*.*

Note that $\Pi(\mathrm{p}^1, \mathrm{q}) \times \cdots \times \Pi(\mathrm{p}^S, \mathrm{q})$ is compact, since it is the product of compact sets, and $H$ is continuous and non-negative. However, $H$ is not convex and the variable $\mathbf{Y}$ does not belong to a compact set. For this reason, we included the additional hypothesis in the above statement.

*Proof of Proposition B.4.* Since $H$ is non-negative, let

$$a^* := \inf\{H(Y, \pi^1, \dots, \pi^S) \mid \mathbf{Y} \in \mathbb{R}^{M\times M}_{\geq 0},\ \pi^s \in \Pi(\mathrm{p}^s, \mathrm{q})\ \forall s \in [S]\},$$

where $\mathbb{R}^{M\times M}_{\geq 0}$ denotes the subset of $\mathbb{R}^{M\times M}$ of all $M \times M$ matrices with non-negative entries. Notice that since the vectors $\mathrm{p}^1, \dots, \mathrm{p}^S$, and $\mathrm{q}$ are fixed, we can rewrite the functional $H$ as

$$\begin{aligned} H(\mathbf{Y}, \pi^1, \dots, \pi^S) &= \sum_{s\in[S]} \lambda_s \sum_{i\in[N^s],j\in[M]} \sum_{k\in[N^s],l\in[M]} |\mathbf{X}^s_{ik} - \mathbf{Y}_{jl}|^2 \pi^s_{ij}\pi^s_{kl} \\ &= \sum_{s\in[S]} \sum_{i,k\in[N]} \lambda_s (\mathbf{X}^s_{ik})^2 \mathrm{p}^s_i \mathrm{p}^s_k + \sum_{j,l\in[M]} (\mathbf{Y}_{jl})^2 \mathrm{q}_j \mathrm{q}_l \\ &\quad - 2 \sum_{s\in[S]} \sum_{i\in[N^s],j\in[M]} \sum_{k\in[N^s],l\in[M]} \lambda_s \mathbf{X}^s_{ik} \mathbf{Y}_{jl} \pi^s_{ij}\pi^s_{kl} \end{aligned}$$

(as in (49) in the previous proof). Thus, when working under the hypothesis that all the matrices have non-negative entries, we have

$$\begin{aligned} H(\mathbf{Y}, \pi^1, \dots, \pi^S) &\geq \sum_{j,l\in[M]} (\mathbf{Y}_{jl})^2 \mathrm{q}_j \mathrm{q}_l - 2 \sum_{s\in[S]} \sum_{i\in[N^s],j\in[M]} \sum_{k\in[N^s],l\in[M]} \lambda_s \mathbf{X}^s_{ik} \mathbf{Y}_{jl} \pi^s_{ij}\pi^s_{kl} \\ &\geq \sum_{j,l\in[M]} (\mathbf{Y}_{jl})^2 \mathrm{q}_j \mathrm{q}_l - \left(2 \sum_{s\in[S]} \sum_{i,k\in[N^s]} \lambda_s \mathbf{X}^s_{ik}\right) \sum_{j,l\in[M]} \mathbf{Y}_{jl} \\ &\geq k_1 \|\mathbf{Y}\|^2_{\mathrm{Frob}} - k_2 \|\mathbf{Y}\|_{\mathrm{Frob}} \end{aligned} \tag{51}$$

for some positive constants $k_1, k_2$ (which do not depend on $\pi^s$), where we used that all the norms in $\mathbb{R}^{M\times M}$ are equivalent, and previously we used that $0 \leq \pi^s_{ij} \leq 1$. Thus, (51) shows that if $\|\mathbf{Y}\|_{\mathrm{Frob}} \to \infty$, then $H(\mathbf{Y}, \pi^1, \dots, \pi^S) \to \infty$. This implies that for all $a > a^*$, there exists $R > 0$ such that

$$a^* < a \leq H(\mathbf{Y}, \pi^1, \dots, \pi^s) \qquad \forall \mathbf{Y} \in \mathbb{R}^{M\times M}_{\geq 0} \setminus B_R,$$

where

$$B_R := \left\{\mathbf{Y} \in \mathbb{R}^{M\times M}_{\geq 0} \mid \|\mathbf{Y}\|_{\mathrm{Frob}} \leq R\right\}.$$

Thus,

$$\begin{aligned} a^* &= \inf\{H(Y,\pi^1,\dots,\pi^S) \mid \mathbf{Y}\in B_R,\ \pi^s\in\Pi(\mathrm{p}^s,\mathrm{q})\,\forall s\in[S]\} \\ &= \min\{H(Y,\pi^1,\dots,\pi^S) \mid \mathbf{Y}\in B_R,\ \pi^s\in\Pi(\mathrm{p}^s,\mathrm{q})\,\forall s\in[S]\}, \end{aligned}$$

where the last expression holds since $H$ is continuous and we are minimizing it over a compact set. In particular,

$$\begin{aligned} &\inf\{H(Y,\pi^1,\dots,\pi^S) \mid \mathbf{Y}\in \mathbb{R}^{M\times M}_{\geq 0},\ \pi^s\in\Pi(\mathrm{p}^s,\mathrm{q})\,\forall s\in[S]\} \\ &= \min\{H(Y,\pi^1,\dots,\pi^S) \mid \mathbf{Y}\in \mathbb{R}^{M\times M}_{\geq 0},\ \pi^s\in\Pi(\mathrm{p}^s,\mathrm{q})\,\forall s\in[S]\}. \end{aligned}$$

Finally, from the general fact that given a function $f$, if $f(x_0,y_0)=\min_{x,y} f(x,y)$ for some point $(x_0,y_0)$, then $\min_{x,y} f(x,y)=\min_x\min_y f(x,y)$, we obtain

$$\begin{aligned} &\min\{H(Y,\pi^1,\dots,\pi^S) \mid \mathbf{Y}\in \mathbb{R}^{M\times M}_{\geq 0},\ \pi^s\in\Pi(\mathrm{p}^s,\mathrm{q})\,\forall s\in[S]\} \\ &= \min_{\mathbf{Y}\in\mathbb{R}^{M\times M}_{\geq 0}} \min_{\{\pi^s\in\Pi(\pi^s,\mathrm{q})\}_{s=1}^S} H(Y,\pi^1,\dots,\pi^S) \\ &= \min_{\mathbf{Y}\in\mathbb{R}^{M\times M}_{\geq 0}} \sum_{s\in[S]} \lambda_s GW((\mathbf{X}^s,\mathrm{p}^s),(\mathbf{Y},\mathrm{q}))^2, \end{aligned}$$

that is, the last minimum is well-defined, meaning that there exists at least one solution $\mathbf{Y}_\lambda\in\mathbb{R}^{M\times M}_{\geq 0}$ of problem (9) under the assumption that the template matrices have non-negative entries. □

**Example B.5** (Illustrative Example Related to Remark 3.5)**.** *To illustrate the point made in Remark 3.5 more clearly, let us analyze the following simple example. For a single template* $(\mathbf{X},\mathrm{p})\in\mathbb{R}^{N\times N}\times\mathcal{P}_N$ *(i.e.,* $S=1$*), consider the particular case of problem* (9) *for* $M=N$ *and* $\mathrm{q}=\mathrm{p}$*, that is,*

$$\min_{\mathbf{Y}\in\mathbb{R}^{N\times N}} GW((\mathbf{X},\mathrm{p}),(\mathbf{Y},\mathrm{p}))^2.$$

*Clearly,* $\mathbf{X}\in\arg\min_{\mathbf{Y}\in\mathbb{R}^{N\times N}} GW((\mathbf{X},\mathrm{p}),(\mathbf{Y},\mathrm{p}))^2$*. Then, Theorem 3.3 implies that*

$$\mathbf{X}=\frac{1}{\mathrm{p}\mathrm{p}^T}\odot(\pi^*)^T\mathbf{X}\pi^* \qquad \forall\pi^*\in\Pi(\mathrm{p},\mathrm{p})\ \textit{optimal for}\ GW((\mathbf{X},\mathrm{p}),(\mathbf{X},\mathrm{p})). \tag{52}$$

*To reinforce* (52)*, let us verify it by exhaustion in the case* $N=M=2$*,* $\mathbf{X}$ *anti-diagonal matrix and* p *uniform. That is, consider* $\mathbf{X}=\begin{pmatrix}0 & c\\ c & 0\end{pmatrix}$ *for some* $c>0$ *and* $\mathrm{p}=(.5,.5)$*. Then*

$$\pi_1=\begin{pmatrix}.5 & 0\\ 0 & .5\end{pmatrix} \qquad \textit{and} \qquad \pi_2=\begin{pmatrix}0 & .5\\ .5 & 0\end{pmatrix}$$

*are all the possible* optimal *plans for* $GW((\mathbf{X},\mathrm{p}),(\mathbf{X},\mathrm{p}))$*. It is easy to check that in fact*

$$\mathbf{X}_1^*:=\frac{1}{\mathrm{p}\mathrm{p}^T}\odot\pi_1^T\mathbf{X}\pi_1=\mathbf{X} \qquad \textit{and} \qquad \mathbf{X}_2^*:=\frac{1}{\mathrm{p}\mathrm{p}^T}\odot\pi_2^T\mathbf{X}\pi_2=\mathbf{X}^T=\mathbf{X},$$

*showing that* $\mathbf{X}_1^*=\mathbf{X}_2^*$ *and so further supporting that* (13) *does not depend on the choice of the GW OT plans.*

B.3. **Weak Isomorphisms.**

Let $\mathbb{X},\mathbb{Y}$ be two mm-spaces. By [38, Thm. 5.1] $GW(\mathbb{X},\mathbb{Y})=0$ if and only if $\mathbb{X}$ and $\mathbb{Y}$ are strongly isomorphic. In more generality, if $\mathbb{X},\mathbb{Y}$ are two networks, then $GW(\mathbb{X},\mathbb{Y})=0$ if and only if $\mathbb{X}$ and $\mathbb{Y}$ are weakly isomorphic [12, Thms. 2.3 and 2.4]. As a consequence, two mm-spaces are strongly isomorphic if and only if they are weakly isomorphic. To gain some intuition we provide a proof for the finite case. The proof of the general case follows the same ideas but requires some technical results such as [38, Lem. 2.2 or Lem. 10.4].

**Proposition B.6.** *If two finite metric measure spaces are weakly isomorphic, then they are strongly isomorphic.*

*Proof.* Let $\mathbb{X} = (X, d_X, \mu_X)$, $\mathbb{Y} = (Y, d_Y, \mu_Y)$ be two metric measure spaces over finite sets $X = \{x_i\}_{i=1}^N$ and $Y = \{y_j\}_{j=1}^M$ such that $\mathbb{X} \sim^w \mathbb{Y}$. Assume, without loss of generality that the support of the measures $\mu_X$ and $\mu_Y$ are exactly $X$ and $Y$, respectively. Let $(Z, \mu_Z)$ be a 'pivoting' finite measure space and maps $\varphi_X : Z \to X$, $\varphi_Y : Z \to Y$ as in Definition 2.3. In fact, since the spaces are finite, the second property in the definition of weak isomorphism (Definition 2.3) takes the form

$$d_X(\varphi_X(z), \varphi_X(z')) = d_Y(\varphi_Y(z), \varphi_Y(z')) \qquad \forall z, z' \in Z. \tag{53}$$

Moreover, $\varphi_X$ and $\varphi_Y$ are surjective functions onto $X$ and $Y$, respectively. This is a consequence of the first property in the definition of weak isomorphism (Definition 2.3), because for each $x \in X$ and each $y \in Y$,

$$\begin{aligned} 0 \neq \mu_X(\{x\}) = (\varphi_X)_\# \mu_Z(\{x\}) = \mu_Z\left(\{z \mid \varphi_X(z) = x\}\right), \\ 0 \neq \mu_Y(\{y\}) = (\varphi_Y)_\# \mu_Z(\{y\}) = \mu_Z\left(\{z \mid \varphi_Y(z) = y\}\right), \end{aligned}$$

that is, for each $x \in X$ there exists at least one point $z \in Z$ such that $\varphi_X(z) = x$; similarly, for each $y \in Y$ there exists at least one point $z \in Z$ such that $\varphi_Y(z) = y$.

Let us define the function $\varphi : X \to Y$ as follows: for $x \in X$, set $\varphi(x) := \varphi_Y(z_x)$, where $z_x$ is some point in $Z$ such that $\varphi_X(z_x) = x$. Let us show the following properties of $\varphi$:

(1) It is a well-defined function: It does not depend on the representative $z_x$, that is, if $z_x, z'_x \in Z$ are such that $\varphi_X(z_x) = x = \varphi_X(z'_x)$, then

$$d_Y(\varphi_Y(z_x), \varphi_Y(z'_x)) = d_X(\varphi_X(z_x), \varphi_X(z'_x)) = d_X(x, x) = 0,$$

thus $\varphi_Y(z_x) = \varphi_Y(z'_x)$. Notice that we have applied the identity of indiscernibles for distances.

(2) It is an isometry: For every $x, x' \in X$ we have,

$$d_Y(\varphi(x), \varphi(x')) = d_Y(\varphi_Y(z_x), \varphi_Y(z_{x'})) = d_X(\varphi_X(z_x), \varphi_X(z_{x'})) = d_X(x, x').$$

(3) It is a bijection: In analogy to the definition of $\varphi$, we can define a new map $\phi : Y \to X$ by $\phi(y) := \varphi_X(z_y)$ for any $z_y \in Z$ such that $\varphi_Y(z_y) = y$. It is a well-defined function by the same argument as in the first item. Moreover, $\phi = \varphi^{-1}$, since, by definition

$$\begin{aligned} \varphi(\phi(y)) = \varphi(\varphi_X(z_y)) = \varphi_Y(z_y) = y, \qquad \forall y \in Y, \\ \phi(\varphi(x)) = \phi(\varphi_Y(z_x)) = \varphi_X(z_x) = x, \qquad \forall x \in X. \end{aligned}$$

(4) $\varphi_\# \mu_X = \mu_Y$: For every $y \in Y$,

$$\begin{aligned} \varphi_\# \mu_X(\{y\}) &= \mu_X(\{x \mid \varphi(x) = y\}) = (\varphi_X)_\# \mu_Z(\{x = \phi(y)\}) \\ &= \mu_Z(\{z \mid \varphi_X(z) = \phi(y)\}) = \mu_Z(\{z \mid \varphi(\varphi_X(z)) = y\}) \\ &= \mu_Z(\{z \mid \varphi_Y(z) = y\}) = (\varphi_Y)_\# \mu_Z(\{y\}) = \mu_Y(\{y\}). \end{aligned}$$

□

**Example B.7** (Weak Isomorphism)**.** *Figure 10 is an illustration of a weak isomorphism between two networks* $\mathbb{X}$ *and* $\mathbb{Y}$*. The network* $\mathbb{X}$ *consists of a measure space* $(X, \mu_X)$ *with two points having masses* 0.6 *and* 0.4*, and* $\omega_X$ *represented by the* $2 \times 2$ *matrix*

$$\mathbf{X} = \begin{pmatrix} 3 & 2 \\ 2 & 0 \end{pmatrix}.$$

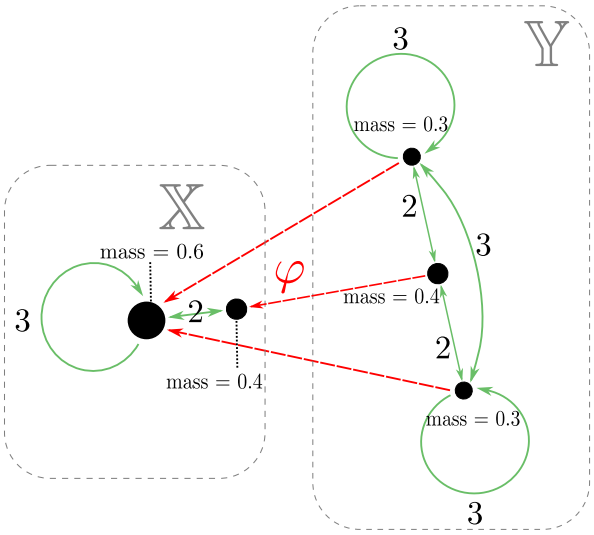



**Figure 10.** Illustration of two weakly isomorphic spaces $\mathbb{X} \sim^w \mathbb{Y}$.

*The network* $\mathbb{Y}$ *is given by the measure space* $(Y, \mu_Y)$ *consisting of three points with mass* 0.3, 0.3, *and* 0.4, *and* $\omega_Y$ *represented by the* $3 \times 3$ *matrix*

$$\mathbf{Y} = \begin{pmatrix} 3 & 3 & 2 \\ 3 & 3 & 2 \\ 2 & 2 & 0 \end{pmatrix}.$$

*Similarly as in Figure 4, the pivoting space* $(Z, \mu_Z)$ *in Definition 2.3 can be taken as* $(Y, \mu_Y)$, *with* $\varphi_X = \varphi$ *(red assignment) and* $\varphi_Y$ *the identity map, getting* $\mathbb{X} \sim^w \mathbb{Y}$.

*As an informal interpretation, under weak isomorphism two nodes* $y, y' \in Y$ *are* 'the same' *if they have the same* internal connectivity, *i.e.,* $\omega_Y(y, y) = \omega_Y(y, y') = \omega_X(y', y) = \omega_Y(y', y')$, *and the same* external connectivity, *i.e.,* $\omega_Y(y, a) = \omega_Y(y', a)$ *and* $\omega_Y(a, y) = \omega_Y(a, y')$ *for all* $a \in Y$ [13]. *In our example, the two nodes in the space* $Y$ *with mass* 0.3 *are* 'the same'.

**Remark B.8** (Log Map)**.** *By using the blow-up technique (i.e., by using Algorithm 3 with an optimal coupling for* $GW(\mathbb{X}, \mathbb{Y})$*), the* logarithmic map $Log_{[\mathbb{Y}]} : \mathcal{GM} \longrightarrow \mathrm{Tan}_{[\mathbb{Y}]}$, *that is, the local inverse of the exponential map (27), can be written as:* $Log_{[\mathbb{Y}]}([\mathbb{X}]) := [\mathbf{X}_b - \mathbf{Y}_b]$. *We refer the reader to* [14, Sec. 3.4].

**Remark B.9** (Geodesics)**.** *By using the blow-up technique, the curve (for* $t \in [0, 1]$*)*

$$\gamma(t) := [(X_b \times Y_b, (1-t)\omega_{X_b} + t\omega_{Y_b}, \pi_b)] \text{ or, equivalently, } \gamma(t) := [((1-t)\mathbf{X}_b + t\mathbf{Y}_b, \mathrm{q}_b)],$$

*is a* $GW$ geodesic *between* $[\mathbb{X}]$ *and* $[\mathbb{Y}]$, *in the sense that* $GW(\gamma(t), \gamma(s)) = |t-s| GW(\mathbb{X}, \mathbb{Y})$ *for all* $0 \le s, t \le 1$. *In particular,* $\omega_{X_b} - \omega_{Y_b}$ *(represented by the matrix* $\mathbf{X}_b - \mathbf{Y}_b$*) can be viewed as its* velocity. *We refer the reader to* [56, 14]. *As a consequence, the GW barycenter between two references* $[\mathbb{X}]$, $[\mathbb{Y}]$ *with uniform weights* $\lambda = (1/2, 1/2)$ *is given by the network class* $\gamma(1/2) = [(\frac{1}{2}\mathbf{X}_b + \frac{1}{2}\mathbf{Y}_b, \mathrm{q}_b)]$. *Indeed, by using the triangle inequality, for every network*

*class* $[\mathbb{Z}]$ *we have:*

$$\begin{aligned}\frac{1}{2}GW^2(\mathbb{X},\gamma(1/2))+\frac{1}{2}GW^2(\mathbb{Y},\gamma(1/2)) &= \frac{1}{2}GW^2(\gamma(0),\gamma(1/2))+\frac{1}{2}GW^2(\gamma(1),\gamma(1/2))\\ &= \frac{1}{2}\frac{1}{4}GW^2(\mathbb{X},\mathbb{Y})+\frac{1}{2}\frac{1}{4}GW^2(\mathbb{X},\mathbb{Y})\\ &= \frac{1}{4}GW^2(\mathbb{X},\mathbb{Y})\\ &\leq \frac{1}{4}\left(GW(\mathbb{X},\mathbb{Z})+GW(\mathbb{X},\mathbb{Z})\right)^2\\ &= \left(\frac{1}{2}GW(\mathbb{X},\mathbb{Z})+\frac{1}{2}GW(\mathbb{X},\mathbb{Z})\right)^2\\ &\leq \frac{1}{2}GW^2(\mathbb{X},\mathbb{Z})+\frac{1}{2}GW^2(\mathbb{X},\mathbb{Z}).\end{aligned}$$

*In general,* $\gamma(t)$ *is a GW barycenter between* $[\mathbb{X}]$ *and* $[\mathbb{Y}]$ *with weights* $\lambda=(1-t,t)$ *because for every network class* $[\mathbb{Z}]$ *we have:*

$$\begin{aligned}(1-t)\,GW^2(\mathbb{X},\gamma(t))+t\,GW^2(\mathbb{Y},\gamma(t)) &= (1-t)\,t^2\,GW^2(\mathbb{X},\mathbb{Y})+t\,(1-t)^2\,GW^2(\mathbb{X},\mathbb{Y})\\ &= t(1-t)\,GW^2(\mathbb{X},\mathbb{Y})\\ &\leq t(1-t)\,\left(GW(\mathbb{X},\mathbb{Z})+GW(\mathbb{Y},\mathbb{Z})\right)^2\\ &\leq (1-t)\,GW^2(\mathbb{X},\mathbb{Z})+t\,GW^2(\mathbb{Y},\mathbb{Z}),\end{aligned}$$

*where in the last step we used the inequality* $t(1-t)(a+b)^2\leq(1-t)a^2+tb^2$ *(which arises from expanding squares or completing the square* $((1-t)a-tb)^2\geq 0$*). However, this procedure cannot be adapted when considering more than 2 templates.*

**Remark B.10** (First-Order Optimality in GW Space with the Formal Riemannian-Like Structure Defined in [14] and Used in This Work)**.** *Let us show that a minimizer* $[\mathbb{Y}^*]$ *of a differentiable functional in GW space,* $G:\mathcal{GW}\to\mathbb{R}$*, must satisfy the* first-order optimality condition*, that is,* $\nabla G([\mathbb{Y}^*])=0$*. First, by assumption we have that* $G([\mathbb{Y}^*])\leq G([\mathbb{Y}])$ *for all* $[\mathbb{Y}]\in\mathcal{GW}$*. In particular,* $G([\mathbb{Y}^*])\leq G(Exp_{[\mathbb{Y}^*]}(tv))$ *for all* $[v]\in \mathrm{Tan}_{[\mathbb{Y}^*]}$*. Thus,*

$$\langle[v],\nabla G([\mathbb{Y}^*])\rangle_{\mathrm{Tan}_{[\mathbb{Y}^*]}}=D_vG([\mathbb{Y}])=\lim_{t\searrow 0}\frac{G(Exp_{[\mathbb{Y}^*]}(tv))-G([\mathbb{Y}^*])}{t}\geq 0,\quad\forall[v]\in\mathrm{Tan}_{[\mathbb{Y}^*]}.$$

*In particular, for the direction* $[v]=-\nabla G([\mathbb{Y}^*])$ *(which exists because tangent vectors are modeled as elements of* $L^2$*-spaces) we have*

$$0\leq\langle-\nabla G([\mathbb{Y}^*]),\nabla G([\mathbb{Y}^*])\rangle_{\mathrm{Tan}_{[\mathbb{Y}^*]}}=-\|\nabla G([\mathbb{Y}^*])\|^2_{\mathrm{Tan}_{[\mathbb{Y}^*]}}\leq 0,$$

*which is only possible if* $\nabla G([\mathbb{Y}^*])=0$*.*

*Thus, the authors in* [14] *develop a* first-order calculus *on GW space–comprising directional derivatives of functionals, gradients as linear functionals (or vectors), first-order optimality conditions for minimizers, and linear approximations of functions around a point–by equipping it with a formal tangent space at each point* $[\mathbb{Y}]$*, based on a Riemannian-like framework. This ends the remark.*

For completeness, we revisit the proof of Proposition 4.3, originally presented in [14, Prop. 8]. Before doing so, we state the following lemma and a subsequent observation.

**Lemma B.11.** *Given a finite network* $\mathbb{Y}=(Y,\omega_Y,\mu_Y)$ *and a measure space* $(Z,\mu_Z)$ *with an associated function* $\varphi:Z\to Y$ *such that* $\varphi_\#\mu_Z=\mu_Y$*. Then*
*(1)* $(Z,\varphi^*\omega_Y,\mu_Z)\in[\mathbb{Y}]$*.*

*(2) For any* $v \in L^2(Y \times Y, \mu_Y \otimes \mu_Y)$, $v \simeq \varphi^* v \in L^2(Z \times Z, \mu_Z \otimes \mu_Z)$ *(i.e.,* $[v] = [\varphi^* v] \in \mathrm{Tan}_{[\mathbb{Y}]}$*).*

*Proof.* It follows from the fact that the plan in $\Pi(\mu_Z, \mu_Y)$ induced by the map $\varphi$ (i.e., $\pi(\{z, y\}) = \mu_Z(\{z\})\delta_{y=\varphi(z)}$) achieves $GW((Z, \varphi^*\omega_Y, \mu_Z), \mathbb{Y}) = 0$. □

**Remark B.12.** *Let* $\mathbb{Y} = (Y, \omega_Y, \mu_Y) = (\mathbf{Y}, \mathrm{q})$ *and* $\mathbb{Y}' = (Y', \omega_{Y'}, \mu_{Y'}) = (\mathbf{Y}', \mathrm{q}')$ *be finite networks such that* $\mathbb{Y} \sim^w \mathbb{Y}'$ *(i.e., both belong to the same class* $[\mathbb{Y}]$*). Let* $\pi \in \Pi(\mathrm{q}, \mathrm{q}')$ *be a GW OT plan between* $\mathbb{Y}$ *and* $\mathbb{Y}'$*, i.e., it achieves* $GW((\mathbf{Y}, \mathrm{q}), (\mathbf{Y}', \mathrm{q}')) = 0$*. Apply the blow-up procedure between* $\mathbb{Y}$ *and* $\mathbb{Y}'$ *with respect to* $\pi$ *(see Definition 4.2 and the follow up properties). Therefore, after relabeling the nodes if necessary, one obtains a new set of nodes* $Y_b = Z = Y'_b$*, with cardinality equal to that of the support of* $\pi$*, and new distribution of mass* $\mu_{Y_b} = \mu_Z = \mu_{Y'_b}$ *on such nodes. Moreover, there exist functions* $\varphi_Y : Z \to Y$, $\varphi_{Y'} : Z \to Y'$ *(defined implicitly in parts 2 and 3 of Definition 4.2) such that* $(\varphi_Y)_{\#}\mu_Z = \mu_Y$ $(\varphi_{Y'})_{\#}\mu_Z = \mu_{Y'}$ *and* $(\varphi_Y)^*\omega_Y = (\varphi_{Y'})^*\omega_{Y'}$*.*

*Now, consider* $[v], [v'] \in \mathrm{Tan}_{[\mathbb{Y}]}$ *with representatives* $v \in L^2(Y \times Y, \mu_Y \otimes \mu_Y)$ *and* $v' \in L^2(Y' \times Y', \mu_{Y'} \otimes \mu_{Y'})$*. As a consequence of Lemma B.11, we can obtain new representatives* $(\varphi_Y)^* v$ *and* $(\varphi_{Y'})^* v'$ *defined over the same underlying space* $Z \times Z$*, i.e.,* $(\varphi_Y)^* v, (\varphi_{Y'})^* v' \in L^2(Z \times Z, \mu_Z \otimes \mu_Z)$*, satisfying* $(\varphi_Y)^* v \simeq v$ *and* $(\varphi_{Y'})^* v' \simeq v$*.*

*Proof of Proposition 4.3.*

**Case** $S = 1$**:** For simplicity, we start by fixing only one finite template $[\mathbb{X}]$, and considering the functional $[\mathbb{Y}] \longmapsto \frac{1}{2} GW^2(\mathbb{X}, \mathbb{Y})$ defined over classes of finite networks, which we denote by $G$. Given a finite network $[\mathbb{Y}]$, we want to compute $\nabla G([\mathbb{Y}])$ according to Definition 4.1.

Let $(\mathbf{X}, \mathrm{p})$ and $(\mathbf{Y}, \mathrm{q})$ be representatives of the weak classes of equivalence of $[\mathbb{X}]$ and $[\mathbb{Y}]$ after blow-up (for simplicity in the notation we avoid the subindex '$b$' from Definition 4.2). In particular, both $\mathbf{X}$ and $\mathbf{Y}$ are matrices of the same size, $M \times M$. Moreover, we can assume that a GW OT plan in $\Pi(\mathrm{p}, \mathrm{q})$ for $GW(\mathbb{X}, \mathbb{Y}) = GW((\mathbf{X}, \mathrm{p}), (\mathbf{Y}, \mathrm{q}))$ is induced by the identity map, after permuting and relabeling the nodes if necessary, and so we can also assume $\mathrm{p} = \mathrm{q}$. Thus,

$$GW^2(\mathbb{X}, \mathbb{Y}) = \sum_{i,j \in [M]} |\mathbf{X}_{ij} - \mathbf{Y}_{ij}|^2 \mathrm{q}_i \mathrm{q}_j, \tag{54}$$

that is, a GW OT plan is a diagonal matrix whose diagonal is given by q, and we denote it as $\mathrm{diag}(\mathrm{q})$.

Consider the $M \times M$ matrix $\mathbf{X} - \mathbf{Y}$. The candidate for $\nabla G([\mathbb{Y}])$ is $[\mathbf{X} - \mathbf{Y}]$. Let $[v] \in \mathrm{Tan}_{[\mathbb{Y}]}$ be an arbitrary tangent vector at $[\mathbb{Y}]$. We want to show that

$$D_v G([\mathbb{Y}]) = \langle [v], [\mathbf{X} - \mathbf{Y}] \rangle_{\mathrm{Tan}_{[\mathbb{Y}]}}.$$

From Remark B.12 applied to $[v]$ and $[\mathbf{X} - \mathbf{Y}]$ in $\mathrm{Tan}_{[\mathbb{Y}]}$, we can consider representatives that are matrices of the same size. Therefore, without loss of generality, and by abuse of notation, we can assume that $v$ and $\mathbf{X} - \mathbf{Y}$ are representatives of $[v]$ and $[\mathbf{X} - \mathbf{Y}]$, respectively, of the same size $M \times M$ (after a new blow-up, possible enlargement, realignment, and relabeling). Thus,

$$\langle [\mathbf{X} - \mathbf{Y}], [v] \rangle_{\mathrm{Tan}_{[\mathbb{Y}]}} = \sum_{i,j \in [M]} (\mathbf{X}_{ij} - \mathbf{Y}_{ij}) v_{ij} \mathrm{q}_i \mathrm{q}_j, \tag{55}$$

where the inner product is given by the weighted trace inner product with weight $\mathrm{q} \otimes \mathrm{q}$.

For $t \geq 0$, consider $\pi^t$ a GW optimal $M \times M$ coupling in $\Pi(\mathrm{q}, \mathrm{q})$ between $(\mathbf{X}, \mathrm{q})$ (representative of $[\mathbb{X}]$) and $(\mathbf{Y} + tv, \mathrm{q})$ (representative of $Exp_{[\mathbb{Y}]}(tv)$) such that $\lim_{t \to 0} \pi^t = \mathrm{diag}(\mathrm{q})$

(notice that $Exp_{[\mathbb{Y}]}(0) = [\mathbb{Y}]$). On the one hand, we have:

$$\begin{aligned}
GW^2(\mathbb{X}, Exp_{[\mathbb{Y}]}(tv)) &= \sum_{i,j\in[M]}\sum_{k,l\in[M]} |\mathbf{X}_{ik} - \mathbf{Y}_{jl} - tv_{jl}|^2 \pi^t_{ij}\pi^t_{kl} \\
&= \sum_{i,j\in[M]}\sum_{k,l\in[M]} |\mathbf{X}_{ik} - \mathbf{Y}_{jl}|^2 \pi^t_{ij}\pi^t_{kl} + t^2 \sum_{i,j\in[M]}\sum_{k,l\in[M]} |v_{jl}|^2 \pi^t_{ij}\pi^t_{kl} \\
&\quad + 2t \sum_{i,j\in[M]}\sum_{k,l\in[M]} (\mathbf{X}_{ik} - \mathbf{Y}_{jl}) v_{jl}\pi^t_{ij}\pi^t_{kl} \\
&= \sum_{i,j\in[M]}\sum_{k,l\in[M]} |\mathbf{X}_{ik} - \mathbf{Y}_{jl}|^2 \pi^t_{ij}\pi^t_{kl} + t^2 \sum_{i,j\in[M]} |v_{ij}|^2 \mathrm{q}_i\mathrm{q}_j \\
&\quad + 2t \sum_{i,j\in[M]}\sum_{k,l\in[M]} (\mathbf{X}_{ik} - \mathbf{Y}_{jl}) v_{jl}\pi^t_{ij}\pi^t_{kl} \\
&\geq GW^2(\mathbb{X}, \mathbb{Y}) + t^2 \sum_{i,j\in[M]} |v_{ij}|^2 \mathrm{q}_i\mathrm{q}_j + 2t \sum_{i,j\in[M]}\sum_{k,l\in[M]} (\mathbf{X}_{ik} - \mathbf{Y}_{jl}) v_{jl}\pi^t_{ij}\pi^t_{kl}. \qquad (56)
\end{aligned}$$

On the other hand, using (54) and since $\mathrm{diag}(\mathrm{q})$ is an admissible coupling but not necessarily optimal for $GW^2(\mathbb{X}, Exp_{[\mathbb{Y}]}(tv))$, we have:

$$\begin{aligned}
GW^2(\mathbb{X}, Exp_{[\mathbb{Y}]}(tv)) &= \sum_{i,j\in[M]}\sum_{k,l\in[M]} |\mathbf{X}_{ik} - \mathbf{Y}_{jl} - tv_{jl}|^2 \pi^t_{ij}\pi^t_{kl} \\
&\leq \sum_{i,j\in[M]} |\mathbf{X}_{ij} - \mathbf{Y}_{ij} - tv_{ij}|^2 \mathrm{q}_i\mathrm{q}_j \\
&= \sum_{i,j\in[M]} |\mathbf{X}_{ij} - \mathbf{Y}_{ij}|^2 \mathrm{q}_i\mathrm{q}_j + t^2 \sum_{i,j\in[M]} |v_{ij}|^2 \mathrm{q}_i\mathrm{q}_j + 2t \sum_{i,j\in[M]} (\mathbf{X}_{ij} - \mathbf{Y}_{ij}) v_{ij}\mathrm{q}_i\mathrm{q}_j \\
&= GW^2(\mathbb{X}, \mathbb{Y}) + t^2 \sum_{i,j\in[M]} |v_{ij}|^2 \mathrm{q}_i\mathrm{q}_j + 2t \sum_{i,j\in[M]} (\mathbf{X}_{ij} - \mathbf{Y}_{ij}) v_{ij}\mathrm{q}_i\mathrm{q}_j. \qquad (57)
\end{aligned}$$

In what follows we use (56) and (57) to provide upper and lower bounds for the directional derivative

$$2\, D_v G([\mathbb{Y}]) = \lim_{t\to 0} \frac{GW^2(\mathbb{X}, Exp_{[\mathbb{Y}]}(tv)) - GW^2(\mathbb{X}, \mathbb{Y})}{t}.$$

- *Upper bound:*

$$\frac{GW^2(\mathbb{X}, Exp_{[\mathbb{Y}]}(tv)) - GW^2(\mathbb{X}, \mathbb{Y})}{t} \leq \sum_{i,j\in[M]} \left(t|v_{ij}|^2 + 2(\mathbf{X}_{ij} - \mathbf{Y}_{ij})v_{ij}\right) \mathrm{q}_i\mathrm{q}_j.$$

  Thus,

$$\lim_{t\to 0} \frac{GW^2(\mathbb{X}, Exp_{[\mathbb{Y}]}(tv)) - GW^2(\mathbb{X}, \mathbb{Y})}{t} \leq 2 \sum_{i,j\in[M]} (\mathbf{X}_{ij} - \mathbf{Y}_{ij}) v_{ij}\mathrm{q}_i\mathrm{q}_j. \qquad (58)$$

- *Lower bound:*

$$\begin{aligned}
&\frac{GW^2(\mathbb{X}, Exp_{[\mathbb{Y}]}(tv)) - GW^2(\mathbb{X}, \mathbb{Y})}{t} \\
&\geq t \sum_{i,j\in[M]} |v_{ij}|^2 \mathrm{q}_i\mathrm{q}_j + 2 \sum_{i,j\in[M]}\sum_{k,l\in[M]} (\mathbf{X}_{ik} - \mathbf{Y}_{jl}) v_{jl}\pi^t_{ij}\pi^t_{kl}.
\end{aligned}$$

Thus,

$$\lim_{t\to 0}\frac{GW^2(\mathbb{X}, Exp_{[\mathbb{Y}]}(tv)) - GW^2(\mathbb{X},\mathbb{Y})}{t} \geq 2\sum_{i,j\in[M]}(\mathbf{X}_{ij}-\mathbf{Y}_{ij})v_{ij}\mathrm{q}_i\mathrm{q}_j. \tag{59}$$

As a consequence of (55), (58) and (59), for a fixed $[\mathbb{X}]$, the directional derivative of the functional $G([\mathbb{Y}]) = \frac{1}{2}GW^2(\mathbb{X},\mathbb{Y})$ in the direction of $[v]\in \mathrm{Tan}_{[\mathbb{Y}]}$ at $[\mathbb{Y}]$ is given by

$$\begin{aligned} D_vG([\mathbb{Y}]) &= \frac{1}{2}\lim_{t\to 0}\frac{GW^2(\mathbb{X}, Exp_{[\mathbb{Y}]}(tv)) - GW^2(\mathbb{X},\mathbb{Y})}{t} \\ &= \sum_{i,j\in[M]}(\mathbf{X}_{ij}-\mathbf{Y}_{ij})v_{ij}\mathrm{q}_i\mathrm{q}_j \\ &= \langle[\mathbf{X}-\mathbf{Y}],[v]\rangle_{\mathrm{Tan}_{[\mathbb{Y}]}}. \end{aligned}$$

Therefore, the gradient of the functional $[\mathbb{Y}]\longmapsto \frac{1}{2}GW^2(\mathbb{X},\mathbb{Y})$ can be identified with the matrix $\mathbf{X}-\mathbf{Y}$, obtained after blow-up.

Moreover, notice that for the case $S=1$, we have:

$$GW^2(\mathbb{X},\mathbb{Y}) = \mathrm{tr}_{\mathrm{q}}\left((\mathbf{X}-\mathbf{Y})^T(\mathbf{X}-\mathbf{Y})\right) = \|[\mathbf{X}-\mathbf{Y}]\|^2_{\mathrm{Tan}_{[\mathbb{Y}]}}.$$

**General Case $S\geq 1$:** Let us fix a collection $\{[\mathbb{X}^s]\}_{s=1}^S$ of classes of finite networks, $\lambda\in\Delta_{S-1}$, and the functional $G:\mathcal{GW}\to\mathbb{R}_{\geq 0}$ given in (31). Given a finite network $[\mathbb{Y}]$, we want to compute $\nabla G([\mathbb{Y}])$ according to Definition 4.1.

Following the outline provided by the authors in [14], suppose that each $\mathbb{X}^s$ has been aligned to $\mathbb{Y}$, that is, suppose we have applied Algorithm 3 so that each network of $\{\mathbb{Y}=(\mathbf{Y},\mathrm{q}),\mathbb{X}^1=(\mathbf{X}^1,\mathrm{q}),\ldots,\mathbb{X}^S=(\mathbf{X}^S,\mathrm{q})\}$ has $M$ nodes with mass distribution q, and the identity map from $[M]$ to $[M]$ is optimal for each $GW(\mathbb{X}^s,\mathbb{Y})$, in the sense that:

$$GW^2(\mathbb{X}^s,\mathbb{Y}) = \sum_{i,j\in[M]}|\mathbf{X}^s_{ij}-\mathbf{Y}_{ij}|^2\mathrm{q}_i\mathrm{q}_j, \qquad \forall s\in[S].$$

Consider the $M\times M$ matrix $\sum_{s=1}^S\lambda_s\mathbf{X}^s-\mathbf{Y}$. The candidate for $\nabla G([\mathbb{Y}])$ is $[\sum_{s=1}^S\lambda_s\mathbf{X}^s-\mathbf{Y}]\in\mathrm{Tan}_{[\mathbb{Y}]}$. Let $[v]\in\mathrm{Tan}_{[\mathbb{Y}]}$ be an arbitrary tangent vector at $[\mathbb{Y}]$. As before, we can consider representatives of $[\sum_{s=1}^S\lambda_s\mathbf{X}^s-\mathbf{Y}]$ and $[v]$ that are matrices of the same size. By abuse of notation, we denote such representatives as $\sum_{s=1}^S\lambda_s\mathbf{X}^s-\mathbf{Y}$ and $v$, assuming they belong to the space of $M\times M$ matrices endowed with the weighted Frobenius norm, with weight $\mathrm{q}\otimes\mathrm{q}$:

$$\begin{aligned} \langle[v],[\sum_{s\in[S]}\lambda_s\mathbf{X}^s-\mathbf{Y}]\rangle_{\mathrm{Tan}_{[\mathbb{Y}]}} &= \sum_{i,j\in[M]}\left(\sum_{s\in[S]}\lambda_s\mathbf{X}^s_{ij}-\mathbf{Y}_{ij}\right)v_{ij}\,\mathrm{q}_i\mathrm{q}_j \\ &= \sum_{s\in[S]}\lambda_s\sum_{i,j\in[M]}\left(\mathbf{X}^s_{ij}-\mathbf{Y}_{ij}\right)v_{ij}\,\mathrm{q}_i\mathrm{q}_j, \end{aligned} \tag{60}$$

where the second equality holds from the fact that $\sum_{s\in S}\lambda_s=1$. We want to show that $D_vG_\lambda([\mathbb{Y}]) = \langle[v],[\sum_{s\in[S]}\lambda_s\mathbf{X}^s-\mathbf{Y}]\rangle_{\mathrm{Tan}_{[\mathbb{Y}]}}$.

We repeat the same calculations as in the case $S=1$, now for each $s\in[S]$, by considering $\pi^{s,t}$ a GW optimal $M\times M$ coupling in $\Pi(\mathrm{q},\mathrm{q})$ between $(\mathbf{X}^s,\mathrm{q})$ and $(\mathbf{Y}+tv,\mathrm{q})$ (where the last network is a representative of $Exp_{[\mathbb{Y}]}(tv)$), for $t\geq 0$, such that $\lim_{t\to 0}\pi^{s,t}=\mathrm{diag}(\mathrm{q})$,

obtaining

$$\begin{aligned} D_v G_\lambda([\mathbb{Y}]) &= \frac{1}{2}\sum_{s\in[S]}\lambda_s \lim_{t\to 0}\frac{GW^2(\mathbb{X}^s, Exp_{[\mathbb{Y}]}(tv)) - GW^2(\mathbb{X}^s,\mathbb{Y})}{t} \\ &= \sum_{s\in[S]}\lambda_s \sum_{i,j\in[M]}(\mathbf{X}^s_{ij} - \mathbf{Y}_{ij})v_{ij}\mathrm{q}_i\mathrm{q}_j \\ &= \langle [\sum_{s\in[S]}\lambda_s\mathbf{X}^s - \mathbf{Y}], [v]\rangle_{\mathrm{Tan}_{[\mathbb{Y}]}}, \end{aligned}$$

where the last equality holds from (60). Therefore, $\nabla G_\lambda([\mathbb{Y}])$ can be identified with the matrix $\sum_{s\in[S]}\lambda_s\mathbf{X}^s - \mathbf{Y}$, obtained after applying the blow-up algorithm 3. □

We now proceed with a remark on blow-ups.

**Remark B.13.** *Let $[\mathbb{Y}]$ be any finite network class, and let us apply Algorithm 3 with respect to the given templates $\{[\mathbb{X}^s]\}_{s=1}^S$ to obtain the corresponding blow-ups. On the one hand, we have that the blow-up 3-tuple $(Y_b, \omega_{Y_b}, \mu_{Y_b})$ is a representative of the class $[\mathbb{Y}]$. On the other hand, as a consequence of Proposition 4.3,*

$$\nabla G_\lambda([\mathbb{Y}]) = \left[\sum_{s=1}^S \lambda_s\omega_{X_b^s} - \omega_{Y_b}\right] \in \mathrm{Tan}_{[\mathbb{Y}]},$$

*and so*

$$Exp_{[\mathbb{Y}]}([\nabla G_\lambda([\mathbb{Y}])]) = [(Y_b, \cancel{\omega_{Y_b}} + \sum_{s=1}^S \lambda_s\omega_{X_b^s} - \cancel{\omega_{Y_b}}, \mu_{Y_b})] = [(Y_b, \sum_{s=1}^S \lambda_s\omega_{X_b^s}, \mu_{Y_b})].$$

*Now, assume that $\nabla G_\lambda([\mathbb{Y}]) = 0$ for some $\lambda \in \Delta_{S-1}$. Hence,*

$$[(Y_b, \omega_{Y_b}, \mu_{Y_b})] = [\mathbb{Y}] = Exp_{[\mathbb{Y}]}(0) = Exp_{[\mathbb{Y}]}([\nabla G_\lambda([\mathbb{Y}])]) = [(Y_b, \sum_{s=1}^S \lambda_s\omega_{X_b^s}, \mu_{Y_b})]$$

*implying that*

$$\omega_{Y_b} = \sum_{s=1}^S \lambda_s\omega_{X_b^s} \quad \textit{or, equivalently,} \quad \mathbf{Y}_b = \sum_{s=1}^S \lambda_s\mathbf{X}_b^s. \tag{61}$$

*See also* [14, Rmk. 9]. *It is important to remark that the expression $\sum_{s=1}^S \lambda_s\omega_{X_b^s}$ depends on the given network $\mathbb{Y}$. That is, given another network $\mathbb{Z}$, one has to perform Algorithm 3 to $\mathbb{Z}$ and the templates $\{\mathbb{X}^s\}$ getting new representatives of all the networks involved and then the new corresponding expression $\sum_{s=1}^S \lambda_s\omega_{X_b}$ will be different to the above one (61). Thus, it would be better to denote the new representatives of the templates after blow-up with respect to $\mathbb{Y}$ as*

$$\mathbb{X}^s \sim^w (\mathbf{X}^s_{b,Y}, \mathrm{q}_{b,Y}) \qquad \forall s \in [S],$$

*and after blow-up with respect to $\mathbb{Z}$ as*

$$\mathbb{X}^s \sim^w (\mathbf{X}^s_{b,Z}, \mathrm{q}_{b,Z}) \qquad \forall s \in [S].$$

*By transitivity, it holds that*

$$(\mathbf{X}^s_{b,Y}, \mathrm{q}_{b,Y}) \sim^w (\mathbf{X}^s_{b,Z}, \mathrm{q}_{b,Z}) \qquad \forall s \in [S]$$

*However, in general*

$$\left(\sum_{\lambda_s}\mathbf{X}^s_{b,Y}, \mathrm{q}_{b,Y}\right) \not\sim^w \left(\sum_{\lambda_s}\mathbf{X}^s_{b,Z}, \mathrm{q}_{b,Z}\right).$$

*In particular, there may be more than one critical point of $G_\lambda$. The discussion above was meant to avoid confusion:* the expression $\sum_{s=1}^{S} \lambda_s \mathbf{X}_b^s$ does not depend solely on the templates.

We conclude this section by providing a proof of the second part of Lemma 4.5, which does not rely on the first-order optimality condition in GW space derived from the first-order calculus introduced in [14] and reviewed throughout this work.

*Proof of Lemma 4.5.* Our goal is to provide a direct proof for the implication

$$[\mathbb{Y}^*] \in \mathrm{Bary}(\{[\mathbb{X}^s]\}_{s\in[S]}) \Longrightarrow \mathbb{Y}^* \sim^w \left( \sum_{s=1}^{S} \lambda_s \mathbf{X}_b^s, \mathrm{q}_b \right).$$

The spaces $\mathbb{X}_b^s = (\mathbf{X}_b^s, \mathrm{q}_b)$, for $s \in [S]$, and $\mathbb{Y}_b^* = (\mathbf{Y}_b^*, \mathrm{q}_b)$ are obtained by applying Algorithm 3. Let $M_b$ be the cardinality of these new spaces, that is, $\mathbf{X}_b^s, \mathbf{Y}_b^* \in \mathbb{R}^{M_b \times M_b}$, for all $s \in [S]$, and $\mathrm{q}_b \in \mathcal{P}_{M_b}$. By re-aligning the new nodes, one can consider the identity map as an OT map for each problem $GW(\mathbb{X}_b^s, \mathbb{Y}_b^*)$, $s = 1, \ldots, S$. In other words, as in (30), we have:

$$\begin{aligned} GW^2(\mathbb{X}^s, \mathbb{Y}^*) &= GW^2(\mathbb{X}_b^s, \mathbb{Y}_b^*) \\ &= \sum_{j,k\in[M_b]} |\mathbf{X}_b^s[j,k] - \mathbf{Y}_b^*[j,k]|^2 \, \mathrm{q}_b[j]\mathrm{q}_b[k] \\ &= \mathrm{tr}_{\mathrm{q}_b}\left((\mathbf{X}_b^s - \mathbf{Y}_b^*)^T(\mathbf{X}_b^s - \mathbf{Y}_b^*)\right). \end{aligned}$$

We proceed as in the proof of Theorem 3.3 on the fixed-point approach. Since one can consider the identity map on $[M_b]$ as an optimal map for the problem $GW((\mathbf{X}_b^s, \mathrm{q}_b), (\mathbf{Y}_b^*, \mathrm{q}_b))$, in this case, the functional $J_\lambda : \mathbb{R}^{M_b \times M_b} \to \mathbb{R}_{\geq 0}$ can be written as

$$J_\lambda(\mathbf{Y}) = \sum_{s\in[S]} \lambda_s \sum_{j,k\in[M_b]} |\mathbf{X}_b^s[j,k] - \mathbf{Y}[j,k]|^2 \, \mathrm{q}_b[j]\mathrm{q}_b[k] = \sum_{s\in[S]} \lambda_s \, \mathrm{tr}_{\mathrm{q}_b}\left((\mathbf{X}_b^s - \mathbf{Y})^T(\mathbf{X}_b^s - \mathbf{Y})\right)$$

(compare to the expression (12)). We know that it admits one and only one minimizer, which is in fact given by the expression

$$\sum_{s=1}^{S} \lambda_s \mathbf{X}_b^s.$$

This can be deduced from (38) or simply because minimizing $J_\lambda$ coincides with the barycentric problem within the Euclidean geometry (see (43) in App. A). Also, since $\mathbb{Y}^*$ is a GW

barycenter, we have

$$\begin{aligned}
\sum_{s\in[S]} \lambda_s\, GW^2(\mathbb{X}^s, \mathbb{Y}^*) &= \min_{[\mathbb{Y}]} \sum_{s\in[S]} \lambda_s\, GW^2(\mathbb{X}^s, \mathbb{Y}) \\
&= \min_{[\mathbb{Y}]} \sum_{s\in[S]} \lambda_s\, GW^2(\mathbb{X}^s_b, \mathbb{Y}) \\
&\leq \sum_{s\in[S]} \lambda_s\, GW^2\left((\mathbf{X}^s_b,\, \mathrm{q}_b), \left(\sum_{r\in[S]} \lambda_r \mathbf{X}^r_b,\, \mathrm{q}_b\right)\right) \\
&\leq \sum_{s\in[S]} \lambda_s \sum_{j,k\in[M_b]} \left| \mathbf{X}^s_b[j,k] - \left(\sum_{r\in[S]} \lambda_r \mathbf{X}^r_b\right)[j,k] \right|^2 \mathrm{q}_b[j]\mathrm{q}_b[k] \\
&= \min_{\mathbf{Y}\in\mathbb{R}^{M_b\times M_b}} J_\lambda(\mathbf{Y}) \\
&\leq \sum_{s\in[S]} \lambda_s \sum_{j,k\in[M_b]} \left|\mathbf{X}^s_b[j,k] - \mathbf{Y}^*_b[j,k]\right|^2 \mathrm{q}_b[j]\mathrm{q}_b[k] \\
&= \sum_{s\in[S]} \lambda_s\, GW^2(\mathbb{X}^s_b, \mathbb{Y}^*_b) \\
&= \sum_{s\in[S]} \lambda_s\, GW^2(\mathbb{X}^s, \mathbb{Y}^*)
\end{aligned}$$

(where the second to last of the inequalities follows from the fact that $\mathrm{diag}(\mathrm{q}_b) \in \Pi(\mathrm{q}_b, \mathrm{q}_b)$ is an admissible plan for $GW\left((\mathbf{X}^s_b,\, \mathrm{q}_b), \left(\sum_{r\in[S]} \lambda_r \mathbf{X}^r_b,\, \mathrm{q}_b\right)\right)$ but not necessarily an optimal coupling), establishing that all the inequalities in the chain are actually equalities. Therefore, the matrix $\mathbf{Y}^*_b$ is a minimizer of $J_\lambda$, implying that $\mathbf{Y}^*_b = \sum_{r\in[S]} \lambda_s \mathbf{X}^s_b$ (by uniqueness of the minimum of $J_\lambda$, which is strictly convex due to having $\mathrm{q}_b$ with all entries strictly positive). Hence,

$$\mathbb{Y}^* \sim^w (\mathbf{Y}^*_b, \mathrm{q}_b) = \left(\sum_{s\in[S]} \lambda_s \mathbf{X}^s_b, \mathrm{q}_b\right).$$

□

## Appendix C. Computational Complexity of Algorithms 2 and 4

For simplicity, let us assume that the number of nodes is the same across the templates and the output, that is, assume $N^s = N$ for all $s \in [S]$.

**Computation of GW Distances:** The Gromov–Wasserstein problem is inherently NP-hard due to its formulation as a quadratic assignment problem [31, 50, 10, 47, 74]. In practice, approximation schemes are employed to mitigate this computational burden. For example, if we consider two networks with $N$ and $M$ nodes, respectively, evaluating the GW objective for a fixed coupling matrix incurs a computational cost of $\mathcal{O}(N^2M^2)$ that can be approximated using entropic regularization [46] reducing its cost to $\mathcal{O}((N^2M + NM^2))$. The original optimization problem can then be approximately solved using a sequence of Sinkhorn iterations, with each iteration cost being dominated by the complexity of evaluating the GW objective. Taking $L$ iterations to convergence, the total cost of solving a single GW problem becomes $\mathcal{O}((N^2M + NM^2)L)$.

In our experiments, we adopt this approach with low entropy regularization, aiming for approximations that closely match the true GW cost and optimal transport plan. More precisely, we use the function `ot.gromov.gromov_barycenters` from the POT library [21] based on the fixed-point algorithm proposed in [46], which, under low entropy, is similar to Algorithm 1.

**Algorithm 2:**

(1) Computation of GW distances: First, one needs to solve (or estimate) as many GW problems as templates ($S$). Thus, extending the discussion above to $S$ templates, the overall complexity to *estimate* $\{\pi(\mathbf{Y}, s)\}_{s\in[S]}$ is $\mathcal{O}((N^2M + NM^2)LS)$, using the approximation through the entropic regularized version of the GW distance.
(2) Computing each matrix $F(\mathbf{Y}, s)$ requires $\mathcal{O}(N^2M + NM^2)$ operations, leading to a total complexity of $\mathcal{O}((N^2M + NM^2)S)$.
(3) Each trace operation between two $M \times M$ matrices costs $\mathcal{O}(M^2)$. Therefore, computing the matrix $\mathcal{Q}$ requires $\mathcal{O}(M^2S^2)$ operations (or, more precisely, $\mathcal{O}(M^2\frac{S(S+1)}{2})$ leveraging on the fact that $\mathcal{Q}$ is symmetric).
(4) Solving the quadratic program $\min_{\lambda\in\Delta_{S-1}} \lambda^T\mathcal{Q}\lambda$ is equivalent to $\min_{\lambda\in\Delta_{S-1}} \lambda^T K\lambda - 2\lambda^T b$ (see (24)).

In our simulations, this is done using the iterative Alternating Direction Method of Multipliers (ADMM)-based first-order method, implemented via the function `cvxpy.OSQP` within the `cvxpy` optimization library in Python, which has a computational complexity of $\mathcal{O}(S^3 + L'S^2)$, where $L'$ is the number of iterations.

In practice, the number of iterations $L'$ can be much larger than $S$ (since, in this work, our experiments involve a small number $S$) thus making this unnecessarily costly. A heuristic to reduce this is to relax the linear problem $K\lambda = b$ s.t. $\lambda \in \Delta_{S-1}$ by only considering the equality restriction $\sum_{s\in[S]} \lambda_s = 1$. This is done using linear solvers that cost $\mathcal{O}(S^3)$.

This yields a total complexity of $\mathcal{O}((N^2M + NM^2)LS + M^2S^2 + S^3)$ (under the entropic regularization scheme). Since the number of templates $S$ is typically much smaller than the number of nodes $N$, we can conclude that the computational complexity of Algorithm 2 is comparable to solving $S$ Gromov–Wasserstein optimization problems (8). This could be further improved by parallelizing the $S$ Gromov-Wasserstein computations.

**Algorithm 4:**

(1) Blow-up step: The computational complexity of Algorithm 3, is essentially equivalent to solving $S$ Gromov-Wasserstein optimization problems. In practice, we approximate each GW computation with its regularized version (using low entropy).

The $S$ concatenated GW problems that we need to solve are defined between networks whose sizes increase with $S$. Specifically, after performing the first blow-up between the first template $\mathbb{X}^1$, with $N$ nodes, and $\mathbb{Y}$, with $M$ nodes, we obtain new networks that are weakly isomorphic to the originals but have size $|\mathrm{supp}(\pi^1)| \geq \max\{N, M\}$, where $\pi^1 \in \Pi(\mathrm{p}^1, \mathrm{q})$ is an optimal coupling for $GW(\mathbb{X}^1, \mathbb{Y})$. This process continues similarly for subsequent steps, involving blow-ups for the rest of the templates $\mathbb{X}^2, \ldots, \mathbb{X}^S$ with respect to $\mathbb{Y}$, possibly increasing the number of nodes at each iteration $s \in [S]$.

In the case of classical OT, any optimal coupling–which is a feasible solution of the corresponding linear program–has support size at most $N + M - 1$, assuming the source and target discrete measures have support of size $N$ and $M$, respectively (see, e.g., [47, Prop. 3.4]). Linear programming theory does not apply in the GW case due

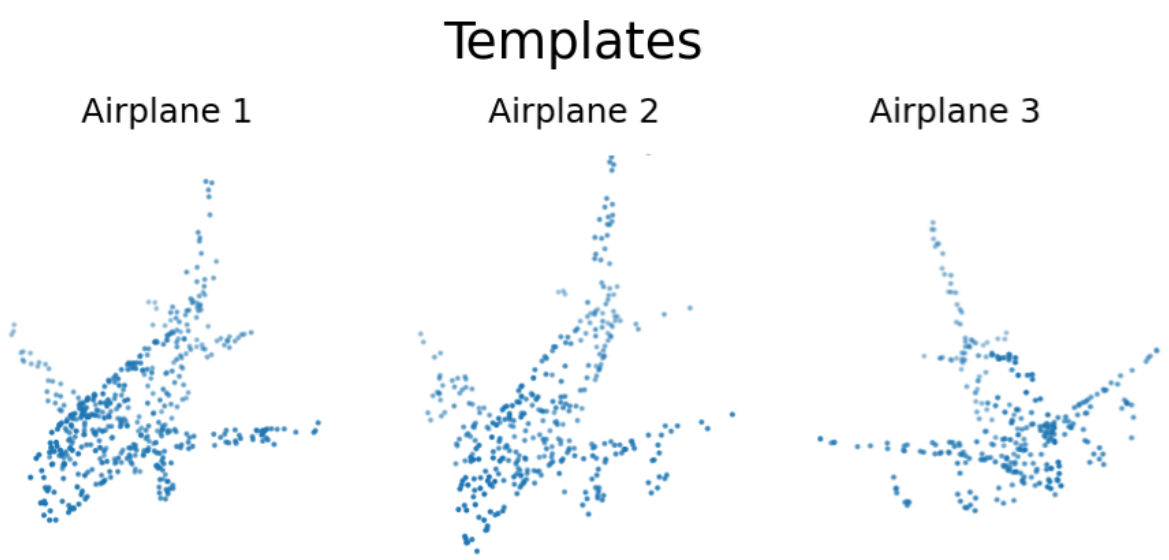



**Figure 11.** Three sample point clouds from the category 'airplane' in the ModelNet40 dataset. For each point cloud, we randomly select between 300 and 500 samples.

to the quadratic nature of the objective, even though the optimization is performed over the same set of transport plans (or couplings). As a result, no support size bound analogous to that in classical OT is currently known. For empirical insight, we refer the reader e.g. to [14, App., Sec. C], where the authors observe that representations often occur in a space much smaller than the naive requirement of size $NM$.

As a result, accurately estimating the total computational cost of this step is challenging.

(2) Suppose that, after the blow-up step, each $\mathbb{X}^s$ has been aligned to $\mathbb{Y}$, so that the collection $\{\mathbb{Y}_b = (\mathbf{Y}, \mathrm{q}_b), \mathbb{X}_b^1 = (\mathbf{X}^1, \mathrm{q}_b), \dots, \mathbb{X}_b^S = (\mathbf{X}^S, \mathrm{q}_b)\}$ consists of networks with $M_b$ nodes. Then, similarly to Algorithm 2, computing the matrix $\mathcal{A}$ is of order $\mathcal{O}(M_b^2 S^2)$, and solving the quadratic program over the simplex $\min_{\lambda \in \Delta_{S-1}} \lambda^T \mathcal{Q} \lambda$ costs approximately $\mathcal{O}(S^3)$.

## Appendix D. Experiments

This section aims to supplement Section 5 with additional visualizations and experiments. App. D.1 and App. D.3 expand on the material in Sections 5.1 and 5.2, respectively. App. D.4 presents an additional application of the proposed GW-BCM.

### D.1. Reconstruction Performance of Algorithms 2 and 4 Under the GW-BCM.

D.1.1. *Experiments with 3D Point Clouds.* In addition to Figures 6 and 7 in the main text, we include the following:

- Figure 11: The templates from the ModelNet40 - Princeton 3D Object Dataset [70], used for synthesizing GW barycenters in all the figures dealing with 3D data.
- Figure 12: By using the templates in Figure 11 and uniform weights $\lambda = (\frac{1}{3}, \frac{1}{3}, \frac{1}{3})$, in Figure 6 in the main text, we start by synthesizing a GW barycenter following the fixed-point approach (i.e., by using the function `ot.gromov.gromov_barycenters` from the POT Library [21]). Instead, in the new Figure 12, the synthesis of the initial barycenter is performed as suggested in Proposition 4.3, using a convex combination of *some* blow-up templates, $\mathbf{Y} = \sum_{s=1}^{S} \mathbf{X}_b^s$. That is, in Figure 6, the synthetic barycentric shape belongs to a GW barycenter space of the form (10), while in Figure 12, emulates to belong to the space of the form (33).

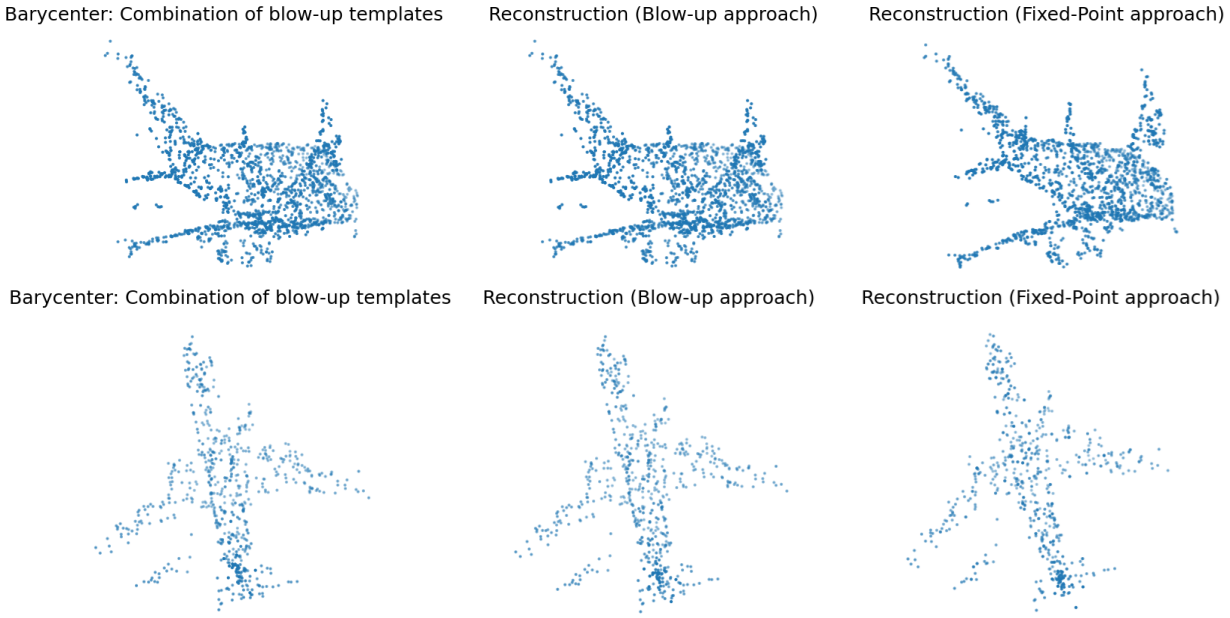



**Figure 12.** Reconstructions of synthetic GW-like barycenters built as suggested in Section 3.1, using *three* (top panel) and *two* (bottom panel) template point clouds of the same class ('airplane'), and uniform vector of weights, i.e., $\lambda = (\frac{1}{3}, \frac{1}{3}, \frac{1}{3})$ (top panel), and $\lambda = (\frac{1}{2}, \frac{1}{2})$ (bottom panel). **Left-most panels:** Unlike Figure 6, here we synthesize convex combinations (top panel) $\mathbf{Y} = \sum_{s=1}^{3} \frac{1}{3}\mathbf{X}_b^s$ and (bottom panel) $\mathbf{Y} = \sum_{s=1}^{2} \frac{1}{2}\mathbf{X}_b^s$, where $\mathbf{X}_b^s$ are blow-up template matrices. According to Remark B.9, in the case of considering 2 templates, such convex combination gives rise to an element in the GW barycenter space generated by those 2 templates. **Middle panels:** MDS of the matrices given by expression (40) after applying Algorithm 4 to estimate $\lambda$. The computed error between the true $\lambda$-vector and its estimate is numerically zero, within floating-point precision (float64), and the GW distance between the two shapes in the top left and bottom right panels is $GW((\mathbf{Y}, \mathrm{q}_b), (\mathbf{Y}_{\mathrm{barybu}}, \mathrm{q}_b)) \approx 10^{-17}$. **Right-most panels:** MDS of the matrices given by expression (39) after applying Algorithm 2 to estimate the vector $\lambda$. The computed error between the true $\lambda$-vector and its estimation is of order $10^{-1}$ (top panel) and $10^{-2}$ (bottom panel), and the GW distance between the first and last shapes is $GW((\mathbf{Y}, \mathrm{q}_b), (\mathbf{Y}_{\mathrm{bary}}, \mathrm{q}_b)) \approx 10^{-3}$.

- Figure 14: We also include Figure 14, which builds on Figures 7a and 7b: Using the three 3D template point clouds from the ModelNet40 dataset shown in Figure 11, we visualize the performance of the two analysis algorithms (Algorithms 2 and 4) in estimating random GW barycentric coordinates $\lambda$ corresponding to GW barycenters constructed through different techniques.

**Comparison and Analysis of the Experiments Illustrated in Figures 6 and 7 in the Main Text and in the New Figures 12, 13, 14:** Algorithm 2 is derived from a fixed-point formulation for computing GW barycenters, compatible with the POT function `ot.gromov.gromov_barycenters` (Section 3). In contrast, Algorithm 4 is based on defining functional gradients and Karcher means within the GW setting via the blow-up technique (Section 4). The experiments visualized in Figure 6 in the main text and in Figure 12 illustrate the qualitative and quantitative performance of our algorithms in their native settings, while also assessing how well each performs when applied outside its original framework. The results show that Algorithm 2 performs with high accuracy when using fixed-point barycenters (Figure 6, bottom left; Figures 7a and 7b, left; and Figure 14, top left), but less effectively with blow-up-based ones (Figure 12, left-most panel; and Figure 14, bottom left). Conversely, Algorithm 4 performs best when using blow-up-based barycenters (Figure 12, middle panel; and Figure 14, bottom right), but still

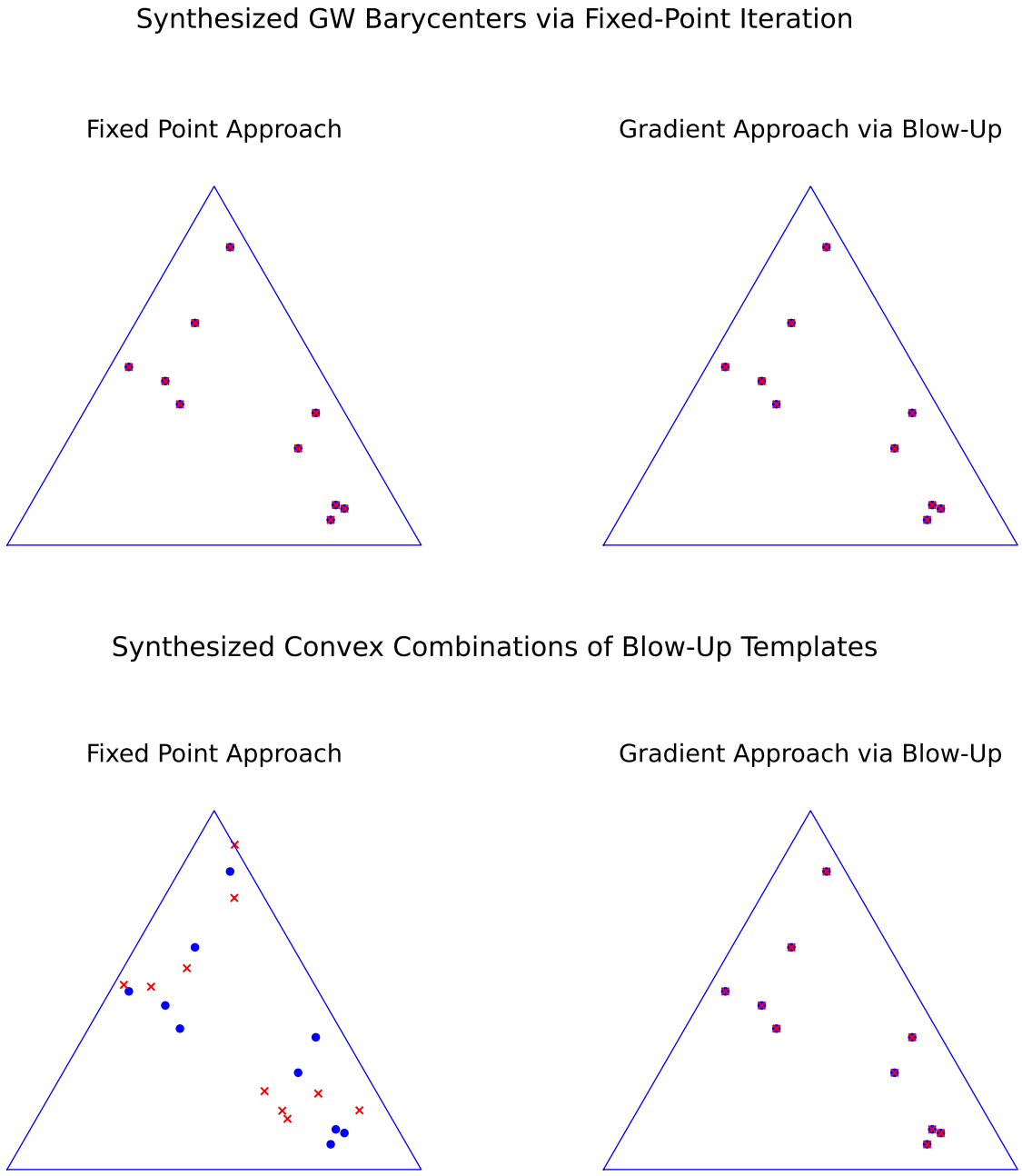



**Figure 13.** Depiction of 10 randomly generated GW barycenter coordinates $\lambda \in \Delta_2$ (blue dots) and their estimations (red crosses) via Algorithms 2 (**first column**) and 4 (**second column**). GW barycenters are synthesized for each $\lambda$ using the templates from Figure 11 *sampled at the same rate* (each with 150 points). **Top row:** Same as Figure 7a. **Bottom row:** Templates $\{\mathbf{X}^s\}_{s=1}^S$ are blown-up to $\{\mathbf{X}_b^s\}_{s=1}^S$ (same size) to allow interpretation of barycenters as convex combinations $\sum_{s=1}^S \lambda_s \mathbf{X}_b^s$.

yields reasonable results with fixed-point ones (Figures 6, 7a, 7b, right panels; and Figure 14, top right). Finally, when the fixed-point iteration scheme is used to synthesize the barycenters, Algorithm 4 for recovering the GW barycentric coordinates performs better when the templates are of the same size (compare the right panels of Figures 7a and 7b).

It is important to highlight that, in the synthesis of point clouds for the experiments in Figure 12 and the bottom panels of Figures 13 and 14, convex combinations of blow-up templates correspond to true GW barycenters when only two templates are involved,

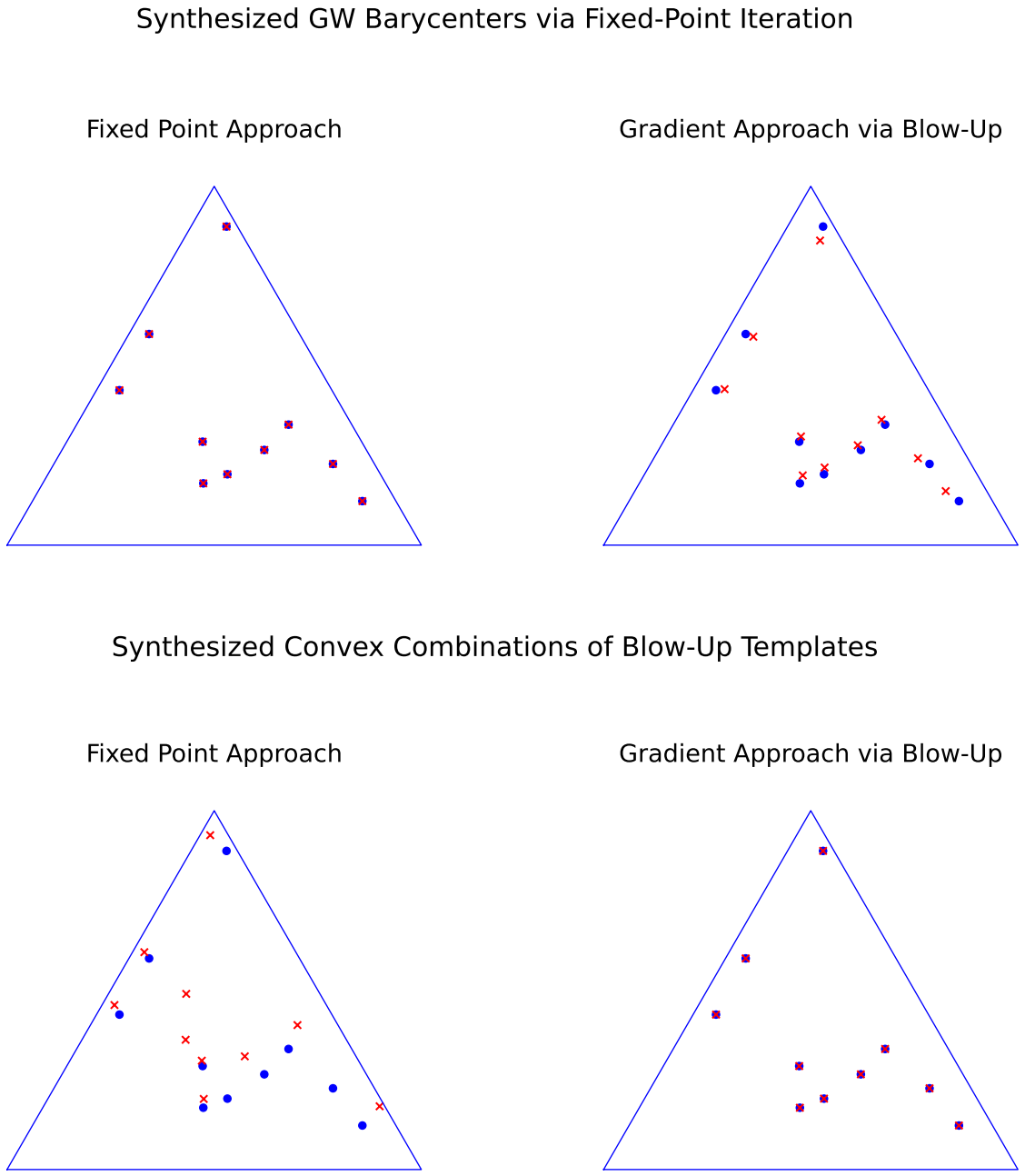



**Figure 14.** Depiction of 10 randomly generated GW barycenter coordinates $\lambda \in \Delta_2$ (blue dots) and their estimations (red crosses) via Algorithms 2 (**first column**) and 4 (**second column**). GW barycenters are synthesized for each $\lambda$ using the templates from Figure 11 *sampled at different rates*, at random, each point cloud having between 50 and 150 points. **Top row:** Same as Figure 7b. **Bottom row:** Templates $\{\mathbf{X}^s\}_{s=1}^S$ are blown-up to $\{\mathbf{X}_b^s\}_{s=1}^S$ (same size) to allow interpretation of barycenters as convex combinations $\sum_{s=1}^S \lambda_s \mathbf{X}_b^s$.

as noted in Remark B.9. However, when more than two templates are considered–as in the top panel of Figure 12 and in Figures 13 and 14–such convex combinations do not necessarily yield *true* GW barycenters. This may help explain why Algorithm 2 performs poorly in the bottom-left panel of Figure14.

D.2. **Experiments with 2D Point Clouds.** In a similar manner to Figure 6 and Figure 12, Figures 15 and 16 provide a visualization of the performance of Algorithms 2

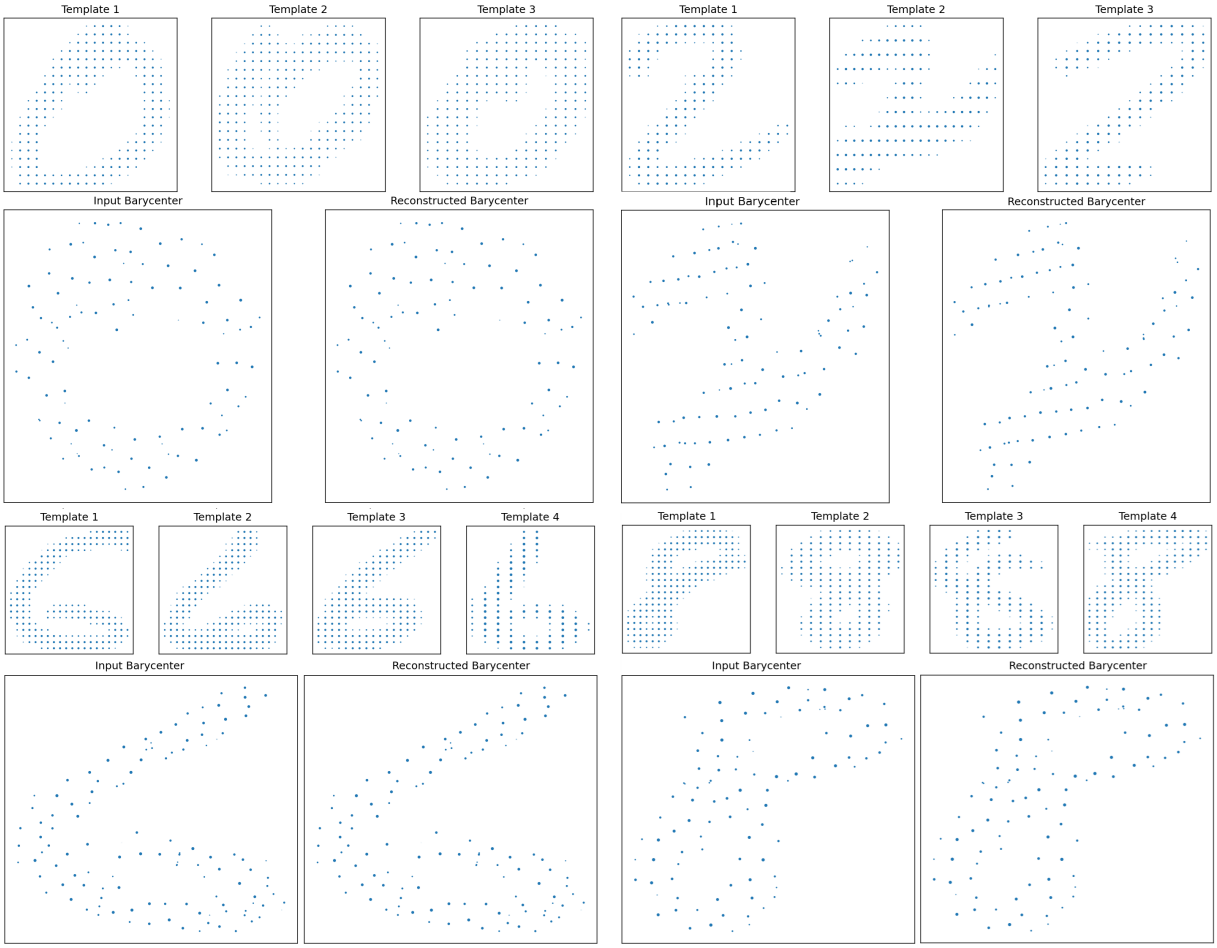



**Figure 15.** In this figure, we depict the following procedure. First, select a digit class and choose $S$ templates within that class. Then, sample a random vector $\lambda$ from the simplex $\Delta_{S-1}$, and synthesize a GW barycenter using these weights via the function `ot.gromov.gromov_barycenters` from the POT Library. Next, attempt to recover $\lambda$ via Algorithm 2 and reconstruct the barycenter as in formula (39). MDS is used for visualization. In this example, we consider digits 0, 2, 6, and 8 from the Point Cloud MNIST 2D dataset [23]. We select 3 templates for classes 0 and 2, and 4 templates for classes 6 and 8.

and 4 on 2D point clouds (instead of 3D) under the GW-BCM assumption. We use the Point Cloud MNIST 2D dataset [23]. On the one hand, in Figure 15 we use the function `ot.gromov.gromov_barycenters` from the POT Library [21], which is based on a fixed-point algorithm similar to Algorithm 1, to synthesize GW barycenters, and then we apply Algorithm 2 to recover the GW barycentric coordinates $\lambda$. On the other hand, in Figure 16 we synthesize a GW barycenter as a convex combination of *some* blow-up template matrices (all of the same size); and then we then apply Algorithm 4 to recover the GW barycentric coordinates $\lambda$, that is, the coefficients of the convex combination.

D.3. **Classification.** We provide supplementary material that builds on Section 5.2 (see App. D.3.1), and two additional classification methods based on the proposed GW-BCM approach (see App. D.3.3 and App. D.3.2).

D.3.1. *t-SNE in the GW Barycentric Coordinate Space.* In addition to Figures 8 and 9, we provide Figures 17, 18, 19 and 20 where, besides showing the t-SNE embedding, we

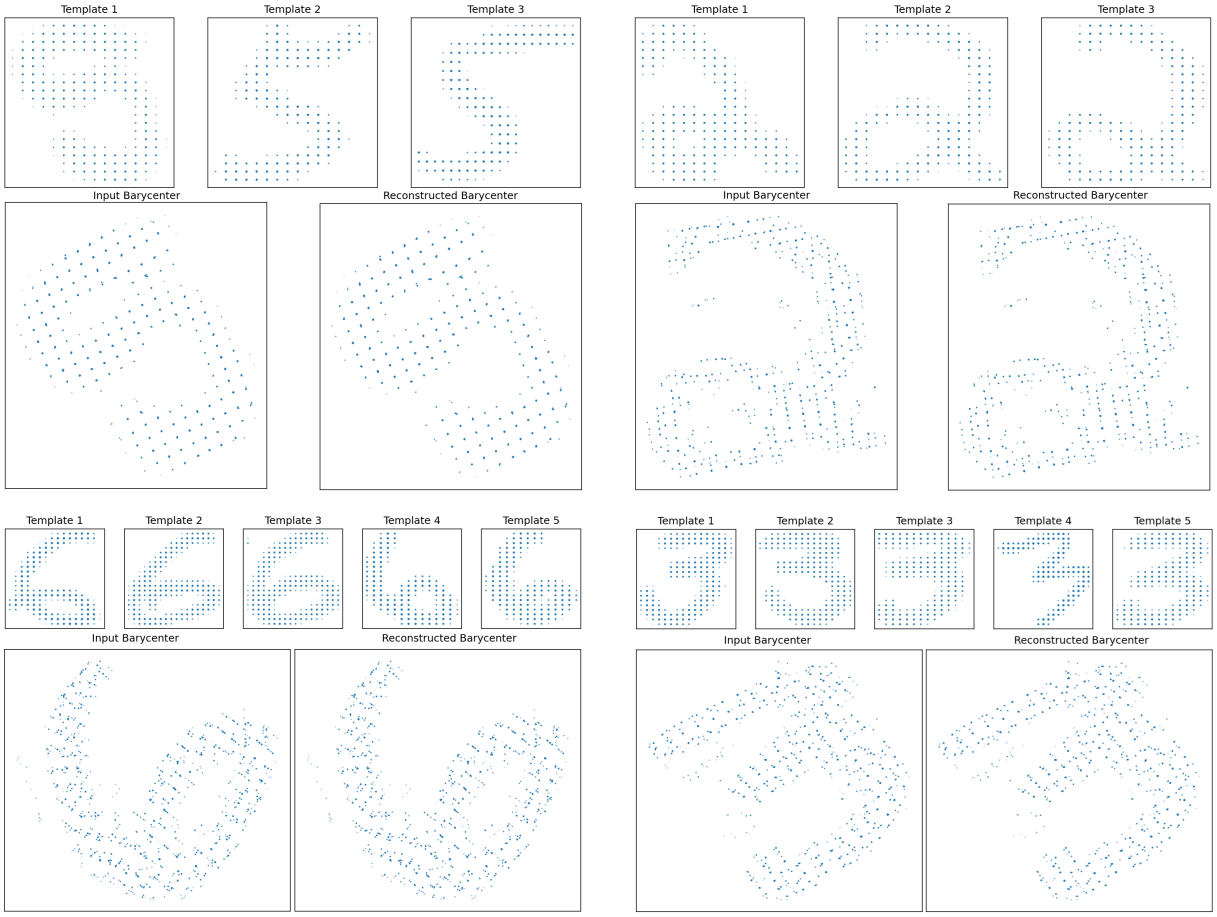


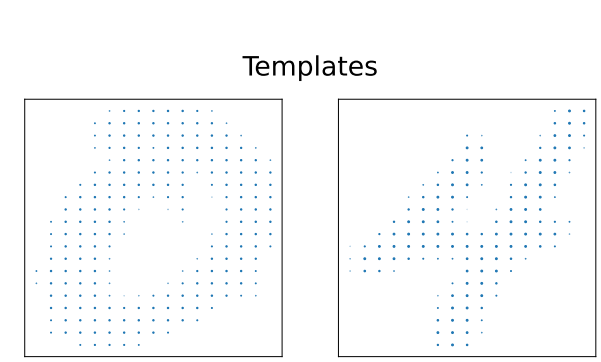

**Figure 16.** In this figure, we depict the following procedure. First, select a digit class and choose $S$ templates within that class, and perform their blow-up obtaining $S$ matrices $\{\mathbf{X}_b^s\}_{s=1}^S$ of the same size. Then, sample a random vector $\lambda$ from the simplex $\Delta_{S-1}$, and synthesize convex combinations of the blow-up template matrices $\sum_{s=1}^S \lambda_s \mathbf{X}_b^s$. Next, attempt to recover $\lambda$ via Algorithm 4 and reconstruct the barycenter as in formula (40). MDS is used for visualization. In this example, we consider digits 5, 2, 6, and 3 from the Point Cloud MNIST 2D dataset [23]. We select 3 templates for classes 5 and 2, and 5 templates for classes 6 and 3.

include the *K-Means clusters* and the corresponding *confusion matrix*[19]. For the first three mentioned figures (17, 18 and 19) we use Algorithm 2 for estimating GW barycentric coordinates, and for the last one (20) we use Algorithm 4.

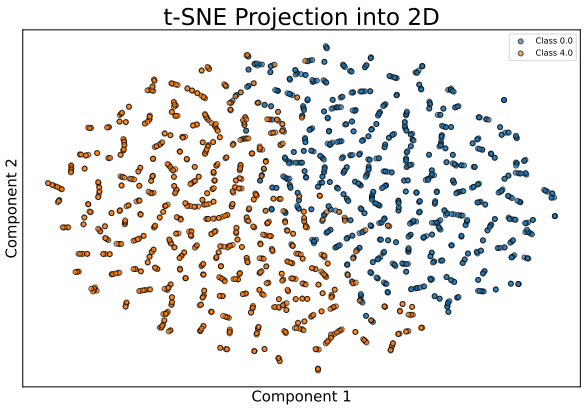
D.3.2. *Minimum GW Barycenter Loss - Experimental Setup.*

(1) Let $n$ be the number of classes in a dataset. Select $S$ random points of each class.
(2) If needed, preprocess each data point, obtaining elements of the form $(\mathbf{X}, \mathrm{p})$: a dissimilarity or edge weight matrix between nodes, together with a mass distribution on its nodes.
(3) Given an input $(\mathbf{X}, \mathrm{p})$ from the data set, compute the GW barycentric coordinates (i.e., apply Algorithm 2 or 4) using the references from each class separately getting a set of $n$ vectors $\{\lambda_i\}_{i=1}^n$, where $\lambda_i \in \Delta_{S-1}$.

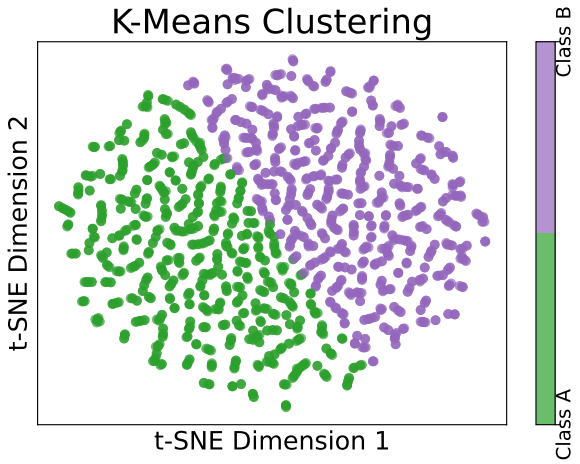
[19]Each cell $(i, j)$ shows the number of samples from true class $i$ that were assigned to cluster $j$, thus a strong diagonal pattern suggests high clustering accuracy, meaning most points were assigned to the correct cluster, while off-diagonal values indicate misclassified samples.



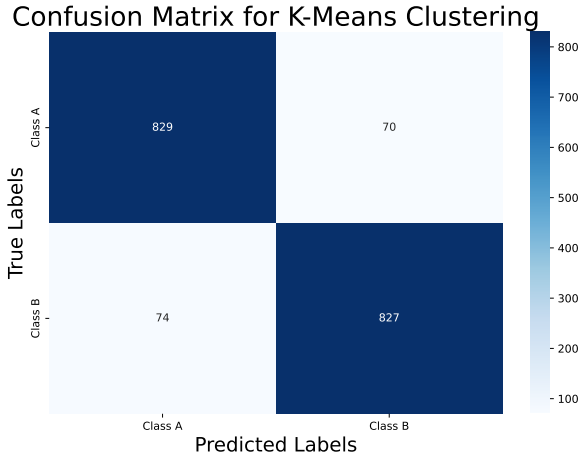

**(a)** Two classes, one template per class.




**(b)** t-SNE embedding.




**(c)** K-Means clustering.




**(d)** Confusion matrix.

**Figure 17.** As in Figure 8 (A), we select one template from the digit classes 0 and 4, and consider 1800 random training samples from the Point Cloud MNIST 2D dataset [23] corresponding to those classes. To estimate GW barycentric coordinates we applied Algorithm 2. Clustering Accuracy: 0.9 via K-Means.

(4) Synthesis set: For each vector $\lambda_i$, synthesize the corresponding GW barycenters using the $S$ templates, obtaining a total of $n$ matrices $\{\mathbf{X}_{\lambda_i}\}_{i=1}^n$ (with probability vectors $\{\mathrm{p}_{\lambda_i}\}_{i=1}^n$).

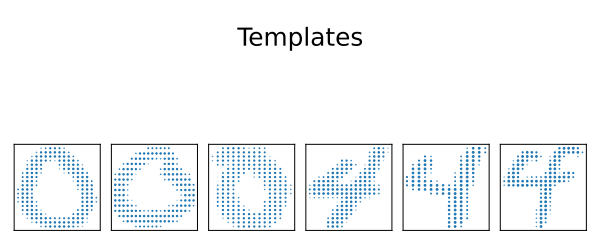
(5) Compute GW distances between input and the synthesized GW barycenters, and select the class with the minimum GW distance, that is:

$$\text{Predicted class for input } (\mathbf{X}, \mathrm{p}) = \arg\min_{1\leq i\leq n} GW((\mathbf{X}, \mathrm{p}), (\mathbf{X}_{\lambda_i}, \mathrm{p}_{\lambda_i})). \tag{62}$$

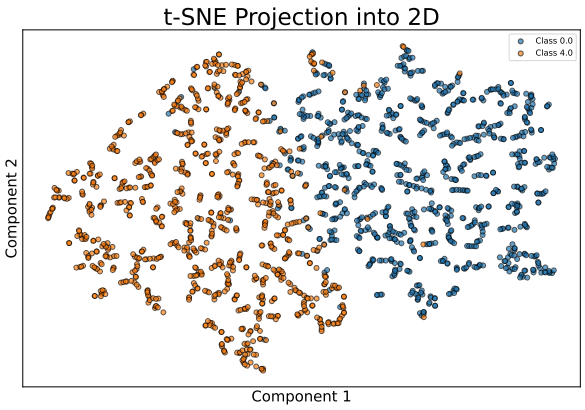
As a proof of concept, we apply the methodology described above to the MNIST Point-Cloud dataset [23] and compute the accuracy between the true and predicted labels. Results are reported below:

- For classifying digit classes 0 and 1 within a set of 400 point cloud digits, the overall accuracy obtained using $S = 1$ or $S = 2$ sample point clouds per class is around 0.91. When increasing $S$ to 4, the accuracy improves to 0.96.
- For classifying digit classes 0, 1, and 2 within a set of 600 point cloud digits, the overall accuracy obtained using $S = 1$ or $S = 2$ sample point clouds per class is 0.8. When increasing $S$ to 4, the accuracy does not improve.

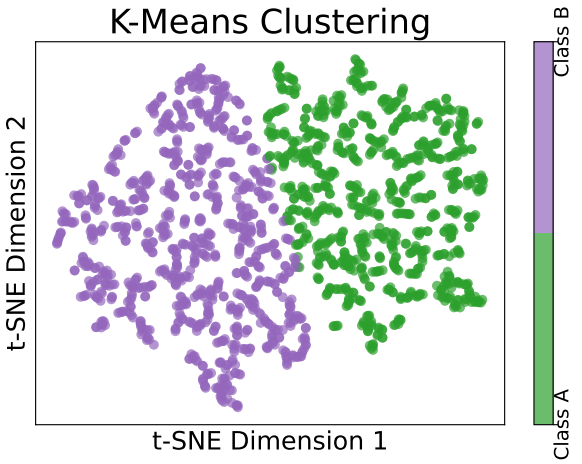
In conclusion, the performance of this approach is not particularly strong, and since it involves GW synthesis with estimated GW barycentric coordinates, along with multiple



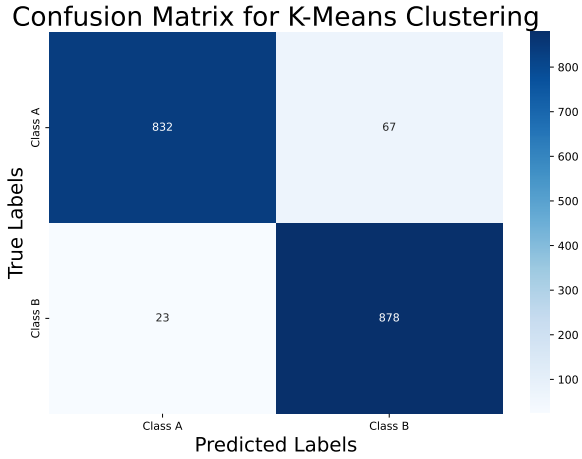

**(a)** Two classes, three templates per class.




**(b)** t-SNE embedding.




**(c)** K-Means clustering.




**(d)** Confusion matrix.

**Figure 18.** Similarly to Figure 9 (A), we select 3 reference templates from the digit classes 0 and 4, and consider 1800 random training samples from the Point Cloud MNIST 2D dataset [23] corresponding to those classes. To estimate GW barycentric coordinates we applied Algorithm 2. Clustering Accuracy: 0.95 via K-Means.

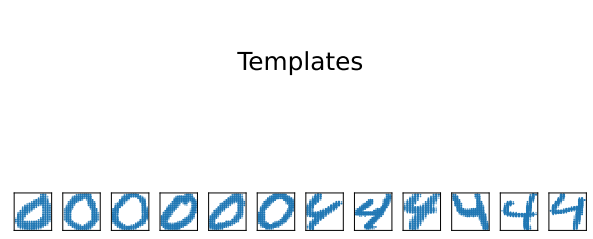
GW computations for classification (see (62)), it is computationally expensive. In the next section, we outline an alternative classification method based on a criterion defined directly on the space of GW barycentric coordinates $\lambda$.

D.3.3. *Maximum Coordinate.* In addition to Figure 3, we provide a complementary illustration that helps interpret the meaning of GW barycentric coordinates. While Figure 3 considers two classes from the Point Cloud MNIST 2D dataset [23], the new Figure 21 extends the setting to three classes.

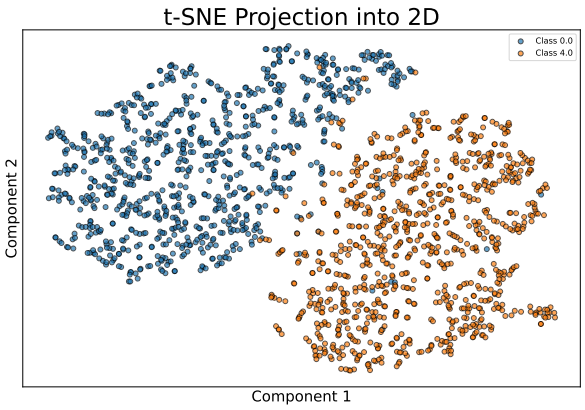
**Description of Figure 21:** From the Point Cloud MNIST 2D dataset [23], we consider three digit classes: 0, 4, and 7. We select one reference point cloud per class, and compute and plot GW barycentric coordinates $(\lambda_1, \lambda_2, \lambda_3)$ for each point cloud in the set. The visualization provided in Figure 21 highlights how GW barycentric coordinates capture meaningful structure in the data, with a particularly clear clustering around the template for digit class 0. In contrast, digit classes 4 and 7 exhibit overlap, suggesting the presence of shared geometric shapes between them.

For further classification, the following general approach could be employed:

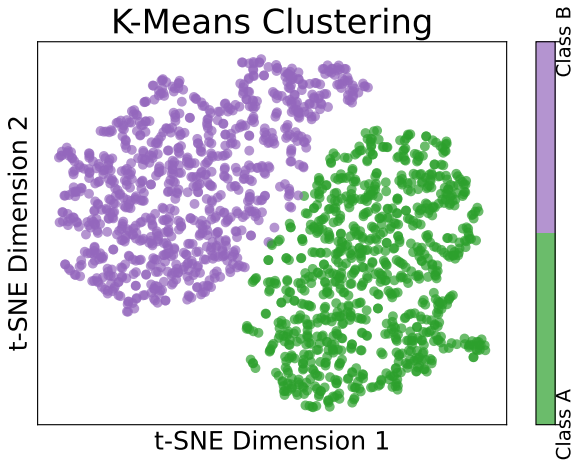
(1) Select templates from each class of the dataset ($k$ samples per class).



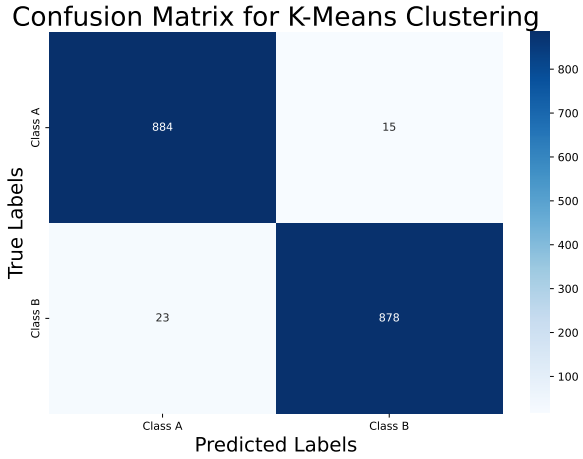

**(a)** Two classes, six templates per class.




**(b)** t-SNE embedding.




**(c)** K-Means clustering.




**(d)** Confusion matrix.

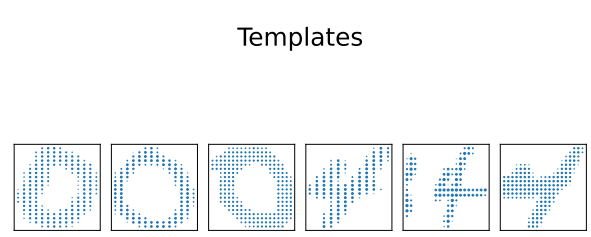
**Figure 19.** Similarly to Figure 9 (B), we select 6 reference templates from the digit classes 0 and 4, and consider 1800 random training samples from the Point Cloud MNIST 2D dataset [23] corresponding to those classes. To estimate GW barycentric coordinates we applied Algorithm 2. Clustering Accuracy: 0.978 via K-Means. Classes are more separated in comparison to Figures 18 and 18 and thus, the accuracy when clustering is higher

.

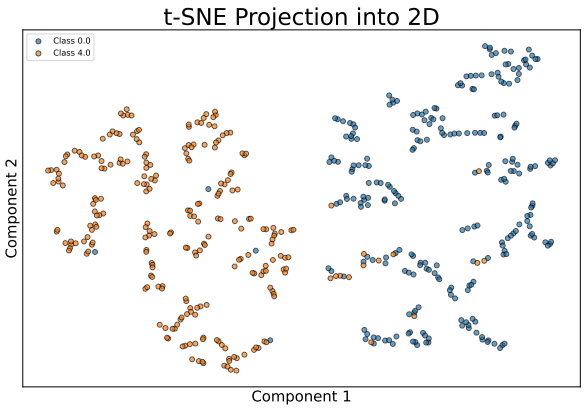
(2) If needed, preprocess each data point, obtaining elements of the form $(\mathbf{X}, \mathrm{p})$: a dissimilarity or edge weight matrix between nodes, together with a mass distribution on its nodes.
(3) Given an input $(\mathbf{X}, \mathrm{p})$, compute its GW barycentric coordinates (i.e., apply Algorithm 2 or 4).
(4) Classify the input into the class corresponding to the template-label with the highest coordinate in the vector of GW barycentric coordinates.

Indeed, in Figure 3, the predicted labels are assigned by selecting the index corresponding to the highest coordinate in the vector $\lambda$.

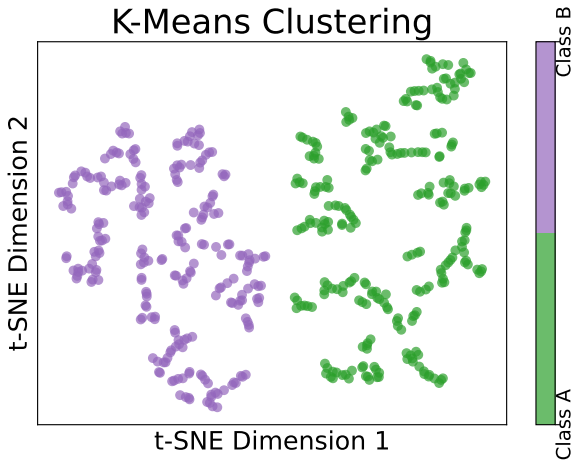
D.4. **Point Cloud Corruption due to Occlusion.** In real-world applications, data corruption is inevitable due to factors such as scene complexity, sensor inaccuracies, and processing imprecision. For point cloud data, we focus on a specific form of corruption: the occlusion of portions of the point cloud. Below, we describe the experimental setup used to address this issue. In our experiments we use the Euclidean distance (in $\mathbb{R}^2$ or $\mathbb{R}^3$) for the dissimilarity matrices, i.e., $\mathbf{Y}_{ij} = \|y_i - y_j\|$. All the synthesized GW barycenters



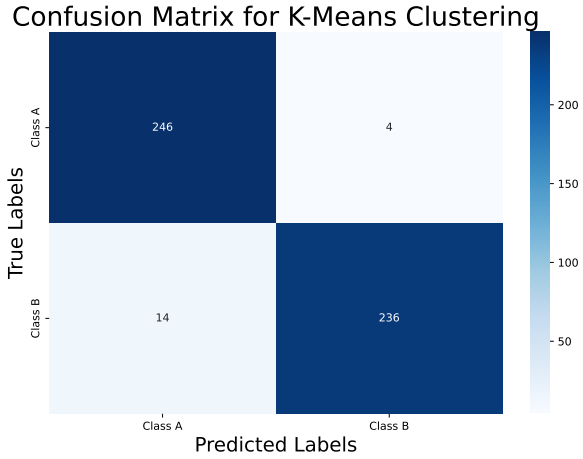

**(a)** Two classes, three templates per class.




**(b)** t-SNE embedding.




**(c)** K-Means clustering.




**(d)** Confusion matrix.

**Figure 20.** Similarly to Figure 18, we select 6 reference templates from the digit classes 0 and 4, and consider 500 random training samples from the Point Cloud MNIST 2D dataset [23] corresponding to those classes. To estimate GW barycentric coordinates we applied Algorithm (3) followed by Algorithm 4. Overall Clustering Accuracy: 0.96 via K-Means.

are computing by applying the function `ot.gromov.gromov_barycenters` from the POT Library [21].

**Experimental Setup:**

(1) Input a 2D or 3D point cloud represented by the discrete probability measure $\mu_Y = \sum_{j=1}^{M} \mathrm{q}[j]\delta_{y_j}$, where $\mathrm{q} \in \mathcal{P}_M$. Compute the dissimilarity matrix $\mathbf{Y}$ between the nodes $\{y_j\}_{j=1}^{M}$. Simulate occlusion by computing $\widetilde{\mu_Y}$ from $\mu_Y$ with a removed portion. Re-normalize the corresponding vector of weights $\widetilde{\mathrm{q}}$ so that it has total mass 1. Compute the dissimilarity matrix $\widetilde{\mathbf{Y}}$ between the remaining nodes.

(2) From the dataset that is used as a model for the given input, select a set of samples to serve as the reference measures $\mu_{X^s} = \sum_{i=1}^{N^s} \mathrm{p}^s[i]\delta_{x_i^s}$, for $s \in [S]$ (if $\mu_Y$ was taken from such dataset, select templates in the same class as $\mu_Y$). Compute the dissimilarity matrices $\mathbf{X}^s$. Perturb the templates letting $\widetilde{\mu_{X^s}}$ be as $\mu_{X^s}$ with a removed portion (the same one as the simulated in step (1)), and re-normalized the vector of weights getting $\widetilde{\mathrm{p}^s}$, for each $s \in [S]$. Compute the new dissimilarity matrices $\widetilde{\mathbf{X}^s}$ across the remaining nodes.

(3) Apply Algorithm 2 (or Algorithm 4) with inputs $\{(\widetilde{\mathbf{X}^s}, \widetilde{\mathrm{p}^s})\}_{s\in[S]}$, $(\widetilde{\mathbf{Y}}, \widetilde{\mathrm{q}})$ to compute estimated coordinates $\widetilde{\lambda}$. After that, apply Algorithm 1 (or Algorithm 4) with inputs

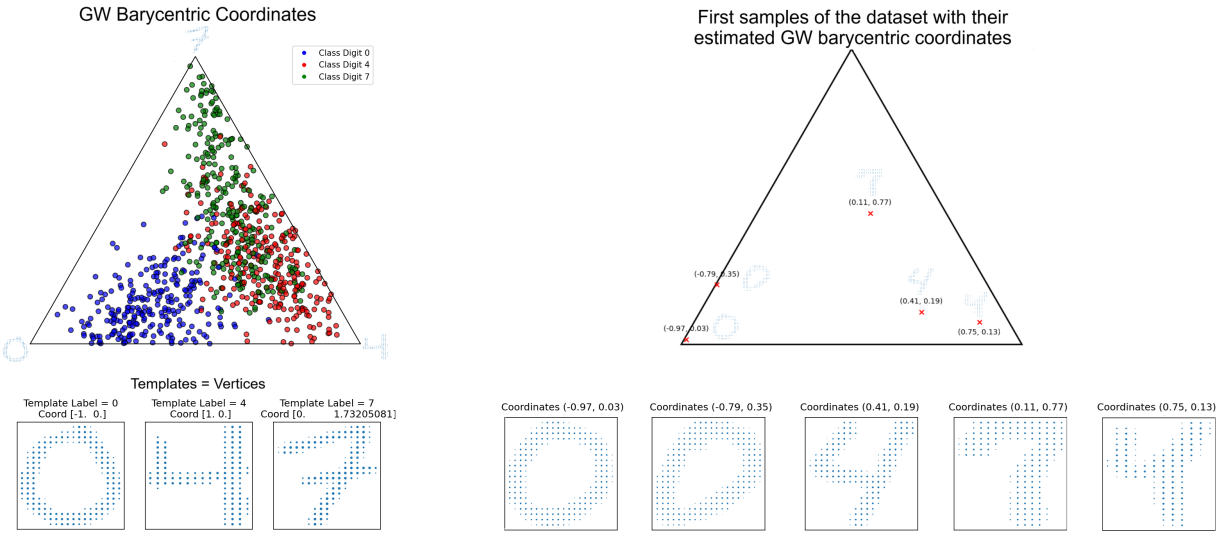



**Figure 21.** From the Point Cloud MNIST 2D dataset [23], we consider three digit classes: 0, 4, and 7. One representative sample from each class is selected and used as a template, placed at the vertices of an equilateral triangle that represents the 2-simplex $\Delta_2$. Then, for 900 randomly selected samples from the dataset, we estimate their GW barycentric coordinates using Algorithm 2, and project them into the triangle (left panel). Each point is colored according to its true class label. As an additional illustration, the right panel shows the first five point clouds from the dataset together with their positions within the triangle according to their computed GW barycentric coordinates.

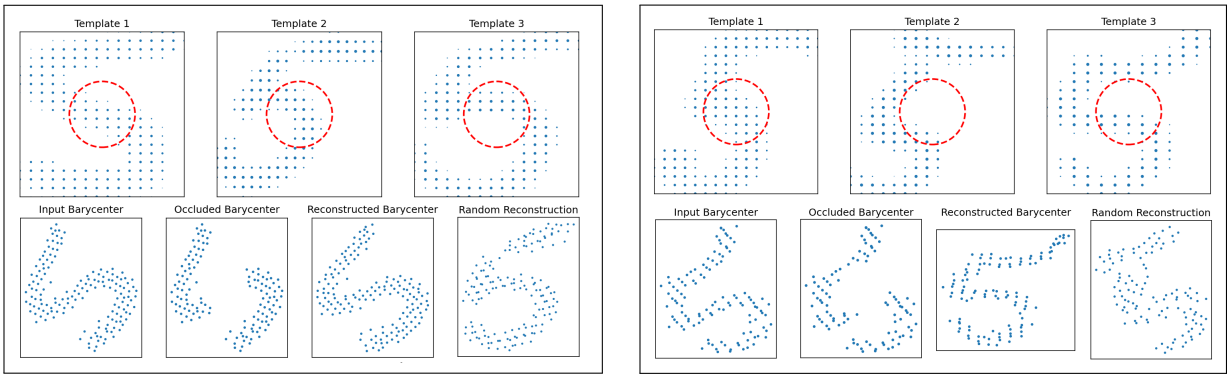



**Figure 22.** Occlusion with a circular mask (rotation-invariant) and reconstruction (two examples). **Top row:** Templates. **Bottom row from left to right:** Synthetic GW barycenter; its perturbation (via occlusion of the central region using a circular mask); the reconstructed point cloud using our proposed method (i.e., GW barycenter coordinates to the corrupted templates are computed using Algorithm 2 and then used to synthesize a GW barycenter with the unperturbed templates); and a random reconstruction (i.e., a synthesized barycenter using a random weight vector $\lambda \in \Delta_2$ and the unperturbed templates).

$\{(\mathbf{X}^s, \mathrm{p}^s)\}_{s\in[S]}$, $\widetilde{\lambda}$, q, $M$ in order to synthesize a barycenter $\mathbf{Y}_{\widetilde{\lambda}}$ from the original (unperturbed) templates. We refer to $\mathbf{Y}_{\widetilde{\lambda}}$ as a reconstruction of $\mathbf{Y}$. Apply MDS embedding (with 2 or 3 components) to $\mathbf{Y}_{\widetilde{\lambda}}$ in order to visualize the recovered point cloud.

In the examples shown in Figure 22, the BCM paradigm proves to be an effective approach to image reconstruction, as evidenced by its ability to recover the missing regions of a perturbed Gromov–Wasserstein (GW) barycenter. A synthetic barycenter is partially occluded using a circular mask, simulating structured data loss. Leveraging geometric

information from the original templates (top panel), the BCM framework successfully reconstructs the barycenter (bottom right).

## Appendix E. Wasserstein Barycenters and Gromov-Wasserstein Barycenters

In the context of the Wasserstein space, both approaches for computing Wasserstein barycenters, namely the fixed-point scheme and the gradient method, can be interpreted as the same. Indeed, let us consider templates $\{\mu^s\}_{s=1}^S$ in the space $\mathcal{P}_2(\mathbb{R}^d)$ of probability measures on $\mathbb{R}^d$ with finite second moments. Given $\lambda \in \Delta_{S-1}$, the functional $G_\lambda$ in (31) is replaced by

$$\mathcal{P}_2(\mathbb{R}^d) \ni \nu \longmapsto \frac{1}{2}\sum_{s=1}^S \lambda_s W_2^2(\nu, \mu^s). \tag{63}$$

If all measures are absolutely continuous with respect to the Lebesgue measure on $\mathbb{R}^d$, its Fréchet derivative [22] can be written as

$$\sum_{s=1}^S \lambda_s (Id - T^{\nu\to\mu^s}), \tag{64}$$

where $Id : \mathbb{R}^d \to \mathbb{R}^d$ is the identity map, and $T^{\nu\to\mu^s} : \mathbb{R}^d \to \mathbb{R}^d$ is the *OT map*[20] from $\nu$ to $\mu^s$. Thus, if $\nu_\lambda$ is a Wasserstein barycenter, it must satisfy the first-order optimality condition for the functional (63)[21], that is,

$$\sum_{s=1}^S \lambda_s (Id - T^{\nu_\lambda\to\mu^s}) = 0 \quad \text{almost everywhere w.r.t. } \nu_\lambda. \tag{65}$$

Moreover, it can be proven that under certain assumptions critical points (or Karcher means), that is, measures $\nu_\lambda$ satisfying (65) and Wasserstein barycenters (i.e., minimizer of the functional described by (63)) coincide (see [68] and [43, Thm. 3.1.15]). As a consequence, to find such a Wasserstein barycenter $\nu_\lambda$, one can adopt the following fixed-point scheme based on (Wasserstein) gradient descent on the variance functional (63):

$$\nu_{n+1} = \left( Id - \eta \sum_{s=1}^S \lambda_s (Id - T_n^s) \right)_{\#} \nu_n,$$

where $T_n^s$ is the OT map from the current iterate $\nu_n$ to $\mu^s$, and $\eta > 0$ is a suitable step size. This iteration seeks a stationary point of the Wasserstein barycenter functional by successively updating $\nu_n$ via a transport-based averaging of the maps $T_n^s$ (we refer the reader to [2], and also to the recent work [11]). In conclusion, the well-defined geometric structure of the Wasserstein space allows gradient and fixed-point methods to work together, complementing each other, when addressing the Wasserstein synthesis problem.

In the context of this paper, that is, under the Gromov–Wasserstein (GW) structure, the objective functional $G_\lambda$ (see (31)) plays the role analogous to that of (63) in the Wasserstein setting. Its gradient can be computed using the blow-up technique (see Proposition 4.3), and it serves as the counterpart to the Fréchet derivative in (64). In [14], the authors propose an iterative Fréchet mean algorithm based on the work of Pennec [45], interpreting it as a gradient descent method for minimizing the Fréchet functional $G_\lambda$ over the space of finite networks. This approach parallels the procedure described in the Wasserstein

[20] $T^{\nu\to\mu^s}$ is the *OT map* in the sense that $T^{\nu\to\mu^s}_{\#}\nu = \mu^s$, and it realizes the Wasserstein distance as $W_2^2(\nu,\mu^s) = \int_{\mathbb{R}^d} \|x - T^{\nu\to\mu^s}(x)\|^2 \, d\nu(x)$.

[21] In other words, $\nu_\lambda$ is a probability measure such that the identity map equals the weighted average of the OT maps from $\nu_\lambda$ to the templates $\{\mu^s\}_{s=1}^S$, i.e., $Id = \sum_{s=1}^S \lambda_s T^{\nu_\lambda\to\mu^s}$.

setting but is adapted to the GW framework, following Pennec's ideas on averaging in finite-dimensional Riemannian manifolds. However, to the best of our knowledge, there are no theoretical guarantees in the literature that critical points of $G_\lambda$ are minimizers of (4), that is, true GW barycenters. Our Lemma 4.5 represents a step in this direction.

## References


[1] M. Agueh and G. Carlier, *Barycenters in the Wasserstein space*, SIAM Journal on Mathematical Analysis, 43 (2011), pp. 904–924.

[2] P. C. Álvarez-Esteban, E. Del Barrio, J. Cuesta-Albertos, and C. Matrán, *A fixed-point approach to barycenters in wasserstein space*, Journal of Mathematical Analysis and Applications, 441 (2016), pp. 744–762.

[3] D. Alvarez-Melis and T. S. Jaakkola, *Gromov-Wasserstein alignment of word embedding spaces*, preprint arXiv:1809.00013, (2018).

[4] L. Ambrosio, N. Gigli, and G. Savaré, *Gradient flows: in metric spaces and in the space of probability measures*, Springer Science & Business Media, 2008.

[5] Y. Bai, R. Diaz Martin, A. Kothapalli, H. Du, X. Liu, and S. Kolouri, *Partial Gromov-Wasserstein metric*, ICLR, (2025).

[6] F. Beier and R. Beinert, *Tangential fixpoint iterations for Gromov-Wasserstein barycenters*, preprint arXiv:2403.08612, (2024).

[7] F. Beier, R. Beinert, and G. Steidl, *On a linear Gromov–Wasserstein distance*, IEEE Transactions on Image Processing, 31 (2022), pp. 7292–7305.

[8] N. Bonneel, G. Peyré, and M. Cuturi, *Wasserstein barycentric coordinates: histogram regression using optimal transport.*, ACM Transactions on Graphics, 35 (2016), pp. 71–1.

[9] L. Chapel, M. Z. Alaya, and G. Gasso, *Partial optimal tranport with applications on positive-unlabeled learning*, NeurIPS, 33 (2020), pp. 2903–2913.

[10] J. Chen, B. T. Nguyen, S. Koh, and Y. S. Soh, *Semidefinite relaxations of the Gromov-Wasserstein distance*, NeurIPS, 37 (2024), pp. 69814–69839.

[11] Z. Chen, A. Neufeld, and Q. Xiang, *Provably convergent stochastic fixed-point algorithm for free-support wasserstein barycenter of continuous non-parametric measures*, preprint arXiv:2505.24384, (2025).

[12] S. Chowdhury and F. Mémoli, *Distances and isomorphism between networks and the stability of network invariants*, preprint arXiv:1708.04727, (2017).

[13] ——, *The Gromov–Wasserstein distance between networks and stable network invariants*, Information and Inference: A Journal of the IMA, 8 (2019), pp. 757–787.

[14] S. Chowdhury and T. Needham, *Gromov-Wasserstein averaging in a Riemannian framework*, in Proceedings of the IEEE/CVF CVPR Workshops, 2020, pp. 842–843.

[15] ——, *Generalized spectral clustering via Gromov-Wasserstein learning*, in AISTATS, 2021, pp. 712–720.

[16] H. S. M. Coxeter, *Introduction to geometry*, John Wiley & Sons, Inc., 1961.

[17] A. Cutler and L. Breiman, *Archetypal analysis*, Technometrics, 36 (1994), pp. 338–347.

[18] M. Cuturi and A. Doucet, *Fast computation of Wasserstein barycenters*, in ICML, 2014, pp. 685–693.

[19] T. DeRose and M. Meyer, *Harmonic coordinates*, Tech. Rep. 06-02, Pixar Technical Memo, 2006.

[20] T. Dumont, T. Lacombe, and F.-X. Vialard, *On the existence of Monge maps for the Gromov–Wasserstein problem*, Foundations of Computational Mathematics, (2024), pp. 1–48.

[21] R. Flamary, N. Courty, A. Gramfort, M. Z. Alaya, A. Boisbunon, S. Chambon, L. Chapel, A. Corenflos, K. Fatras, N. Fournier, L. Gautheron, N. T. Gayraud, H. Janati, A. Rakotomamonjy, I. Redko, A. Rolet, A. Schutz, V. Seguy, D. J. Sutherland, R. Tavenard, A. Tong, and T. Vayer, *POT: Python optimal transport*, Journal of Machine Learning Research, 22 (2021), pp. 1–8.

[22] M. Fréchet, *Les éléments aléatoires de nature quelconque dans un espace distancié*, in Annales de l'institut Henri Poincaré, vol. 10, 1948, pp. 215–310.

[23] C. Garcia, *Point cloud MNIST 2d dataset*, 2023. Accessed: 2024-09-28.

[24] M. Gromov, *Metric structures for Riemannian and non-Riemannian spaces*, Bulletin of the AMS, 38 (2001), pp. 353–363.

[25] F. Gunsilius, M. H. Hsieh, and M. J. Lee, *Tangential Wasserstein projections*, Journal of Machine Learning Research, 25 (2024), pp. 1–41.

[26] R. Hendrikson et al., *Using Gromov-Wasserstein distance to explore sets of networks*, University of Tartu, Master Thesis, 2 (2016).
[27] K. Hormann and N. Sukumar, *Generalized barycentric coordinates in computer graphics and computational mechanics*, CRC press, 2017.
[28] Y. Hur, W. Guo, and T. Liang, *Reversible Gromov–Monge sampler for simulation-based inference*, SIAM Journal on Mathematics of Data Science, 6 (2024), pp. 283–310.
[29] H. Karcher, *Riemannian center of mass and mollifier smoothing*, Communications on Pure and Applied Mathematics, 30 (1977), pp. 509–541.
[30] L. Kong, J. Li, J. Tang, and A. M.-C. So, *Outlier-robust Gromov-Wasserstein for graph data*, NeurIPS, 36 (2024).
[31] N. Kravtsova, *The NP-hardness of the Gromov-Wasserstein distance*, preprint arXiv:2408.06525, (2024).
[32] T. Le Gouic and J.-M. Loubes, *Existence and consistency of Wasserstein barycenters*, Probability Theory and Related Fields, 168 (2017), pp. 901–917.
[33] D. Lee and H. S. Seung, *Algorithms for non-negative matrix factorization*, NeurIPS, 13 (2000).
[34] W. Liu, C. Zhang, J. Xie, Z. Shen, H. Qian, and N. Zheng, *Partial Gromov-Gasserstein learning for partial graph matching*, preprint arXiv:2012.01252, (2020), p. 115.
[35] B. Mallery, J. M. Murphy, and S. Aeron, *Synthesis and analysis of data as probability measures with entropy-regularized optimal transport*, in AISTATS, 2025, pp. 2584–2592.
[36] R. J. McCann, *A convexity principle for interacting gases*, Advances in Mathematics, 128 (1997), pp. 153–179.
[37] A. Mead, *Review of the development of multidimensional scaling methods*, Journal of the Royal Statistical Society: Series D (The Statistician), 41 (1992), pp. 27–39.
[38] F. Mémoli, *Gromov–Wasserstein distances and the metric approach to object matching*, Foundations of Computational Mathematics, 11 (2011), pp. 417–487.
[39] F. Mémoli and T. Needham, *Distance distributions and inverse problems for metric measure spaces*, Studies in Applied Mathematics, 149 (2022), pp. 943–1001.
[40] F. Mémoli and G. Sapiro, *Comparing point clouds*, in Proceedings of the 2004 Eurographics/ACM SIGGRAPH symposium on Geometry processing, 2004, pp. 32–40.
[41] M. Mueller, S. Aeron, J. M. Murphy, and A. Tasissa, *Geometrically regularized wasserstein dictionary learning*, in Topological, Algebraic and Geometric Learning Workshops 2023, 2023, pp. 384–403.
[42] F. Otto, *The geometry of dissipative evolution equations: the porous medium equation*, Communications in Partial Differential Equations, 26 (2001), p. 101–174.
[43] V. M. Panaretos and Y. Zemel, *An invitation to statistics in Wasserstein space*, Springer Nature, 2020.
[44] K. Pearson, *Liii. on lines and planes of closest fit to systems of points in space*, The London, Edinburgh, and Dublin philosophical magazine and journal of science, 2 (1901), pp. 559–572.
[45] X. Pennec, *Intrinsic statistics on Riemannian manifolds: Basic tools for geometric measurements*, Journal of Mathematical Imaging and Vision, 25 (2006), pp. 127–154.
[46] G. Peyré, M. Cuturi, and J. Solomon, *Gromov-wasserstein averaging of kernel and distance matrices*, in ICML, 2016, pp. 2664–2672.
[47] G. Peyré and M. Cuturi, *Computational optimal transport*, Foundations and Trends in Machine Learning, 11 (2019), pp. 355–607.
[48] G. Rioux, Z. Goldfeld, and K. Kato, *Entropic gromov-wasserstein distances: Stability and algorithms*, Journal of Machine Learning Research, 25 (2024), pp. 1–52.
[49] F. Santambrogio, *Optimal Transport for Applied Mathematicians*, vol. 87 of PNLDE, Birkhäuser Boston, 2015.
[50] M. Scetbon, G. Peyré, and M. Cuturi, *Linear-time gromov wasserstein distances using low rank couplings and costs*, in ICML, 2022, pp. 19347–19365.
[51] M. A. Schmitz, M. Heitz, N. Bonneel, F. Ngole, D. Coeurjolly, M. Cuturi, G. Peyré, and J.-L. Starck, *Wasserstein dictionary learning: Optimal transport-based unsupervised nonlinear dictionary learning*, SIAM Journal on Imaging Sciences, 11 (2018), pp. 643–678.
[52] B. Schmitzer and C. Schnörr, *Modelling convex shape priors and matching based on the gromov-wasserstein distance*, Journal of Mathematical Imaging and Vision, 46 (2013), pp. 143–159.
[53] H. Schwerdtfeger, *Introduction to linear algebra and the theory of matrices*, P. Noordhoff, 1961.
[54] T. Séjourné, F.-X. Vialard, and G. Peyré, *The unbalanced gromov wasserstein distance: Conic formulation and relaxation*, NeurIPS, 34 (2021), pp. 8766–8779.

[55] J. Solomon, G. Peyré, V. G. Kim, and S. Sra, *Entropic metric alignment for correspondence problems*, ACM Transactions on Graphics, 35 (2016), pp. 1–13.
[56] K.-T. Sturm, *The space of spaces: curvature bounds and gradient flows on the space of metric measure spaces*, AMS, 2012.
[57] A. Thual, Q. H. Tran, T. Zemskova, N. Courty, R. Flamary, S. Dehaene, and B. Thirion, *Aligning individual brains with fused unbalanced Gromov Wasserstein*, NeurIPS, 35 (2022), pp. 21792–21804.
[58] V. Titouan, R. Flamary, N. Courty, R. Tavenard, and L. Chapel, *Sliced gromov-wasserstein*, NeurIPS, 32 (2019).
[59] I. Tošić and P. Frossard, *Dictionary learning*, IEEE Signal Processing Magazine, 28 (2011), pp. 27–38.
[60] R. Tyrrell Rockafellar, *Convex analysis*, Princeton mathematical series, 28 (1970).
[61] H. Van Assel, C. Vincent-Cuaz, N. Courty, R. Flamary, P. Frossard, and T. Vayer, *Distributional reduction: Unifying dimensionality reduction and clustering with Gromov-Wasserstein*, preprint arXiv:2402.02239, (2024).
[62] T. Vayer, *A contribution to optimal transport on incomparable spaces*, preprint arXiv:2011.04447, (2020).
[63] T. Vayer, L. Chapel, R. Flamary, R. Tavenard, and N. Courty, *Fused Gromov-Wasserstein distance for structured objects*, Algorithms, 13 (2020), p. 212.
[64] C. Villani, *Topics in Optimal Transportation*, AMS, 2003.
[65] ——, *Optimal transport: old and new*, Springer, 2009.
[66] W. Wang, D. Slepčev, S. Basu, J. A. Ozolek, and G. K. Rohde, *A linear optimal transportation framework for quantifying and visualizing variations in sets of images*, International Journal of Computer Vision, 101 (2013), pp. 254–269.
[67] J. Warren, S. Schaefer, A. N. Hirani, and M. Desbrun, *Barycentric coordinates for convex sets*, Advances in Computational Mathematics, 27 (2007), pp. 319–338.
[68] M. Werenski, R. Jiang, A. Tasissa, S. Aeron, and J. M. Murphy, *Measure estimation in the barycentric coding model*, in ICML, 2022, pp. 23781–23803.
[69] M. Werenski, B. Mallery, S. Aeron, and J. M. Murphy, *Linearized wasserstein barycenters: Synthesis, analysis, representational capacity, and applications*, in AISTATS, 2025, pp. 4555–4563.
[70] Z. Wu, S. Song, A. Khosla, F. Yu, L. Zhang, X. Tang, and J. Xiao, *3d shapenets: A deep representation for volumetric shapes*, in CVPR, 2015, pp. 1912–1920.
[71] Y. Zemel and V. M. Panaretos, *Fréchet means and Procrustes analysis in Wasserstein space*, Bernoulli, 25 (2019), pp. 932–976.
[72] J. Zhang, B. Deng, Z. Liu, G. Patanè, S. Bouaziz, K. Hormann, and L. Liu, *Local barycentric coordinates*, ACM Transactions on Graphics, 33 (2014), pp. 1–12.
[73] Z. Zhang, Z. Goldfeld, K. Greenewald, Y. Mroueh, and B. K. Sriperumbudur, *Gradient flows and Riemannian structure in the Gromov-Wasserstein geometry*, preprint arXiv:2407.11800, (2024).
[74] Z. Zhang, Z. Goldfeld, Y. Mroueh, and B. Sriperumbudur, *Duality and sample complexity for the Gromov-Wasserstein distance*, in NeurIPS 2023 Workshop Optimal Transport and Machine Learning, 2023.
[75] Z. Zhang, Y. Mroueh, Z. Goldfeld, and B. Sriperumbudur, *Cycle consistent probability divergences across different spaces*, in AISTATS, 2022, pp. 7257–7285.

Rocío Díaz Martín, Tufts University, Department of Mathematics, Medford, MA 02155, USA
*Email address*: rocio.diaz_martin@tufts.edu

Ivan V. Medri, University of Virginia, Department of Biomedical Engineering, Charlottesville, VA 22904, USA
*Email address*: pzr7pr@virginia.edu

James M. Murphy, Tufts University, Department of Mathematics, Medford, MA 02155, USA
*Email address*: jm.murphy@tufts.edu